The lithostratigraphy and structural components of the Eureka Shear Zone, southern Namibia

by

Moses Tuutaleni Angombe

Thesis presented in fulfilment of the requirements for the degree of
Master of Science in the Faculty of Science at
Stellenbosch University

Supervisor: Dr. Jodie Miller
Co-supervisor: Dr. Paul Macey

December 2016

Stellenbosch University https://scholar.sun.ac.za

Declaration

By submitting this thesis electronically, I declare that the entirety of the work contained therein is my own, original work, that I am the sole author thereof (save to the extent explicitly stated otherwise), that reproduction and publication thereof by Stellenbosch University will not infringe any third party rights and that I have not previously in its entirety or in part submitted it for obtaining any qualification.

Signature: ..... Date: December 2016

Copyright © 2016 Stellenbosch University
All rights reserved

Stellenbosch University https://scholar.sun.ac.za

Abstract

The newly recognised Eureka Shear Zone (ESZ) in southern Namibia is a Late-Mesoproterozoic to Early Neoproterozoic high strain zone in the Namaqua sector of the Namaqua Natal Metamorphic Province (NNMP). Its current outcrop trace is closely aligned with the previously identified terrane boundary between the Paleoproterozoic Richtersveld Subprovince and the Mesoproterozoic Gordonia Subprovince (South Africa) or Grünau Terrane (Namibia). This has given rise to the question of what this high strain zone represents in terms of its lithostratigraphy and tectonic history. A joint mapping program between the Geological Survey of Namibia and the Council for Geoscience in South Africa has redefined and clarified aspects of the regional geology and the relationship between different crustal blocks within the Namaqua sector. Chief amongst these are the redefinition of: (1) the Paleoproterozoic Richtersveld Subprovince into the Richtersveld Magmatic Arc (comprised of the greenschist-facies Vioolsdrif Domain and the amphibolite-facies Pella Domain) in both South Africa and Namibia; (2) the Mesoproterozoic Grünau Terrane into the Kakamas Domain in Namibia; (3) the SW-vergent, subhorizontal Lower Fish River-Onseepkans Thrust (LFROT) that juxtaposes the granulite-facies Kakamas Domain on top of the Pella Domain and (4) a zone of highly deformed and imbricated units on top of the LFROT that reworks the Kakamas Domain, referred to as the Lower-Fish-River-Onseepkans Thrust Zone (LFROTZ) and which also includes unique units not found in the Kakamas or Pella domains. In this study, detailed field mapping, petrography, structural analysis and U-Pb zircon dating on the ESZ was undertaken to understand its relationship to the LFROTZ and the nearby Marshall Rocks-Pofadder Shear Zone (MRPSZ) with a view to understanding the evolution of the ESZ in the broader context of the Namaqua sector and NNMP. The ESZ is a ~2 to 5 km wide, 50 km long and WNW-trending zone of intense shearing. It is dominantly composed of two distinct lithostratigraphic packages: (1) the Eureka Complex (EC) in the north, a heterogeneous sheared garnet-bearing gneiss with isolated m-scale and lens-shaped remnants of pelitic granulite whose metamorphic grade and detrital zircon patterns correlate it to the Kakamas Domain; and (2) fault/thrust-bounded packages of interlayered quartz-feldspar gneiss and amphibolite (MQ), that occur as sigmoid-shaped mega-lenses within the EC and which are correlated to units considered to be unique to the LFROTZ. South of the EC and MQ units, the ESZ shears migmatitic volcanoclastic rocks of the Pella Domain. Petrographic studies indicate that the rocks of the ESZ were affected by retrograde metamorphism at mid to upper greenschist facies during shearing. Fault rock textures in the ESZ vary from phyllonite to cataclasite dominant, with rarer mylonitic textures. This implies a complex interplay between rheological contrast, slip rate and crustal depth under shearing conditions where potassium feldspar was brittle and quartz was plastic. The orientation of the shear fabrics varies with the ESZ but maintains a dominant WNW strike steeply dipping shear foliation accompanied by a NE trending and moderately to steeply plunging lineation. The ESZ was intruded by a significant volume of foliation sub-parallel, sheet-like, pegmatite and leucocratic equigranular granite dykes which date to ~1000 Ma and constrain the age of the shear zone. The geometry, age and strain regime of ESZ is similar to the adjacent MRPSZ, but its lithostratigraphy reveal the presence of rocks found in the LFROTZ making the ESZ a younger shear zone exploiting the older terrane boundary between the Kakamas and Pella domain.

Stellenbosch University https://scholar.sun.ac.za

Acknowledgement

Firstly, I would like to thank my supervisor Dr. Jodie Miller and my co-supervisor Dr. Paul Macey; you have been of active support and great assistance throughout the entire research period. I would also like to extend my gratitude to the members of the southern Namibia joint mapping project between the Geological Survey of Namibia and Council for Geosciences, South Africa. Finally, I would like to thank my colleagues, family, girlfriend, friends and professional leaders, whose unique talents have enabled me to complete this thesis. Thank you all.

Stellenbosch University https://scholar.sun.ac.za

Table of Contents

Stellenbosch University https://scholar.sun.ac.za

Stellenbosch University https://scholar.sun.ac.za

Stellenbosch University https://scholar.sun.ac.za

List of Tables

Stellenbosch University https://scholar.sun.ac.za

List of Figures

Stellenbosch University https://scholar.sun.ac.za

Stellenbosch University https://scholar.sun.ac.za

Stellenbosch University https://scholar.sun.ac.za

Stellenbosch University https://scholar.sun.ac.za

Stellenbosch University https://scholar.sun.ac.za

Stellenbosch University https://scholar.sun.ac.za

Stellenbosch University https://scholar.sun.ac.za

List of Abbreviations

NNMP: Namaqua-Natal Metamophic Province

MRPSZ: Marshall Rocks-Pofadder Shear Zone

LFROT: Lower-Fish River Onseepkans Thrust

LFROTZ: Lower-Fish River Onseepkans Thrust Zone

ESZ: Eureka Shear Zone

SSZ: Sperlingsputs Shear Zone

EC: Eureka Complex

MQ: Interlayered amphibolite and quartzo-feldspathic gneiss

Stellenbosch University https://scholar.sun.ac.za

CHAPTER 1: INTRODUCTION

1.1 BACKGROUND

The Namaqua Sector of the Namaqua-Natal Metamorphic Province (NNMP) is associated with a series of sub-parallel Late Mesoproterozoic / Early Neoproterozoic dextral shear zones of which the most well-known is the Marshall-Rocks Pofadder Shear Zone (MRPSZ) (Beukes, 1973; Blignault, 1977; Blignault et al., 1983; Colliston and Schoch, 2000; Colliston et al., 2014; Coward, 1980; Coward and Potgieter, 1983; Hartnady et al., 1985; Jacobs et al., 1993; Joubert, 1986; Miller, 2008; Moen and Toogood, 2007; Moore, 1981; Thomas et al., 1994; Toogood, 1976). These shear zones, are thought to have developed due to indentor tectonics as the NNMP accreted onto the Kaapvaal Craton during (Jacobs et al., 1993; Thomas et al., 1994) the Namaqua Orogeny at 1.2-1.0 Ga (Cornell et al., 2009; Jacobs et al., 1993; Macey et al., 2015; Thomas et al., 1994). Previous studies of these shear zones focused on the regional scale (1:100 000) as part of PhD research projects (Beukes, 1973; Blignault, 1977; Mclaren, 1988; Toogood, 1976). Detailed work on these shear zones only was carried out during the past five years and mostly concentrated on the MRPSZ (e.g. Colliston and Schoch, 2013; Lambert, 2013; Macey et al., 2015; Melosh et al., 2014).

Recent 1:50000 scale geological mapping done by Macey et al., (2015) in southern Namibia has led to the newly recognised Eureka Shear Zone (ESZ) as one of the parallel high strain zone in the Namaqua Sector. The ESZ forms a 50 km-long and up to 10 km wide WNW-trending high-strain zone, situated north of and sub-parallel to the MRPSZ. Apart from it being a newly recognised shear zone in the Namaqua sector, its structural complexity and poor exposure pose many problems. Some of the major problems associated with the ESZ are the following: (1) the lateral extent and boundaries of the shear zone are not constrained especially underneath the Cenozoic sedimentary cover; (2) the rock units within the shear zone have not been described in detail and hence their relationship to the regional lithotectonic framework is unclear; (3) the structure and orientation of fabric elements have not been studied in detail; (4) the timing of shearing is not constrained; and (5) in the west, both the MRPSZ and ESZ broaden into a 25 km wide high-strain zone making it difficult to define the boundaries and the relationship between the two. Moreover, the geographical position of the ESZ coincides with the inferred line of the older Lower-Fish River-Onseepkans Thrust (LFROT), which marks the boundary between the high grade Gordonia and medium-low grade Richtersveld subprovinces (Blignault et al., 1983; Colliston and Schoch, 2000; Macey et al., 2015). Adding to that, Macey et al (2015) hypothesized that the Eureka shear zone represented a D_4-shearing event that reworked the LFROT and recognised the need for more detailed research into this complex shear zone.

Shear zones in general are studied for their ability in recording deformation processes and rheological behaviours at different pressure and temperature conditions (Carreras, 2001; Means, 1995; Passchier and Trouw, 2005; Ramsay, 1980; Simpson and De Paor, 1993). Modern approach to studying complex ancient exhumed fault zones require a comprehensive detailed study of structures at all scales (Carreras, 2001; Rennie et al., 2013; Stewart et al., 2000). Field based studies are considered useful in

Stellenbosch University https://scholar.sun.ac.za

understanding the distribution, nature and relationship between different deformation mechanism in natural shear zones at all scales (Stewart et al., 2000). Furthermore, in order to understand the controlling factors in regions of frictional, viscous and frictional-viscous transition, detailed field description and petrographic studies is required along the shear zone (Stewart et al., 2000). U-Pb zircon radiometric systems in conjunction with field based investigations are increasingly being used to determine the timescales of tectonic processes and conditions that are affecting the zircons host rocks (Marsh and Stockli, 2015; Whitehouse and Bridgwater, 2001). Therefore, this study will employ detailed petrographical, structural and geochronological methods as an attempt aimed at resolving some of the issues associated the ESZ.

1.2 RESEARCH AIMS AND OBJECTIVES

1.2.1 **Problem Statement**

This study aims to build on the regional geological mapping of the ESZ done by Macey et al (2015) through detailed geological, structural and geochronolgical analysis, in order to reconstruct the tectonic processes that led to the formation the Eureka shear zone. The understanding of the evolution of the Eureka shear zone will be of importance to the broader knowledge of the tectonometamorphic evolution of the NNMP.

1.2.2 **Objectives and Key Questions**

The objectives of this research project are to:

1. To determine the nature of the lithological units that are cut by the fault rocks of the ESZ.
   - ✓ What are the rock types present in the ESZ and do they lead to unique characteristics or lithological packages within the shear zone?
   - ✓ What are the ages of the rocks within the ESZ?
   - ✓ Based on the lithology and age of the rocks in the ESZ, does the ESZ cut the Gordonia Subprovince, the Pella Domain (Richtersveld Subprovince), the tectonic boundary between them or all three?

2. To determine structural elements that characterizes and allows differentiation of the ESZ.
   - ✓ What are the meso- and micro-scale structural elements that characterise the ESZ and do they imply brittle or ductile shearing conditions or both?
   - ✓ What is the style and distribution of the structural elements and can they be used to delineate the boundaries and lateral extent of the shear zone?
   - ✓ How is the shearing intensity distributed within the ESZ and what does this imply about the thermal regime and slip regime within the shear zone?

3. To determine whether there is a link between the ESZ, the MRPSZ and the LFROTZ.
   - ✓ What is the relative timing of the ESZ and the MRPSZ and does this imply a link between the evolutions of the two shear zones?
   - ✓ What is the effect of the older LFROTZ structure on the younger ESZ?

Stellenbosch University https://scholar.sun.ac.za

4. To understand the evolution of the ESZ and clarify its role in the amalgamation of the Namaqua Sector of the NNMP.

1.3 LOCATION OF THE STUDY AREA

The study area is located in the Warmbad District, southern Namibia about 20 km west of the town of Warmbad and 23 km northwest of the Tantalite Valley Massif Complex. The area extends between latitudes 28°22' S and 28°37' S and longitudes 18°16' E and 18° 32' E (Figure 1-1). The area is semi-arid with sparse vegetation consisting mostly of grassland. Commercial farmers occupy the majority of the land, while communal farmers are a minority. The study area is accessed via a well maintained gravel road and by private dirt tracks.

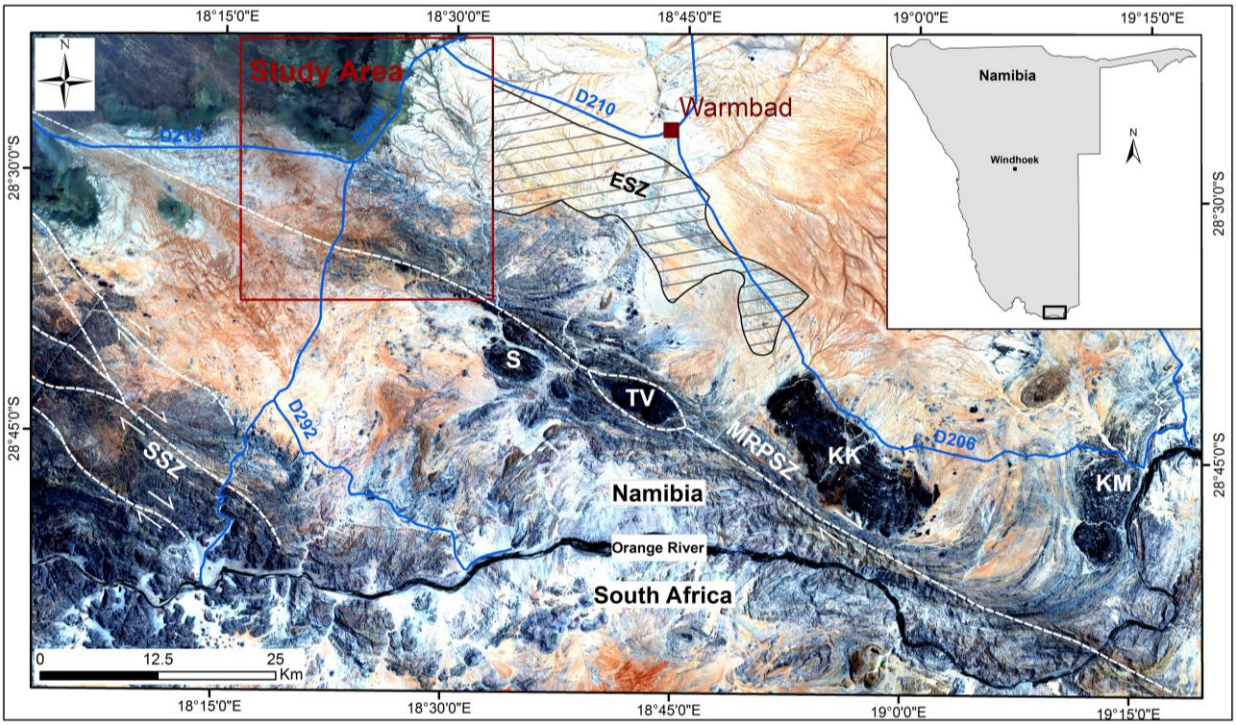

Figure 1-1: Location map of the study area showing the position and extent of the Eureka Shear Zone (black dotted lines) along with two other Namaqua sector late-dextral shear zones, i.e. the Marshall Rocks-Pofadder shear zone and the Sperlingputs Shear Zone (white dotted lines). Image also shows four Gordonia Klippen; KM=Keimasmond, KK=Kum kum, TV=Tantalite Valley massif and Sandfontein klippen. Map background =Landsat (ETM) Image (RGB: 321) of the border region between Namibia and South Africa.

1.4 RESEARCH METHODOLOGY

This study was conducted as part of a regional 1:50 000 scale geological mapping and research project on the Precambrian rocks of the NNMP in southern Namibia. The Council for Geoscience (South Africa) conducted the project, under contract and in cooperation with the Geological Survey of Namibia. During research, the mapping teams (which the author was part of) from both surveys produced a series of 1:50 000 scale geological maps and compiled a map explanation sheet referenced as Macey et al. (2015). The methodological procedures used are discussed below.

Stellenbosch University https://scholar.sun.ac.za

1.4.1 Remote Sensing Data

Prior to field mapping, detailed remote sensing interpretation was done and various basemaps were produced at a scale of 1:35 000. These maps consisted of Landsat, ASTER, hyperspectral and high resolution airborne magnetic imagery. In addition to these maps, topographic maps, existing geological maps and Google Earth images were also compiled for the study area. Google Earth, Corel draw graphic suite, Adobe illustrator CC and ArcGIS 10.1 software's were used in compiling, geo-referencing and exporting various maps and figures. ASTER and Landsat (ETM) data were processed using ENVI 4.8 software, while high resolution airborne magnetic data were processed using Geosoft Software. All the remote sensing datasets were obtained from the digital library of Geological Survey of Namibia.

1.4.2 Field Mapping and Data Collection

A total of 55 days were spent in the field between May 2015 and July 2015. This consisted of 4 weeks between May and July 2014, 2 weeks in September and 9 days in July 2015. During the field mapping, location data was collected with a Garmin 30X GPS and structural measurements were taken using a Freiberg compass set at a magnetic declination of 19˚. Various samples were collected for petrographic, structural and geochronological analyses. List of samples are attached as Appendix A. The oriented structural samples were processed at the University of Stellenbosch and were submitted for thin section preparation at the Council for Geoscience (South Africa) laboratories. A detailed geological map of the study area is provided in Appendix B.

1.4.3 Structural Data Analysis

All structural measurements (foliation, lineation, fold axes and fault planes) collected in the field were compiled into a Microsoft Excel spreadsheets. The data was filtered and grouped into different relative structural domains. The clustered data was imported into Stereonet Windows 8 software (Allemendinger et al., 2012; Cardozo and Allmendinger, 2013) and various Schmidt equal area projected stereonets plots were produced.

Stellenbosch University https://scholar.sun.ac.za

CHAPTER 2: REGIONAL TECTONIC ARCHITECTURE

2.1 OVERVIEW

The Namaqua-Natal Metamorphic Province (NNMP) is a ~100-400 km wide NW-SE trending Proterozoic metamorphic belt that extends across Southern Namibia and South Africa (Blignault, 1977; Blignault et al., 1983; Cornell et al., 2006; Frimmel, 2000; Hartnady et al., 1985; Joubert, 1986; Miller, 2008; Thomas et al., 1994). The rocks of this Proterozoic metamorphic belt were assembled during the formation of the Supercontinent Rodinia between 1.3 and 1.0 Ga, when a series of crustal blocks were accreted onto the southern and southwestern margins of the Kaapvaal Craton (Colliston and Schoch, 2013; Colliston et al., 2014; Eglington and Armstrong, 2003; Hartnady et al., 1985; Hoffman, 1991; Humphreys and Van Bever Donker, 1987; Joubert, 1986; Thomas et al., 1994) (Figure 2-1). The NNMP is subdivided into two segments; 1) the Natal sector in the southeast of South Africa and 2) the Namaqua sector in southern Namibia and northwestern South Africa (Cornell et al., 2006; Frimmel, 2000) (Figure 2-1). The exposures of the Namaqua and Natal sectors are separated by younger Phanerozoic Karoo cover sequences (Eglington and Armstrong, 2003; Frimmel, 2000; Thomas et al., 1994). In Southern Namibia, rocks of the NNMP define a ~100 km wide north-westerly trending belt that extends from Luderitz on the Namibian coast towards the Orange River in the southeast (Becker et al., 2006; Miller, 2012, 2008). This research study area is located in the Namaqua sector, north of the Orange River and south of town Karasburg (Figure 2-1).

Stellenbosch University https://scholar.sun.ac.za

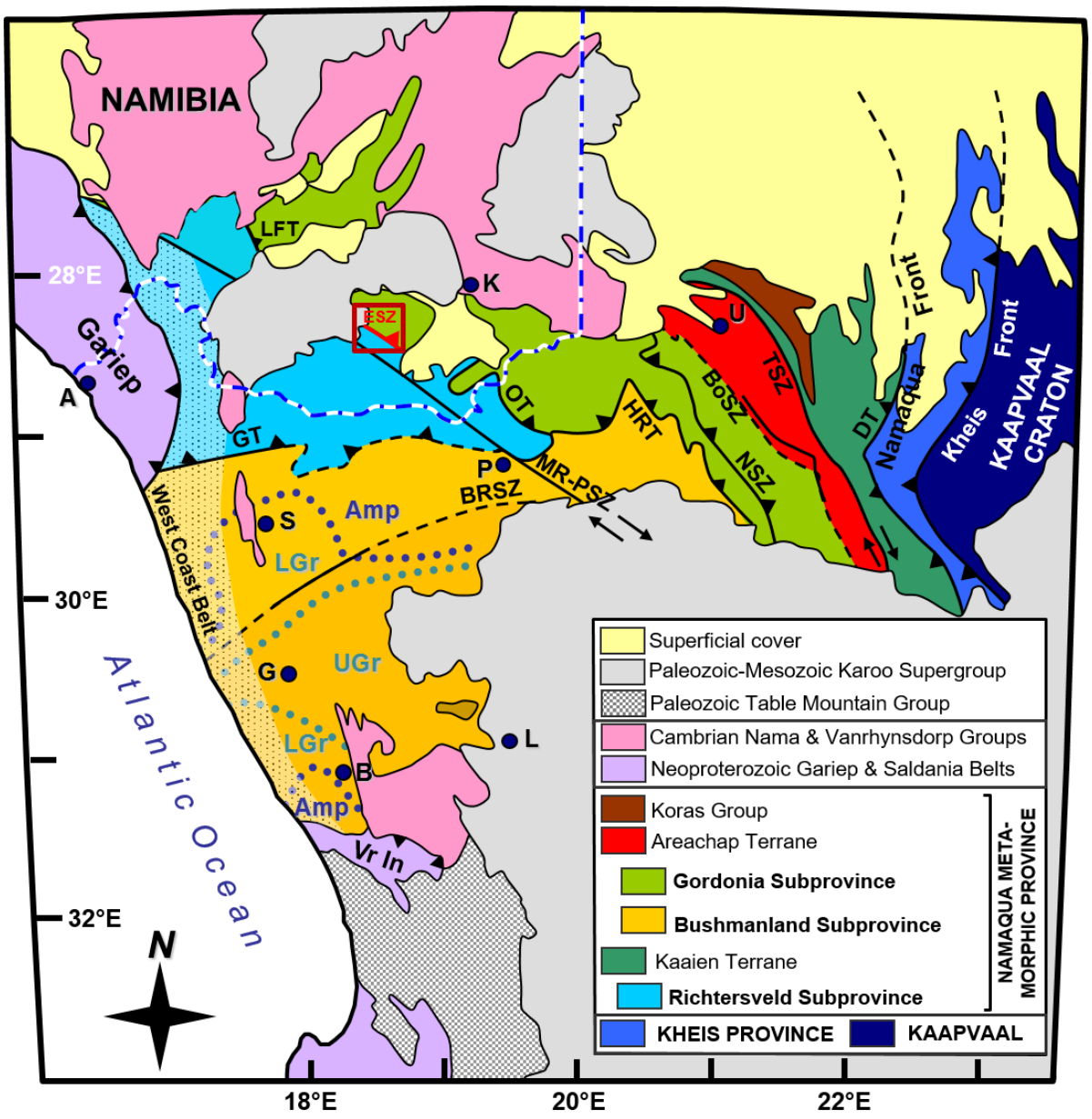

Figure 2-1: Tectonostratigraphic subdivision of the Namaqua sector of the NNMP, adopted from Cornell et al., (2006) *and modified after Macey et al, (2015). Terrane boundaries of Namaqua sector: GT: Groothoek Thrust; OT: Onseepkans Thrust; MR-PSZ:Marshall-Rocks Pofadder Shear Zone; VSZ: Vogelstruislaagte Shear Zone; BPSZ: Brypaal Shear Zone; HBRT: Hartbeest River Thrust; BoSZ: Bovenrug Shear Zone; BBSZ: Brakbos Shear Zone; DT: Dabep Thrust; LFT Lower Fish River Thrust. Place names: A=Alexander Bay; B=Bitterfontein; G=Garies; K=Karasburg; L=Loeriesfontein; P=Pofadder; S=Springbok; U=Upington. Metamorphic isograds after Waters (1986): UGr=upper granulite facies; LGr=lower granulite facies; Amp=amphibolite facies. ESZ=Eureka Shear Zone. Red box=Study area.*

Stellenbosch University https://scholar.sun.ac.za

2.2 LITHOTECTONIC OVERVIEW OF THE NAMAQUA SECTOR

2.2.1 Tectonic Domains and Their Tectonic History

The rocks of the Namaqua sector have been subdivided into several subprovinces, which are futher subdivided into terranes. The latter are bounded by major structural discontinuities and distinguished by differences in lithostratigraphy, tectonic history and metamorphic grade. The major subdivisions in the Namaqua sector are; (1) Richtersveld Subprovince, (2) Bushmanland Subprovince, (3) Gordonia Subprovince, (4) Areachap Terrane and (5) Kaaien Terrane (Blignault et al., 1983; Colliston and Schoch, 2000; Frimmel, 2000; Hartnady et al., 1985; Joubert, 1986; Macey et al., 2015; Miller, 2008; Thomas et al., 1994). The current study area, is located across the boundary between the Richtersveld and Gordonia subprovinces (Blignault et al., 1983; Colliston and Schoch, 2000; Frimmel, 2000; Miller, 2012, 2008) (Figure 2-1).

The Richtersveld Subprovince is comprised of Paleoproterozoic volcanic and volcano-sedimentary rocks of the Orange River Group and intrusive rocks of the Vioolsdrif Suite (Blignault, 1977; Blignault et al., 1983; Hartnady et al., 1985; Minnaar, 2012; Moen and Toogood, 2007; Reid, 1997; Reid et al., 1987). In the vicinity of the study area the Richtersveld Subprovince is subdivided into the Pella and Vioolsdrift Domains (discussed in section 2.2.2) (Colliston and Schoch, 2013, 2002, 2000; Macey et al., 2015; Miller, 2008; Minnaar, 2012). The Gordonia Subprovince is situated east of the Richtersveld Subprovince (Figure 2-1) and incorporates granulite facies metamorphosed metasedimentary and intrusive rocks of the Grünau Terrane (Colliston and Schoch, 2000) also known as the Kakamas Terrane (Thomas et al., 1994) or Kakamas Domain by (Macey et al., 2015). The Richtersveld and Gordonia subprovinces are separated by the Lower-Fish River-Onseepkans Thrust Zone (LFROTZ), which thrusted the high grade rocks on top of the of the medium-low grade rocks (Blignault et al., 1983; Colliston and Schoch, 2013, 2000; Macey et al., 2015; Miller, 2012, 2008; Moen and Toogood, 2007).

Rocks of the Namaqua sector record a complex structural and metamorphic history. Different deformation episodes and tectonic models have been proposed by a number of previous workers (e.g. Beukes, 1973; Blignault, 1977; Blignault et al., 1983; Hartnady et al., 1985; Joubert, 1986; Moen and Toogood, 2007; Toogood, 1976). The commonly accepted structural nomenclature (deformation episodes D_1-D_4) for the study area is adopted from Joubert (1986) and can be summarised as follows. An early deformation episode (D_1), occurred during the Orange River (Eburnian) Orogeny at ~1.9-1.85 Ga (Beukes, 1973; Blignault, 1977; Blignault et al., 1983; Joubert, 1986; Macey et al., 2015). This deformation episode is associated with greenschist facies metamorphism within the Orange River Group rocks of the Richtersveld Subprovince (Beukes, 1973; Blignault, 1977; Blignault et al., 1983; Joubert, 1986; Moen and Toogood, 2007). The effects of the D_1 deformation are present in the low grade western part of the Richtersveld Subprovince (Vioolsdrift Domain) and are not observed in the current study area. The second deformation episode (D_2) occurred during the Namaqua Orogeny at 1.2-1.0 Ga through multiple phases and is characterised by the development of a strong regional fabric and medium to high-grade regional metamorphism (Blignault, 1977; Blignault et al., 1983; Colliston and Schoch, 2013, 2002, 2000;

Stellenbosch University https://scholar.sun.ac.za

Cornell et al., 2009; Joubert, 1986; Macey et al., 2015; Thomas et al., 1994; Toogood, 1976). The effect of D_2 deformation is recorded in the rocks of the eastern Richtersveld Subprovince (Pella Domain) and Kakamas Domain of the Gordonia Subprovince. The terminal phase of D_2 is accompanied by the development of east trending megascopic folds (F_3) at ~1020 Ma (Colliston and Schoch, 2013, 2002, 2000; Joubert, 1986; Moen and Toogood, 2007). The folding event F_3 is considered as a separate deformation episode (D_3) by some authors (e.g. (Colliston and Schoch, 2013, 2002, 2000; Macey et al., 2015). The deformation episode D_4 is associated with the development of a series of sub-parallel dextral shear zones between 1050 and 960 Ma (Colliston and Schoch, 2013, 2002, 2000; Joubert, 1986; Lambert, 2013; Macey et al., 2015; Moen and Toogood, 2007; Toogood, 1976). D_4 is characterized by brittle-ductile deformation accompanied by retrograde metamorphism under amphibolite to greenschist facies conditions (Colliston and Schoch, 2013, 2002, 2000; Lambert, 2013; Macey et al., 2015; Toogood, 1976). A brief summary of these deformation sequences and timing of the major structural events are presented Table 2-1. In the study area, the D_1 deformation episode is not preserved and the D_2 Namaqua Orogeny is considered responsible for the prominent planar and linear ductile fabrics associated with changes in metamorphic grade within the rocks of the Richtersveld and Gordonia subprovinces (Colliston and Schoch, 2000; Macey et al., 2015; Miller, 2008). The D_2 Namaqua Orogeny is also responsible for the development of the complex, low-angle and imbricated LFROTZ (Colliston and Schoch, 2013; Macey et al., 2015) that juxtaposes the granulite facies Kakamas Domain of the Gordonia Subprovince against the amphibolite-facies Pella Domain of the Richtersveld Subprovince (Table 2-1 and Figure 2-2). The two phases of thrusting were accompanied by voluminous bimodal magmatism, represented by porphyritic garnet-biotite granites (Eendoorn Suite; 1250-1190 Ma), leucogranite (e.g Orange Falls Suite; 1210-1120 Ma), gabbroic rocks (Kum Kum Suite; 1225-1215 Ma) and I-type hornblende granites (Komsberg Suites; 1125-1110 Ma) that intruded into the thrust zone and areas adjacent to it (Pella and Kakamas domains host rocks) (Macey et al., 2015).

Stellenbosch University https://scholar.sun.ac.za

Table 2-1: Summary of the deformation sequences and timing of major structural events. Taken from, Macey et al. (2015).

NEOPROTEROZOIC TO CRETACEOUS	POST-NAMAQUA BRITTLE DEFORMATION	D_5	Development of brittle structures (faults, joints and quartz veins) cross-cutting D_1,D_2,D_3 and D_4 fabrics	POST-NAMAQUA
EARLY NEOPROTEROZOIC	(MARSHALL ROCKS-POFADDER, EUREKA & SOUTHERN NAMAQUA	D_4	Development of crustal-scale shear zones associated with brittle-ductile deformation at amphibolite- greenschist facies grade	Development of three brittle-ductile, dextral, NW-SE trending shear zones; the Eureka Shear Zone, Marshall Rocks-Pofadder Shear Zone and Sperlingsputs Shear Zone. Shear zones overprint pre-existing structures and reactivate older thrust boundaries
MESOPROTEROZOIC	NAMAQUA OROGENY (~1200-1000 Ma)	D_3	Mega-scale folding	Development regional scale open fold (F_3), domes and basin structures
		D_2	Two main phases of thrusting & terrane juxtaposition	2) Thrusting of the granulite facies Kakamas Domain of the Gordonia Subprovince on top of the amphibolite facies Pella Domain of the Richtersveld Subprovince along the Lower Fish River Onseepkans Thrust Zone (LOFRTZ).
			Regional high grade ductile deformation	1) Development of regional ductile LS-tectonite fabrics of higher metamorphic (amphibolite and granulite facies) grade in rocks of the Pella and Kakamas domains
PALEOPROTEROZOIC	ORANGE RIVER OROGENY (~1900 - 1850 Ma)	D_1	Greenschist facies deformation	The first deformation recorded in the Namaqua sector, overprinted by D_2 and restricted to the Vioolsdrift Domain (Not observed in the study area.) (western Richtersveld Subprovince).

POST-TERRANE JUXTAPOSING	
SYN-TERRANE JUXTAPOSING	
PRE-TERRANE JUXTAPOSING	

Stellenbosch University https://scholar.sun.ac.za

Along the LFROTZ, rocks of the Richtersveld and Gordonia subprovinces and intrusive rocks are sheared into a wide imbricated melange referred to as the "Lower Fish River-Onseepkans Thrust Zone" (Macey et al., 2015). For clarification Lower Fish River-Onseepkans Thrust (LFROT) *sensu strictu* refers to the basal thrust only (Macey et al., 2015), while Lower Fish River-Onseepkans Thrust Zone (LFROTZ) refers to a wider zone, comprising imbricated sheared rocks of the Pella Domain, Kakamas Domain, Eendoorn Suite and a variety of leucogranite gneisses that are restricted and occur in close proximity to the LFROT (Macey et al., 2015).

The origin of D_2 is thought to have been the accretion of a juvenile mesoproterozoic (1600-1200 Ma) supercrustal and plutonic continetal crust along the southwestern margins of the Archean (>2500 Ma) Kaapvaal Craton (Hartnady et al., 1985). The Namaqua orogeny refer to the the final stages of accretion as a result of arc-continent-continent-collistion between ~1210-1195 Ma (Hartnady et al., 1985; Jacobs and Thomas, 1994; Jacobs et al., 1993; Joubert, 1986; Macey et al., 2015; Thomas et al., 1994). Progessive D_2 deformation started with early crustal thickening, followed by burial, high-temperature metamorphism and wrench-shearing between 1200-1050 Ma (Colliston and Schoch, 2013; Eglington, 2006; Jacobs et al., 1993; Thomas et al., 1994).

The planar S_2 fabrics of the D_2 Namaqua Orogeny have a regional shallow to moderate NE dip direction associated with axial planes of various phases of isoclinal folds, sheath fold, thrusts and mineral lineations (Colliston and Schoch, 2013, 2002, 2000; Macey et al., 2015). Mineral stretching lineations (L_2) are represented by sub-horizontal-stretching mostly NE-trending lineations and fold axes of various phases of isoclinal D_2 folds sub-parallel to the SW-directed tectonic transport direction (Colliston and Schoch, 2013, 2002, 2000; Macey et al., 2015). The terminal phase of D_2 is thought to have been followed by D_3 (Colliston and Schoch, 2013, 2002, 2000; Macey et al., 2015). The age and origin of the D_3 deformation episode remains poorly understood, but it is represented by a regional-scale open F_3 domes (dominant) and basin structures throughout the Namaqua sector (Colliston and Schoch, 2013, 2000; Joubert, 1986; Macey et al., 2015; Toogood, 1976). In the vicinity of the current study area and north of the MRPSZ, D_3 is characterised by km-scale dome-and basin structure with NE-trending long axes. South of the MRPSZ, D_3 is characterized by a series of parallel NE to E, near-upright F_3 antiforms and synforms (Beukes, 1973; Colliston and Schoch, 2013, 2000; Lambert, 2013; Macey et al., 2015; Moen and Toogood, 2007). D_2 and D_3 structures and fabrics were rotated and variably overprinted by D_4 during shearing (Colliston and Schoch, 2013, 2000; Lambert, 2013; Macey et al., 2015; Toogood, 1976).

Stellenbosch University https://scholar.sun.ac.za

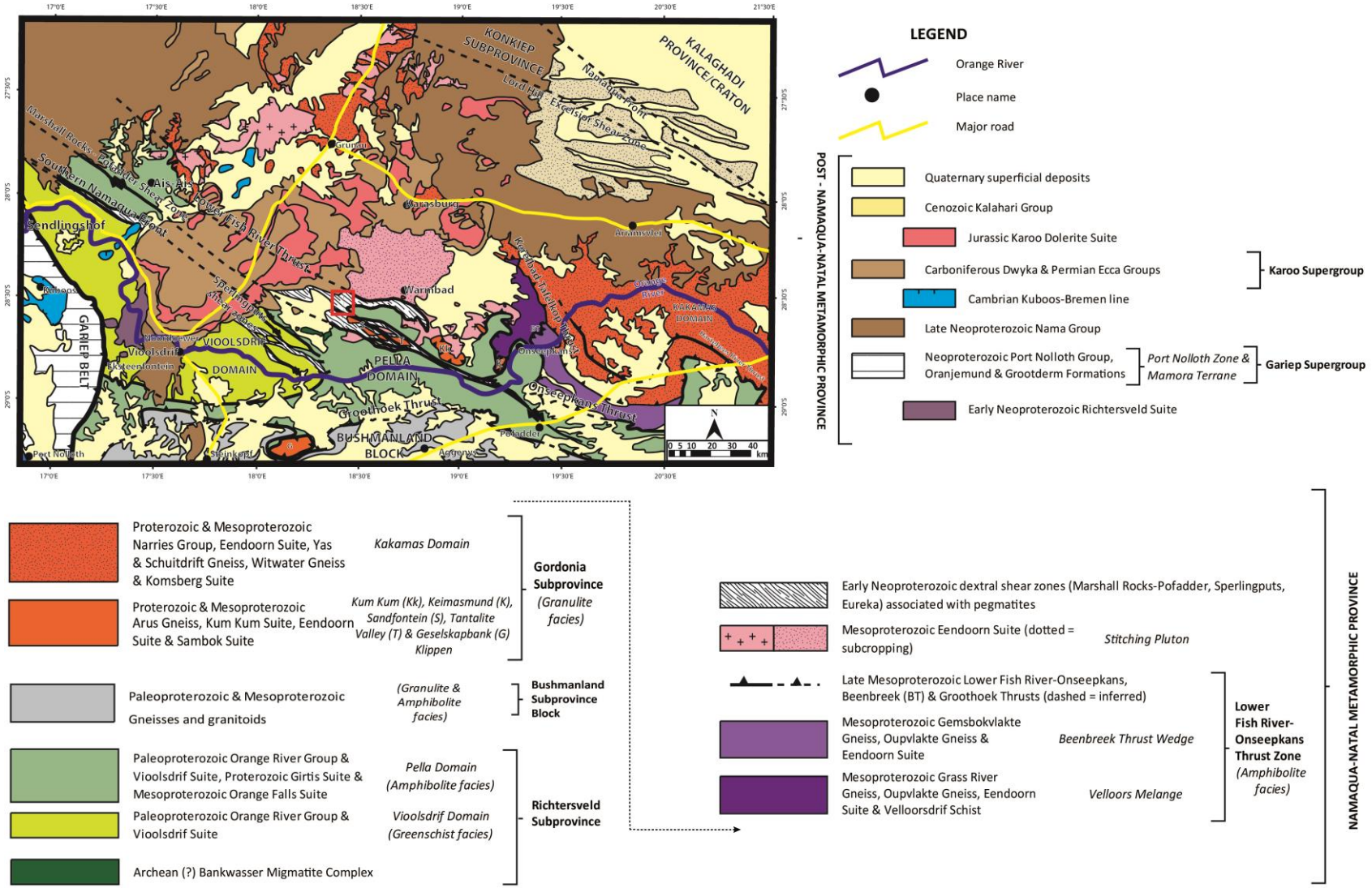

Figure 2-2: Tectonic architecture of the Namaqua sector in the border region (international boundary marked by the Orange River) between Namibia and South Africa. Map taken from Macey et al, 2015 Red box=Study area.

Stellenbosch University https://scholar.sun.ac.za

2.2.2 **The Richtersveld Subprovince**

The Paleoproterozoic Richtersveld Subprovince is an east-west trending, thrust-bounded, ~200 km long tectonic wedge within the Namaqua sector (Colliston et al., 2008; Cornell and Pettersson, 2007; Cornell et al., 2009; Macey et al., 2015; Minnaar, 2012; Reid, 1997; Reid et al., 1987). In the east, the Richtersveld Subprovince is separated from the Gordonia Subprovince by the LFROTZ (Blignault, 1977; Colliston and Schoch, 2013, 2002, 2000; Macey et al., 2015; Minnaar, 2012). In the south, the Richtersveld Subprovince is bounded by the Groothoek Thrust along which the Richtersveld Subprovince was emplaced southward onto the Bushmanland Subprovince (Colliston and Schoch, 2002, 2000; Colliston et al., 2008; Cornell et al., 2006; Hartnady et al., 1985; Joubert, 1986; Macey et al., 2015; Minnaar, 2012; Thomas et al., 1994) (Figure 2-1 and Figure 2-2). In the west, the Richtersveld Subprovince extends to the tectonic boundary with the Pan-African Gariep Belt (Miller, 2008). The rocks of the Richtersveld Subprovince are subdivided into two domains; 1) the greenschist facies Vioolsdrift Domain in the southwest and 2) the amphibolite facies Pella Domain in the south and northeast (Figure 2-2) (Colliston and Schoch, 2013, 2002, 2000; Macey et al., 2015; Miller, 2008; Minnaar, 2012; Reid, 1997; Thomas et al., 1994). The Vioolsdrift and Pella domains are separated by the Southern Namaqua Front, which marks the transition in metamorphic grade from low-grade greenschist facies in the former and to higher-grade amphibolite facies grade in the latter (Blignault, 1977; Blignault et al., 1983).

2.2.2.1 Vioolsdrift Domain

The Vioolsdrift Domain is characterized by greenshist facies volcano-sedimentary rocks (~1900-1850Ma) of the Orange River Group (Hartnady et al., 1985; Macey et al., 2015) (Figure 2-2). Furthermore, the domain is intruded by undeformed, juvenile, calc-alkaline granitoids of the Vioosldrift Suite (1900-1830 Ma) (Blignault, 1977; Macey et al., 2015; Minnaar, 2012; Nordin, 2009; Reid and Barton, 1983; Reid, 1997; Samskog, 2009) (Figure 2-2).The prominent fabric recorded in this domain is a planar S_1 foliation within the Orange River Group rocks that is associated with the Paleoproterozoic D_1 greenschist facies deformation of the Orange River Orogeny (Blignault, 1977; Joubert, 1986; Macey et al., 2015). The timing of D_1 deformation is constrained at ~1.9-1.85 Ga (Blignault, 1977; Blignault et al., 1983; Macey et al., 2015; Minnaar, 2012). The Vioolsdrift Domain largely represents rocks that escaped the main penetrative deformation and metamorphism related to the ~1210-1050 Ma D_2 Namaqua Orogeny (Blignault et al., 1983; Hartnady et al., 1985; Joubert, 1986; Macey et al., 2015; Minnaar, 2012; Reid, 1997).

2.2.2.2 Pella Domain

The Pella Domain also hosts Paleoproterozoic volcanic and volcano-sedimentary rocks of the Orange River Group (2.0-1.87 Ga) (Blignault, 1977; Blignault et al., 1983; Macey et al., 2015) (Figure 2-2). Rocks of the Orange River Group are considered to be the supracrustal foundation into which volcanic arc rocks of the Vioolsdrif Suite intruded (Blignault, 1977; Blignault et al., 1983; Macey et al., 2015; Minnaar, 2012; Reid, 1997). Macey et al., (2015) recognize three lithodemic units of the Orange River Group within the Pella Domain; Guadom, Gaidip and Umeis Gneisses. The Guadom (meta-andesite) and Gaidip gneisses (meta-rhyolite) have a dominant meta-volcanic component and are situated south of the MRPSZ, whereas the migmatitic quartz -feldspar-biotite Umeis gneiss has a higher supercrustal component and is

Stellenbosch University https://scholar.sun.ac.za

confined to the MRPSZ and the area to the north of it (Macey et al., 2015). The rocks of the Pella Domain comprise similar stratigraphic units to those of the Vioolsdrift Domain. However, in the Pella Domain both the Orange River Group and Vioolsdrift suite rocks were strongly deformed and metamorphosed at amphibolite facies grade during D_2 Namaqua Orogeny and contain a penetrative S_2 gneissic foliation and L_2 lineation (Blignault, 1977; Blignault et al., 1983; Joubert, 1986; Macey et al., 2015).

2.2.3 **Gordonia Subprovince**

The Gordonia Subprovince incorporates Mesoproterozoic high grade (upper amphibolite to granulite facies) gneisses and granitoids (Cornell and Pettersson, 2007) rocks of the Kakamas Domain (Hartnady et al., 1985; Macey et al., 2015), Grünau Terrane/Sequence (Blignault et al., 1983; Toogood, 1976) and the Areachab Terrane (Cornell et al., 2006; Eglington, 2006; Macey et al., 2015; Miller, 2008; Moen and Toogood, 2007; Thomas et al., 1994) that are separated from the Richtersveld Subprovince by the LFROTZ (Figure 2-1 and Figure 2-2). In the study area, the Gordonia Subprovince is preserved as a stack of southwest-vergent thrust sheets and nappes (Becker et al., 2006; Macey et al., 2015) comprised of high-grade supracrustal gneisses and intrusive rocks of the Kakamas Domain (Becker et al., 2006; Macey et al., 2015; Thomas et al., 1994), which were thrust over the Paleoproterozoic Richtersveld Subprovince along the LFROTZ (Becker et al., 2006; Colliston and Schoch, 2013, 2000; Macey et al., 2015; Miller, 2008) (Figure 2-2). The high-grade metamorphic and intrusive rocks of the Gordonia Subprovince were most likely derived, or at least are part of a pre-existing older crust of the Richtersveld Subprovince and Areachab Terrane (Cornell et al., 2012; Macey et al., 2015) (Figure 2-1). These rocks have undergone multiple phases of tectonic reworking including: 1) high-grade metamorphism and intense plutonism during the mid-Mesoproterozoic (Bailie et al., 2011; Bial et al., 2015a; Cornell and Pettersson, 2007; Cornell et al., 2012; Macey et al., 2015; Pettersson, 2008); and 2) imbricated thrusting during the mid- to late-Mesoproterozoic D_2 Namaqua Orogeny (Macey et al., 2015). Some of the rocks of the Gordonia Subprovince in the vicinity of the study area are preserved as tectonic outliers overlying the Pella Domain of the Richtersveld Subprovince (Macey et al., 2015). Several tectonic outliers are identified and grouped into a number of klippen, i.e. Sandfontein, Kum Kum and Keimasmund (Macey et al., 2015) (Figure 2-2).

2.3 LATE D_4 SHEARING IN THE NAMAQUA SECTOR

The terminal phase of the Namaqua Orogeny was followed by an unroofing (exhumation) stage (1050 Ma), which led to the cooling of the Namaqua sector rocks to temperatures below ca. 350 °C by ca 950 Ma (Eglington, 2006). This unroofing stage was accompanied by the development and/or reactivation of a series of brittle-ductile, dextral, NW-SE trending shear zones (Figure 2-3) (Coward and Potgieter, 1983; Humphreys and Van Bever Donker, 1987; Jacobs et al., 1993; Maclaren, 1984; Moen and Toogood, 2007; Thomas et al., 1994). The subject of the origin of these shear zones is poorly documented but the geometry and sense of movement on these shear zones are believed to have developed due to the local geometry of the SW margin of the Kaapvaal craton accompanied a SW directed indentor compressional regime (Jacobs et al., 1993; Thomas et al., 1994).

Stellenbosch University https://scholar.sun.ac.za

In the study area, D_4 deformation resulted in the development of three ductile dextral NW-SE-trending shear zones; the Marshall Rocks-Pofadder Shear Zone, the Eureka Shear Zone and the Sperlingsputs Shear Zone (Colliston and Schoch, 2013, 2002, 2000; Lambert, 2013; Macey et al., 2015; Miller, 2008) (Figure 2-3). Most of the previous work done on D_4 focused on the MRPSZ (e.g Colliston and Schoch, 2013; Joubert, 1986; Lambert, 2013; Macey et al., 2015; Melosh et al., 2014; Miller, 2008; Toogood, 1976), mainly because it is the largest and most well exposed in the Namaqua sector and it surrounds the Tantalite valley massif complex mineralised with columbite-tantalite, beryl, rare earth and lithium minerals (Beukes, 1973; Moore, 1981). This research study area falls within a region affected by both the MRPSZ and ESZ and will mainly focus on the D_4 structural imprints imposed by the two shear zones. As the Sperlingsputs Shear Zone lies outside the scope of this study, only a very brief summarly will be given.

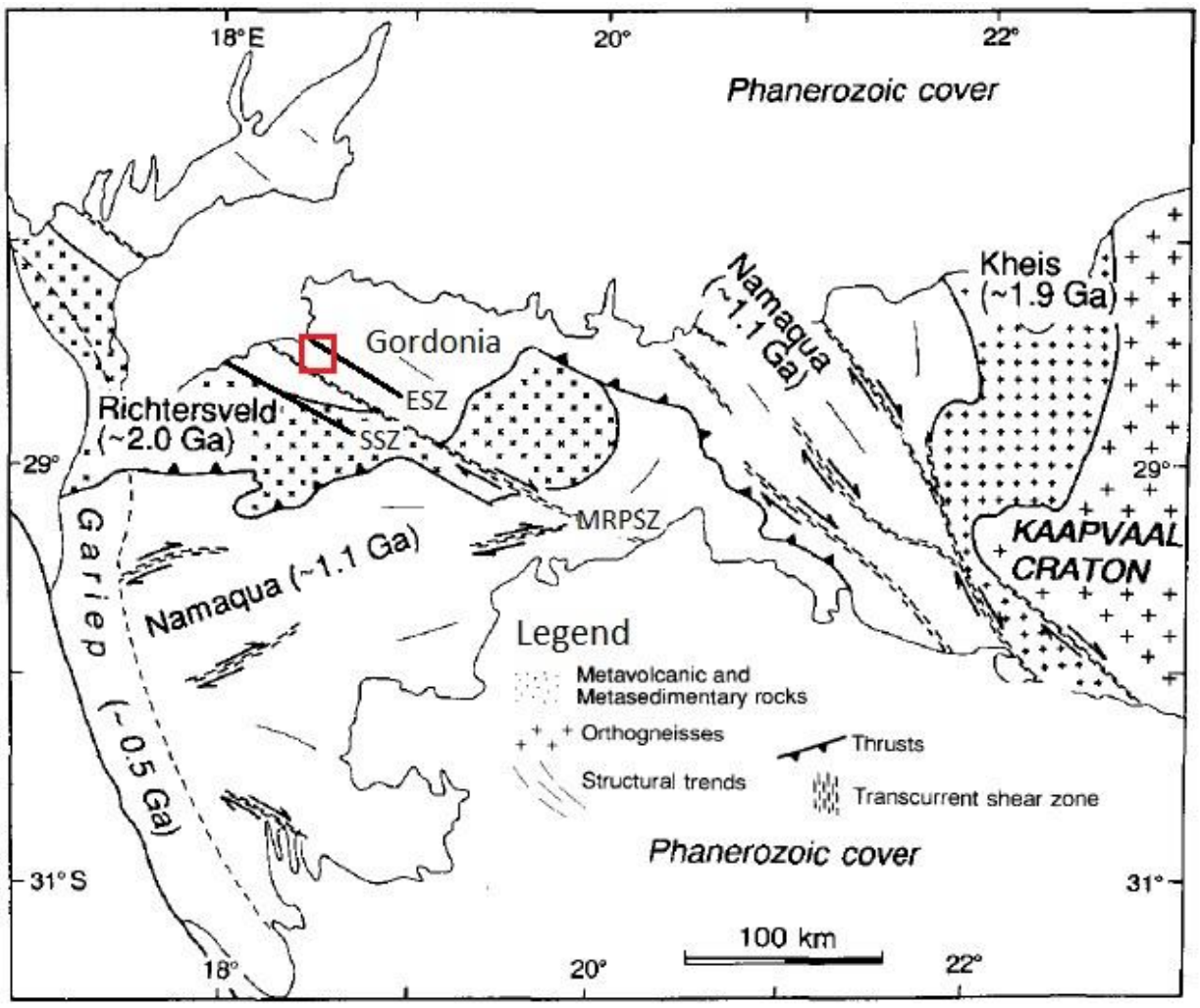

Figure 2-3: Simplified tectonostratigraphic subdivision of the Namaqua sector of the NNMP (Modified after Jacobs et al., (1993); after Joubert, (1986)). Showing positions of major thrust zones and shear zones. ESZ=Eureka Shear Zone, MRPSZ= Marshall Rocks-Pofadder Shear Zone, SSZ=Sperlingsputs Shear Zone. Red box=Study Area.

Stellenbosch University https://scholar.sun.ac.za

2.3.1 **Marshall Rocks-Pofadder Shear Zone.**

The MRPSZ forms a WNW-trending, ~500 km long (Joubert, 1986; Miller, 2008; Moen and Toogood, 2007; Moore, 1981) and up to 10-km wide dextral shear zone (Lambert, 2013; Macey et al., 2015) that extends across most of southern Namibia and terminate near Pofadder in South Africa (Joubert, 1986; Macey et al., 2015; Melosh et al., 2014; Miller, 2008; Moore, 1981; Toogood, 1976) (Figure 2-1, Figure 2-2 and Figure 2-3). It is defined by a steep, north-east dipping 1 to 7 km wide mylonitic core (along with cataclasites and fault beccias) domain and associated with up to 10 km wide zone of apparent dextral drag folding of the wall rocks into the core of the shear zone (Lambert, 2013; Macey et al., 2015; Miller, 2008). The kinematics on the MRPSZ resemble a dextral shear sense dominated by wrench-faultings (Colliston and Schoch, 2013; Lambert, 2013; Macey et al., 2015). Recent work done on the MRPSZ recognizes four deformation episodes subdivisions (D_{4a}, D_{4b}, D_{4c} and D_{4d}) that occurred and overlap in time during progressive deformation D_4 (Colliston and Schoch, 2013; Lambert, 2013; Macey et al., 2015). These four deformation episodes are described below.

The deformation episode **D_{4a}** is defined by an early ductile rotation and folding of the pre-existing planar and linear fabrics (forming composite S_2/S_4 and L_2/L_4) of the gneissic wall rocks into the shear zone at mid-amphibolite facies grade (Lambert, 2013; Macey et al., 2015). It is also accompanied by the development of new (S_{4a}/L_{4a}) fabrics (Lambert, 2013). The brittle-ductile deformation episode **D_{4b}** is characterized by the development of a penetrative planes S_{4b} (NW-SE striking) and linear (L_{4b}) fabrics that overprints D_2, D_3 and D_{4a} fabrics, and it is accompanied by retrogression from amphibolite to greenschist facies grade (Lambert, 2013). D_{4b} is confined to the core zone of the MRPSZ and is thought to have been responsible for the development of mylonitic and cataclasitic textures in the shear zone host rocks (Lambert, 2013; Macey et al., 2015). Lambert (2013) considered D_{4b} to be due to late localisation, retrogression and strain incrimination into the core of the shear zone. The deformation episode **D_{4c}** is restricted to the SE terminous of the MRPSZ and is characterized by a localized high-strain deformation along a narrow 1-30 m wide discrete shear zones. These discrete shear zones are associated with mylonite and ultramylonite in sharp contact with the surrounding wall rocks (Macey et al., 2015). This deformation is oblique, cross-cuts and offsets the earlier D_{4a} and D_{4b} structures at an angle of ~10° (Macey et al., 2015). The deformation episode **D_{4d}** is associated with the cm-scale development of brittle breccias domains within the ultramylonites that were formed during D_{4c} (Macey et al., 2015). It is anticipated to have occurred due to brittle-faulting during the terminal phase of the MRPSZ at ~960 Ma (Lambert, 2013; Macey et al., 2015). The late D_4 fault breccias within the core zone were studied by Melosh et al., (2014) who suggested a sesimic slip under brittle-plastic deformation and linked with sismic activity from earthquakes of a magnitude between 2.8- 5.8 Mw with a rupture length of 0.023-3.3 km. The folding event **F_4** is presumed to have occurred through the progressive deformation (D_{4a} to D_{4b}) in the MRPSZ. Essentially, F_4 developed new folds but also conveyed and re-oriented earlier F_2 and F_3 in the adjacent gneissic wall rocks into the shear zone. Folding F_4 is preserved as tight isoclinal folds associated with an axial planar S_{4a} fabric; in places it is truncated by discrete small-scale S_{4b} shears (Lambert, 2013; Macey et al., 2015). The timing of D_4 deformation along the MRPSZ is constrained by syn-tectonic to late pegmatites dated between 1005 and 958 Ma (Lambert, 2013).

Stellenbosch University https://scholar.sun.ac.za

2.3.2 The Eureka Shear Zone

The Eureka Shear Zone (ESZ) was first documented by Macey et al. (2015), while conducting regional mapping and research in southern Namibia. Macey et al. (2015) described the Eureka Shear Zone as a 5 km wide and 50 km-long, WNW-trending, dextral, brittle-ductile, tectonic melange of early Neoproterozoic age (Figure 2-2 and Figure 2-3). The ESZ is shearing rocks from both the Richtersveld and Gordonia subprovinces and probably strongly reworking the pre-existing LFROTZ (Macey et al., 2015). One of the main problems associated with the ESZ and most of the surrounding study area is poor outcrop exposures. This has led to a lot of confusion among the previous worker (e.g. Beukes, 1973; Blignault et al., 1983; Colliston and Schoch, 2000; Miller, 2008; Moen and Toogood, 2007) on the lateral extent and geometry of both the MRPSZ and LFROT in the area west of the Tantalite valley massif complex. For example; work done by Blignault et al., (1983) and Colliston and Schoch, (2000) suggest that present tectono-stratigraphic position of the ESZ coincides with the lithological boundaries between the Orange river sequence (correlated to Pella Domain) and Grünau terrane (Kakamas Domain) (Blignault et al., 1983). This boundary is interpreted to be associated the LFROT (Colliston and Schoch, 2013, 2000; Macey et al., 2015; Moen and Toogood, 2007). However, Miller, (2008) inferred the LFROT to extend south of the MRPSZ and joins it with the Southern Namaqua Front (also; Sperlingputs Shear Zone(Macey et al., 2015). In the study area, majority of the rocks units are strongly sheared by both the ESZ and MRPSZ to a degree that the boundaries between the two shear zones are not well defined. The stratigraphic sequence and protolith of the rocks units exploited by the D_4 shearing is not clear. Therefore, this study will mainly focus on the D_4 imprints in the ESZ and will attempt to resolve some of the issues.

2.3.3 Sperlingsputs Shear Zone

The Sperlingsputs Shear Zone occurs as a set of parallel NW-trending mylonitic shear zones that anastomase around more rigid granite bodies in the eastern part of the Vioolsdrift Domain of the Richtersveld Subprovince (Figure 2-2 and Figure 2-3). Five main shear zones are recognised including the northeastern reworking of the Namaqua Front separating the Viooldrift Domain and Pella Domain of the Richtersveld Subprovince (Blignault, 1977; Macey et al., 2015). The Sperlingsputs Shear Zones is considered as one of the D_4 Namaqua shears based on orientation, grade and association with foliation subparallel syn-shearing pegmatites similar to those found in the MRPSZ and ESZ.

Stellenbosch University https://scholar.sun.ac.za

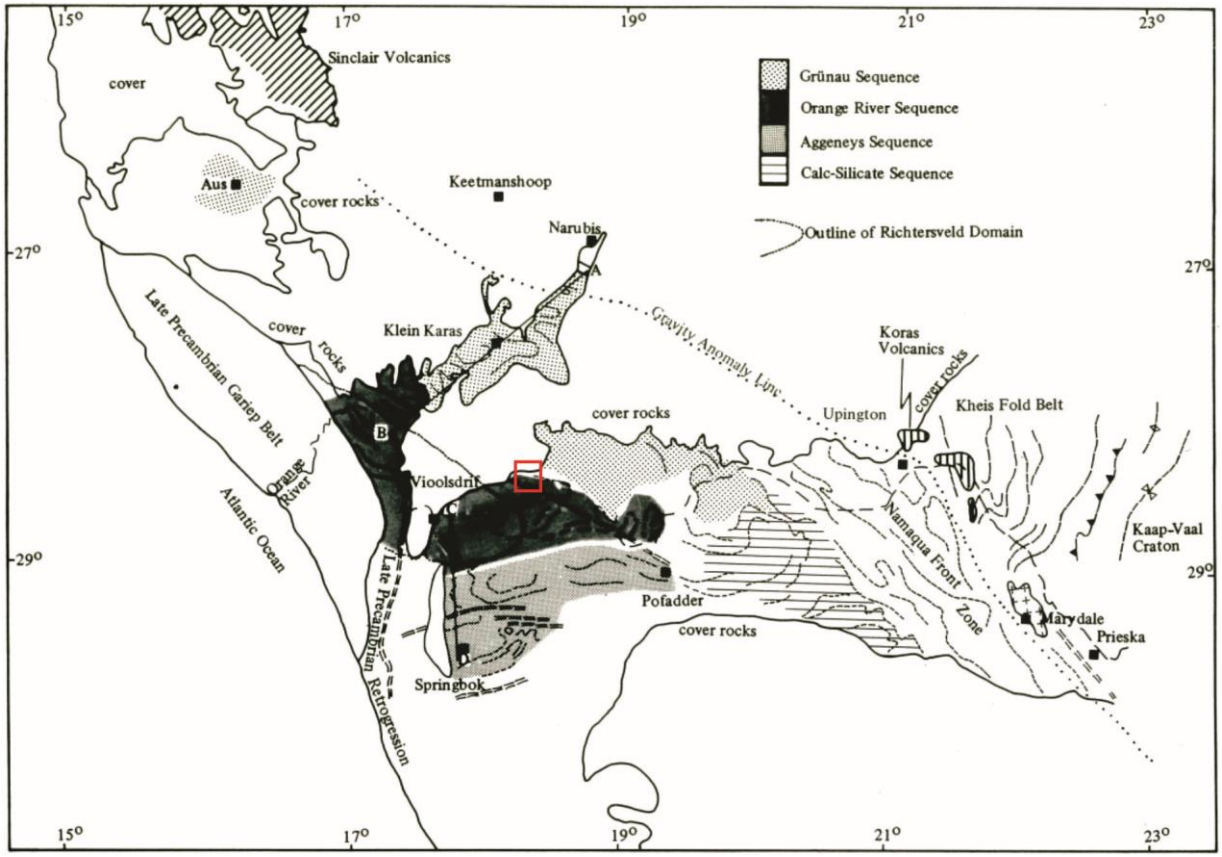

Figure 2-4: Tectonostratigraphic maps of the Namaqua sector of the NNMP. Showing the position of Blignault et al., (1983) *lithological boundaries between Orange River sequence (Pella Domin of the Richtersveld Subprovince) and Grünau Terrane (Kakamas Domain of the Gordonia Subprovince).*

2.4 PREVIOUS LITHOSTRATIGRAPHIC FRAMEWORK OF THE EUREKA SHEAR ZONE AND SURROUNDING AREAS

Beukes (1973) was the first worker to map the area at 1:100000 scale as part of the PhD research. The work of Beukes (1973) recognize the presence of six lithological units, namely Umeis formation, Arus Formation, Eendoorn granite, mafics and ultramafic intrusive rocks, Warmbad granite and pegmatites (Table 2-2). Blignault et al. (1983) of which Beukes was a senior author recognised two major sequences: the Grünau sequence and the Orange River sequence (Figure 2-4 and Table 2-2). The Grünau sequence is comprised of high aluminous metashale/wacke succession (Arus formation) and the Orange River sequence is made up of a volcanic sequence (Blignault et al., 1983). The contact between the two sequences is complex and Blignault et al. (1983) described this boundary to be "*interbanded on the wide scale that the tectonic interbanding seems improbable*". The joint mapping project between the Geological Survey of Namibia and Council for Geoscience, South Africa mapped the area adjacent to the current study area in the year 2013 to 2015. The mapping redefined and subdivided the stratigraphy of the Umeis formation (Orange River sequence) into the Pella domain (comprised of Umeis gneiss and Guadom gneiss), Eureka complex and Ouplvakte Complex (Figure 2-2 and Table 2-2). The mapping also redefined intrusive rocks such as the Eendoorn granite into the Eendoorn suite and mafic-ultramafic rocks as Kum Kum Suite (Figure 2-2 and Table 2-2).

Stellenbosch University https://scholar.sun.ac.za

Table 2-2: Summary of the previous and present lithostratigraphy framework of the study area

Beukes (1973)	**Blignault et al. (1983)**	**Macey et al. (2015)**			**Rock types**
		Domain		**Age**	
Pegmatites		Post-juxtapositing, syn D4	Pegmatites	~1000Ma	Sheared and unsheared pegmatites
Warmbad Granite			Warmbad Suite	?	Biotite-muscovite alkali leucogranite
Mafic and ultramafic intrusive rocks			Kum Kum Suite	~1200Ma	Metagabbro and metagabbronorite
Eendoorn Granite			Eendoorn Suite		K-feldspar-biotite porphyritic/porphyroclastic granodiorite gneiss
Arus Formation	GRUNAU SEQUENCE	Kakamas	Arus Gneiss/Narries Group	~1210 Ma	Restitic sillimanite-K-felsdspar-garnet-cordierite granulitic pelite
Umeis Formation	ORANGE RIVER SEQUENCE	?	Eureka Complex	?	Undefined
		LFROTZ	Oupvlakte Complex	1215 Ma	Sheared amphibolite and mafic granulite
		Pella	Umeis Gneiss / ORANGE RIVER GROUP	~1900Ma	Heterogeneous interlayered package of gneisses dominated by biotite-honblende porphyroblastic gneiss
			Guadom Gneiss / ORANGE RIVER GROUP		Heterogeneous interlayered package of gneisses dominated by migmatitic hornblende-biotite-quartz-feldspar gneiss

Despite of previous work done in the study area, there is still a need for detailed research on the ESZ in order clarify the nature of the shear zone and its tectonic boundary. These can be achieved by studying and understanding the structure and lithostratigraphy of the ESZ and the surrounding area. Therefore, this research will employ detailed geological mapping and geochrology studies to study the structure of the ESZ and its associated rock units. These aspects will in turn help in clearing up whether there is link between the ESZ, MRPSZ and LFROTZ and how the three evolved within the Namaqua Sector of NNMP.

Stellenbosch University https://scholar.sun.ac.za

CHAPTER 3: LITHOLOGICAL FRAMEWORK

3.1 INTRODUCTION

The study area covers an area of ~960 km^2 (Appendix B) and topographically characterized by narrow hills of moderate to low outcrop exposure that are separated by a Cenozoic sediment cover flood plains (Appendix B). Mapping was conducted at a scale of 1:50 000 scale and a detailed geological map is provided as Appendix B. In order to get the overall coverage of the ESZ and the distribution of the major rock types of the study area; a simplified map (Figure 3-1) was created using data collected from this study and those of the previous mappers. The rocks of the study area are dominantly sheared and hosted within the Eureka Shear Zone (ESZ), Marshall Rocks-Pofadder Shear Zone (MRPSZ) and the area between the two (Figure 3-1 and Appendix B). The strong fabrics and poor outcrop exposure across the mapping area made it difficult to differentiate the boundaries between the MRPSZ and ESZ with absolute certainty (Figure 3-1 and Appendix B). However, this study inferred most of the northern region of the study area to mark ESZ (Figure 3-1) and the southern region of the study area to represent the zone affected by the MRPSZ (Figure 3-1). The two shear zones are separated by another zone of intense shearing referred to as an Intermediate domain (Figure 3-1). To clarify the structure of the study area these this study subdivided the area into three structural domains (ESZ, MRPSZ and Intermediate domain) (Figure 3-1) based on the occurrence of distinctive litho-tectonic units and orientation of fabrics (discussed in more details in Chapter 5 and 6).

Majority of the rocks in the study area are intensely folded and, in places, sheared so strongly that their protolith cannot be identified easily. Strong fabrics, discrete shear zones cross-cutting these rocks and poor outcrop exposure also made it difficult to determine the contact relationships between the different rock types (Figure 3-1 and Appendix B). Furthermore, linking weakly deformed rocks to their strongly deformed variety within the study has been difficult. To overcome some of these matters, this study mapped and grouped different rock types that cannot be mapped out separately at a scale of 1: 50000 as large lithotectonic rock packages (Figure 3-1 and Appendix B, MQ and EC lithotectonic packages). Petrographic sections were collected from both strongy and weakly deformed domains in order to link strongly sheared rock types to their respective to unsheared states. Field and petrographic section descriptions of major rock units are described in this chapter and are later correlated to those documented by the previous worker (discussed in Chapter 6). A summary of the major rock types are shown in Table 3.1 and the overall distribution of the fundamental rock types of the area are discussed as following.

Field mapping has identified that the area is comprised of a variety of supracrustal rocks and intrusive rocks. These rocks hosted as large litho-tectonic units bounded and truncated by NW-SE striking shear zones (Figure 3-1 and Appendix B). The Fundamental litho-tectonic units in the study area are identified as; migmatitic banded gneiss, Eureka complex (EC) and interlayered amphibolite and quartzo-feldspathic gneiss (MQ). The three units are found in association and in some localities intruded by mesocratic

Stellenbosch University https://scholar.sun.ac.za

porphyritic granite, leucocratic equigranular granite and pegmatites (Table 3-1). The summary of the major rock types of the study area and their map codes are shown in Table 3-1.

Table 3-1: Summary of the major rock types of the study area and their respective map codes.

Fundamental litho-tectonic units	**Associated rock types**
Migmatitic banded gneiss (MU,MU2 & MUp)	Quartz-biotite gneiss Quartz-feldspar gneiss Amphibolite Hornblende-biotite-quartz-feldspar gneiss
Interlayered quartzo-feldspahic gneiss and amphibolite (MQ)	Quartzo-feldspathic gneiss
	Amphibolites
Eureka Complex (EC & ECp)	Eureka grey gneiss
	Restitic granulitic pelites
Other major rock types	
Mesocratic porphyritic granite (MgEd1, MgEd2 & MgEd)	
Leucocratic equigranular granite (NgWb, NgWbs & Wb=dykes)	± leucocratic porphyritic granite
Pegmatites (Npe & p=dykes)	

The supracrustal rocks identified in the study area are (1) migmatitic banded gneiss, a migmatitic heterogeneous rock dominated by interlayering quartz-biotite gneiss, amphibolite, quartz feldspar gneiss and quartz-biotite ± hornblende gneiss (contains interlayering supracrustal and volcaniclasti layers) (Appendix B) and (2) the Eureka grey gneiss; a heterogeneous garnet-quartz-feldspar gneiss (dominantly restitic) found incorporating and closely associated with remnant resititic granulitic pelites (Appendix B). The Eureka grey gneiss and resititic granulitic pelites in the ESZ could not be mapped out separately at a scale of 1:50 000 and hence, are grouped together to form the Eureka Complex (EC) (Appendix B). Rocks of the EC are differentiated from the migmatitic banded gneiss by being restricted to the ESZ (northern part of the study area), closely associated with resititic granulitic pelites and lacking amphibolites. The migmatitic banded gneiss are restricted to the region south of the ESZ and within the MRPSZ (Appendix B).

The EC package and the margin of the migmatitic banded gneiss is intruded by an interlayered amphibolite and quartzo-feldspathic gneiss (MQ) package (Appendix B). The MQ package is comprised of outcrop scale interlayered amphibolites and quartzo-feldspathic gneiss that occurs as several distinct sigmoidal wedges. The MQ package appears to be restricted to the ESZ and marks the southern margin of it (Figure 3-1 and Appendix B). All three mentioned rock packages are commonly found strongly sheared and are intruded by a number of variably sheared megacrystic granite, amphibolite dykes, leucocratic equigranular granite, pegmatites and quartz veins. Metagabbro and restitic granulitic pelites are also locally present (Appendix B). Detailed descriptions of the major rock types within the study area are provided as following (section 3.2).

Stellenbosch University https://scholar.sun.ac.za

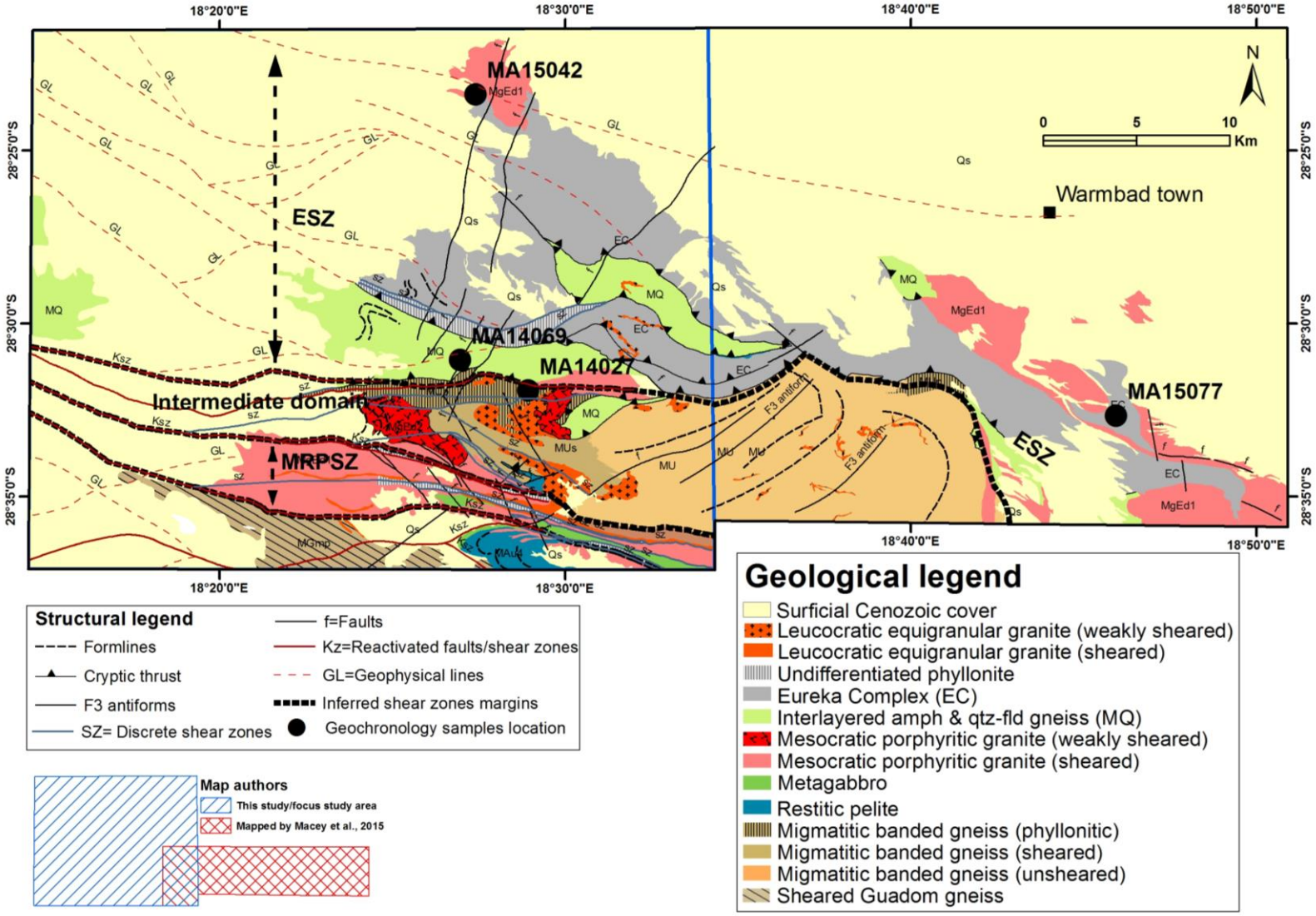

Figure 3-1: Simplified geological map of the ESZ, MRPSZ and surrounding area. The focus study area covers the ESZ and MRPSZ (blue box). A detailed geological map is provided as Appendix B.

Stellenbosch University https://scholar.sun.ac.za

3.2 PETROGRAPHIC DESCRIPTION OF MAJOR ROCKS UNITS

3.2.1 **Migmatitic Banded Gneiss**

The migmatitic banded gneiss occurs mainly in the central and southeastern part of the study area (Figure 3-1 and Appendix B). The unit is very heterogeneous and usually comprises interlayered thin bands (up to 10 mm thick) consisting of both leucosome (quartz-feldspar gneiss) and mesosome to melanosome (amphibolite and quartz-biotite ± hornblende gneiss) (Figure 3-2a and Figure 3-2b). In a few localities the rock found associated with thick amphibolite boudins (Figure 3-2a; top right). Individual interbanded layers recognised in the banded gneiss are hornblende-biotite-quartz-feldspar gneiss, biotite-quartz-feldspar± garnet gneiss, quartz-biotite gneiss and amphibolite. The rock is usually highly deformed, strongly foliated and folded, with various scales of wavy kink asymmetrical folds and crenulation cleavage on the foliation surface (Figure 3-2c and Figure 3-2d).

At meso-scale, the rock weathers reddish-brown with a lustrous leathery surface (Figure 3-2d). When fresh, the rock is melanocratic, fine- to medium-grained (overall grainsize less than 3 mm) and has a gneissic to schistose texture. In petrographic section, the rock is composed of quartz (~35-40%), biotite (~25%), plagioclase (20-15%), microcline (~10%) and garnet (~3%) (Figure 3-2e and Figure 3-2d). Muscovite is replacing biotite and plagioclase has been altered to sericite. Garnet and andalusite locally occur as porphyroblasts and distributed as thin layers within the matrix of the quartz biotite ± hornblende gneiss. Accessory minerals are sphene, zircon and unidentified opaque minerals. Quartz occurs as sub-grains and elongated subparallel recrystallized crystals (Figure 3-2e). The dominant fabric in the rock is defined by sub-parallel alignment of elongated biotite and muscovite. Crenulation cleavage is weakly developed and defined by micro-folds of biotite and muscovite (Figure 3-2e and Figure 3-2f). Field observation suggest that the heterogeneous migmatitic banded gneiss package contains some layers that appears to be of igneous origins such as: quartz-feldspar gneiss, amphibolite and quartz-biotite ± hornblende gneiss. Biotite-quartz-feldspar ± garnet gneiss layer are usually found associated with aluminosilicate minerals (such as garnet and andalusite) and appears to be supracrustal.

Stellenbosch University https://scholar.sun.ac.za

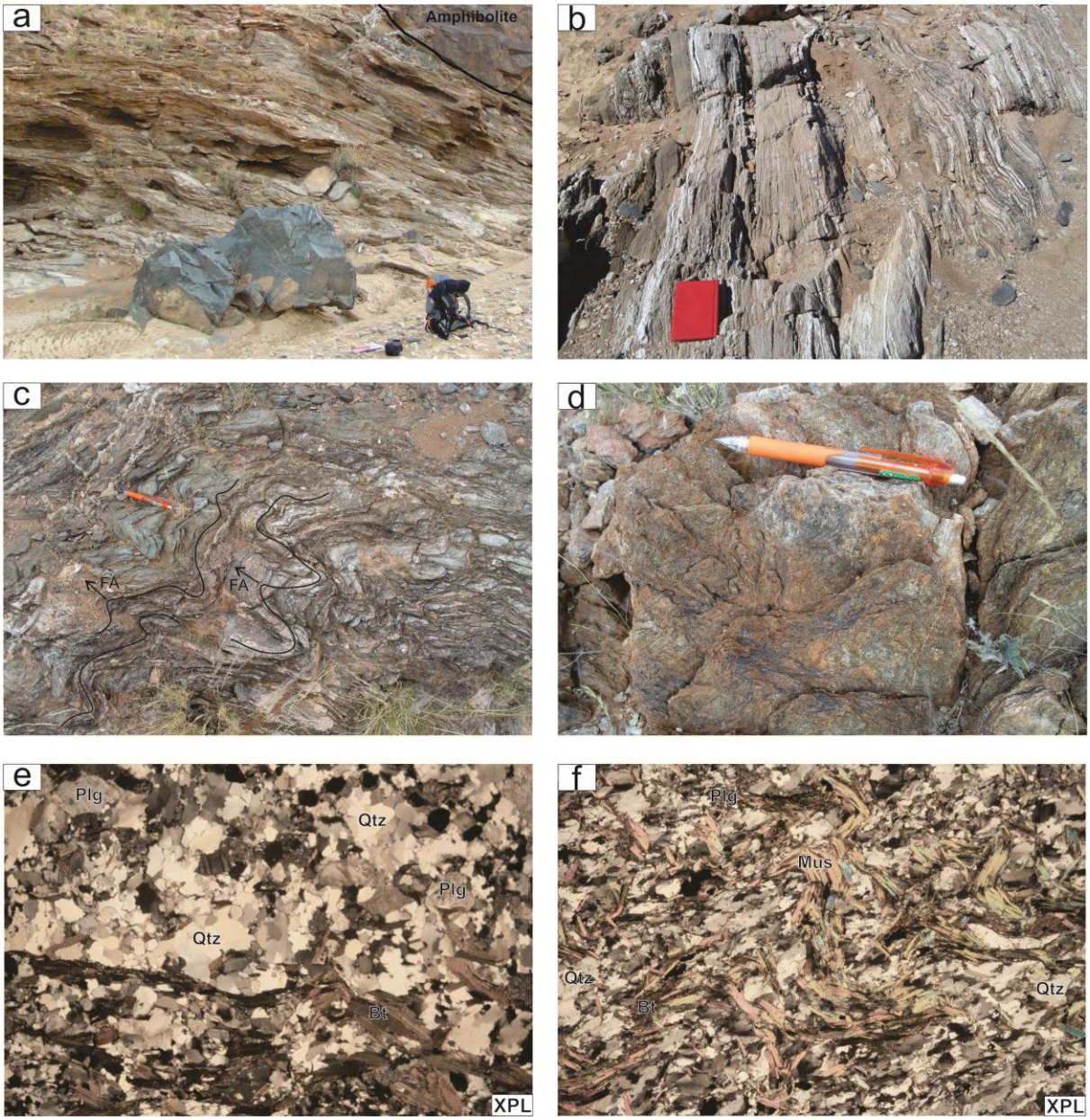

Figure 3-2: a) Outcrop pictures and photomicrograph of the migmatitic banded gneiss. (a) Thin heterogeneous compositional banding layering associated with thick amphibolite boudin (top right). (b) Riverbed pavement showing centimetre scale inter-banding of quart-biotite gneiss, amphibolite, quartz feldspar gneiss and pegmatites of a strongly sheared migmatitic banded gneiss. (c) Parasitic intrafolial folds with moderately plunging fold axial plane (FA). The rock slightly brecciated and dominated by a series of quartz plunged veins. (d) Weakly developed crenulation cleavage on the foliation surface. (e) Photomicrograph (FOV=4.5mm), showing thin elongated and folded biotite (Bt) resting in the matrix of quartz (Qtz) and sericitized plagioclase (Plg). Quartz has irregular shaped grain boundaries. (f) Photomicrograph (FOV=4.5mm), crenulation cleavage of biotite deformed into asymmetric microfolds separated by recrystallized quartz. FOV = Field of view. XPL=Cross polarised light.

Stellenbosch University https://scholar.sun.ac.za

3.2.2 **Interlayered Amphibolite and Quartzo-Feldspathic Gneiss (MQ)**

The interlayered amphibolite and quartzo-feldspathic gneiss occurs as a distinctive mafic (65%)-felsic (35%) interlayered rock package within the central part of the study area (Figure 3-1 and Appendix B). Both units are usually sheared, folded, probably intrusive and cannot be mapped out separately in the field (Figure 3-3a and Figure 3-3b). The largest outcrop of the MQ is a ~15 km long and ~3 km wide wedge in the central part of the study area (Appendix B). Other smaller sigmoidal shaped outcrops of this unit were also mapped across the ESZ and within the EC (Appendix B). The thickness of the amphibolite and quartzo-feldspathic gneiss layers within the package varies in a range of ~10^{th} cm to ~2 m across the area (Figure 3-3a and Figure 3-3b). In strongly foliated domains, the lithological contrast is high and the individual bands have a thickness of ~5 to 50 cm.

3.2.2.1 Amphibolite

Amphibolite is the dominant unit within the MQ package and makes up approximately 65% of the total mafic-felsic package (Figure 3-3a). The amphibolites are fine- to medium-grained (overall grain size less than 1.5 mm) (Figure 3-3c). The mineralogical composition is hornblende (~60-65%), sericitized plagioclase (~30%), chlorite (~5%) and quartz (~<5%). Accessory minerals in the rock are sphene and epidote. The majority of the minerals are anhedral, with irregular inequigranular polygonal grain boundaries (Figure 3-3d). Quartz is recrystallized as elongate grains and has strong undulose extinction (Figure 3-3d). Hornblende occurs as brown (dominantly) to pale green elongated grains and have a preferred orientation that is defining a strong fabric within the rock. Majority of the minerals are distributed in a groundmass of sericitized plagioclase and hence, defining a nematoblastic texture in the rock (Figure 3-3d).

3.2.2.2 Quartzo-feldspathic gneiss

The leucocratic quartzo-feldspathic gneiss is fine- to medium-grained (overall grain size in the range of; ~0.5-1.0 mm) (Figure 3-3e) and composed of plagioclase (~30%), quartz (~25-30%), microcline (~20%) and biotite (15%) (Figure 3-3f). The majority of the plagioclase is replaced by sericite and biotite fish are interweaved between relict grains of quartz and microcline. Biotite is occasionally replaced by chlorite. Quartz is recrystallized, occur as elongate grains and sub-grains within the matrix (quartz microstructures are discussed in more details in chapter 5). The rock has a poikiloblastic texture defined by coarser-grained recrystallized quartz and potassium feldspar within a groundmass of sericitized plagioclase. Microclines have a sub-rounded to angular grain shapes. The fabric mostly is defined by sub-parallel mineral elongation of quartz and biotite (Figure 3-3f).

Stellenbosch University https://scholar.sun.ac.za

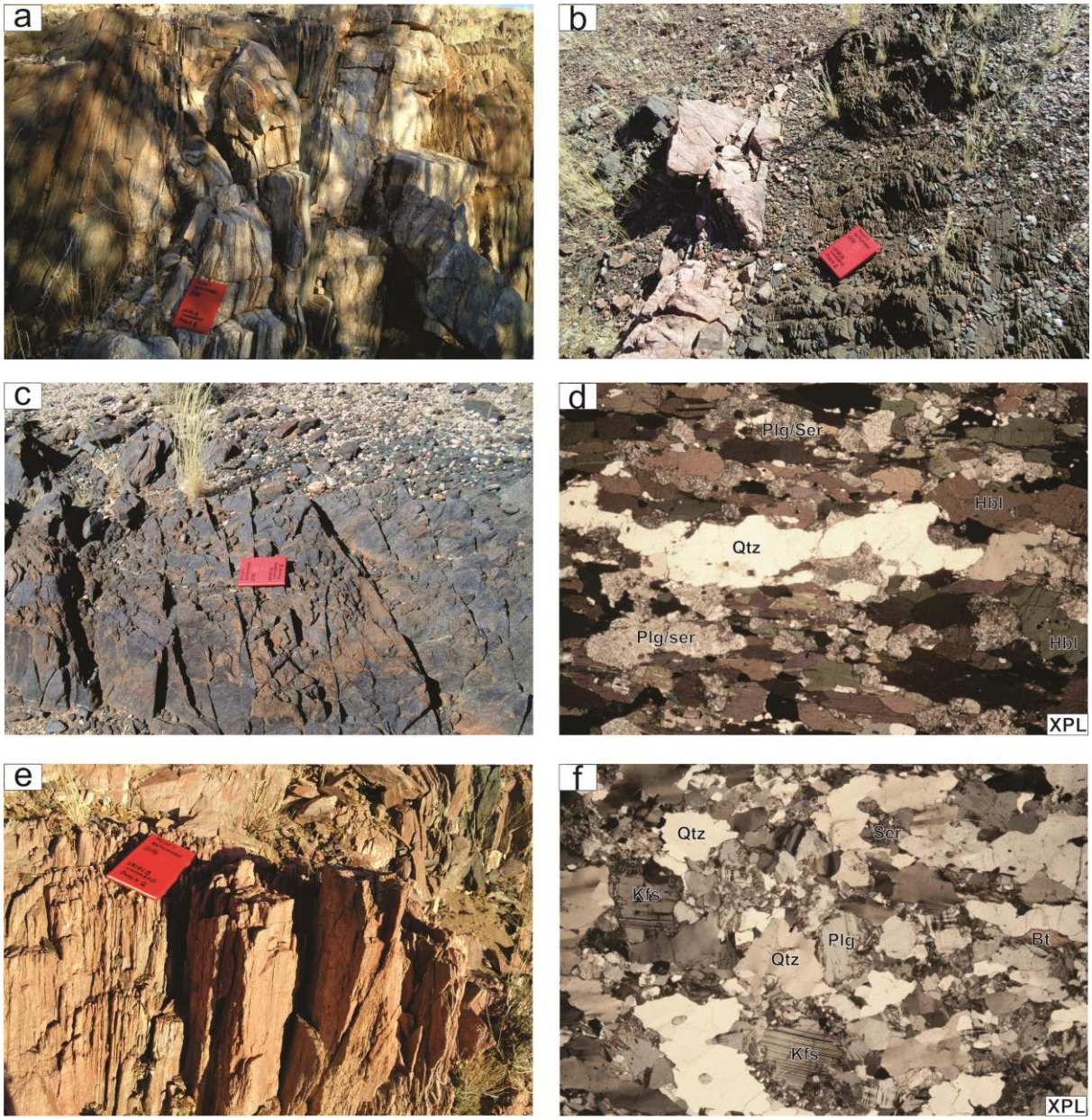

Figure 3-3: Field photos along with photomicrograph of sheared MQ (a) Sheared and asymmetrical folded MQ. (b) Subcropping outcrop of a strongly sheared MQ. (c) Strongly sheared and fractured amphibolite. (d) Photomicrograph (FOV=4.5 mm) of a sheared amphibolite; showing both elongated quartz grain (center) and alteration of plagioclase to sericite (Ser). Dominant shear fabric is defined by elongated quartz grains and sub-parallel alignment of hornblende (Hbl). (e) Strongly foliated and lineated equigranular textured quartzo-feldspathic gneiss. Photomicrograph (FOV=4.5mm) of a sheared quartzo-feldspathic gneiss showing recystallization of quartz and potassium feldspar (Kfs), indicated by irregular inequigranular interlobate grain boundaries and strong undulose extinction. FOV = Field of view. XPL=Cross polarised light.

Stellenbosch University https://scholar.sun.ac.za

3.2.3 **Eureka Complex (EC)**

The Eureka Complex is a generic term given to a poorly exposed rock package comprised of the Eureka grey gneiss and remnant pods/nodules of restitic granulitic pelites and calc-silicates that are dominantly restricted to the northern part of the study area (Figure 3-1 and Appendix B). Rocks of the EC are commonly strongly sheared and intruded by voluminous granitic rocks such as mesocratic porphyritic granite, leucocratic equigranular granite and pegmatites. Amphibolite dykes are not frequently observed in the EC. The the elongated restitic pods/nodules of granulitic pelites and calc-silicate are normally observed in the EC compared to the rest of the study area. The majority of the restitic pods/nodules are hosted as various sizes xenoliths within the matrix of the phyllonites and the Eureka grey gneiss (Appendix B).

3.2.3.1 Eureka grey gneiss

The Eureka grey gneiss is a weakly migmatitic, partly heterogeneous in composition and orange to dark-grey weathering gneissic/schist (Figure 3-4a and Figure 3-4b). Depending on the foliation intensity and mica content, the rock texture can vary from; weakly migmatitic gneiss (~30% mica) and phyllonitic (Figure 3-4b and Figure 3-4c). The weakly migmatitic texture is characterized by less than 30 mm thick leucosomes veins of melts segregated from the massive groundmass of biotite and quartz. When strongly sheared the rock becomes phyllonitic and can be distinguished from other phyllonites by its association with the remnants restitic nodules (Figure 3-4d).

On fresh surfaces, the rock has a mesocratic “grey” colour and is fine- to medium-grained (overall grain size less than 1.5 mm). The Eureka grey gneiss is comprised of quartz (~30-35%), biotite (~25-30%), sericitized plagioclase (20%) and potassium feldspar (<10%) (Figure 3-4 e and Figure 3-4 f). Quartz has been partly recystallized and exhibits pronounced undulose extinction. Muscovite is a minor constituent and chlorite replaces biotite. Garnet is present in some localities and sphene and zircon occur as accessory phases (Figure 3-4f). The rock matrix resembles a granolepidoblastic texture. Elongated biotite and quartz show sub-parallel orientation. The overall rock texture have an equidimensional grain sizes and enhancing a weak mineral preferred orientation (Figure 3-4e and Figure 3-4f).

The elongated restitic calc-silicate finer-grained (sugary textured) nodular pods are dominant (~75%) in the EC (Figure 3-4a and Figure 3-4b) and restitic granulitic pelites pods are a minority (~25%). The elongated restitic nodular pods are widely distributed within the matrix of the Eureka grey gneiss, usually elogated (aspect ratio in the range of; 3:1 and 2:1) and oriented sub-parallel to the rock fabric (Figure 3-4a; Figure 3-4b; Figure 3-4c and Figure 3-4d).

Stellenbosch University https://scholar.sun.ac.za

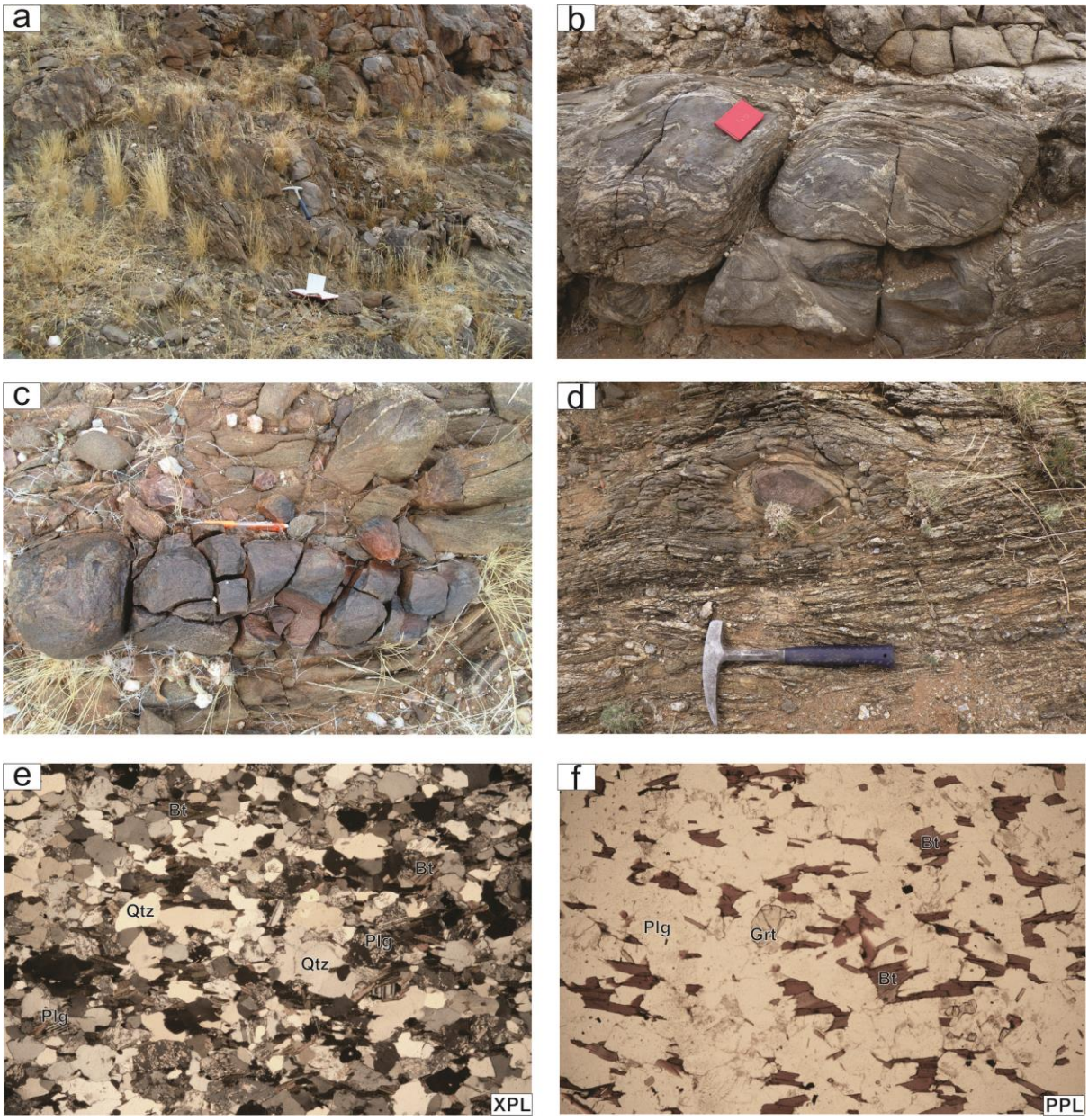

Figure 3-4: Outcrop pictures and photomicrograph of Eureka grey gneiss. (a) Outcrop photo showing texture variation from weakly migmatitic gneissic (top right side of the photograph) to schistose/phylonitic (center to bottom right side of the photograph). (b) Weakly migmatitic Eureka grey gneiss intruded by sheared pegmatite (top) and incorporating an ellipsoidal shaped restitic nodule (center bottom side of the photograph). (c) Elongated fractured restitic calc-silicate nodule, hosted within a sheared and hydrothermally altered (epidote coating) Eureka grey gneiss. (d) Restitic nodule hosted within phyllonites of Eureka grey gneiss. (e) Photomicrograph of Eureka grey gneiss showing a near equigranular texture. Quartz is recrystallized with strong undulose extinction and interlobate grain boundaries. Plagioclase is altered to sericite. Biotite is elongated and altered to sericite. (f) Photomicrograph showing randomly distributed garnet grains within the rock matrix. FOV = Field of view. XPL=Cross polarised light. PPL=plain polarised light.

3.2.3.2 Restitic granulitic pelites

The restitic granulitic pelites in the EC occur either as less than 20 m thick isolated rock units, or as smaller pods within the phyllonites, Eureka grey gneiss and mesocratic porphyritic granite (Figure 3-1 and Appendix B). In the south, close to the MRPSZ, the granulitic pods occur within or in close proximity with the mesocratic porphyritic granite. At outcrop scale, the rock weathers light- to dark-brown and has a fine- to medium-grained texture (Overall grain size less than 2 mm) (Figure 3-5a). The fresh surface is usually

Stellenbosch University https://scholar.sun.ac.za

dark-brown (melanocratic) in colour with partial felsic leucosome veins surrounding massive restitic palaeosome biotite. Rock is comprised of Garnet is usually porphyroblastic, disseminated within the rock matrix and growing more along the leucosome veins (Figure 3-5a and Figure 3-5b). Garnet and cordierite usually appear altered and are probably replaced by biotite (Figure 3-5b). Sillimanites occur as elongate fibrous packets between garnet and quartz.

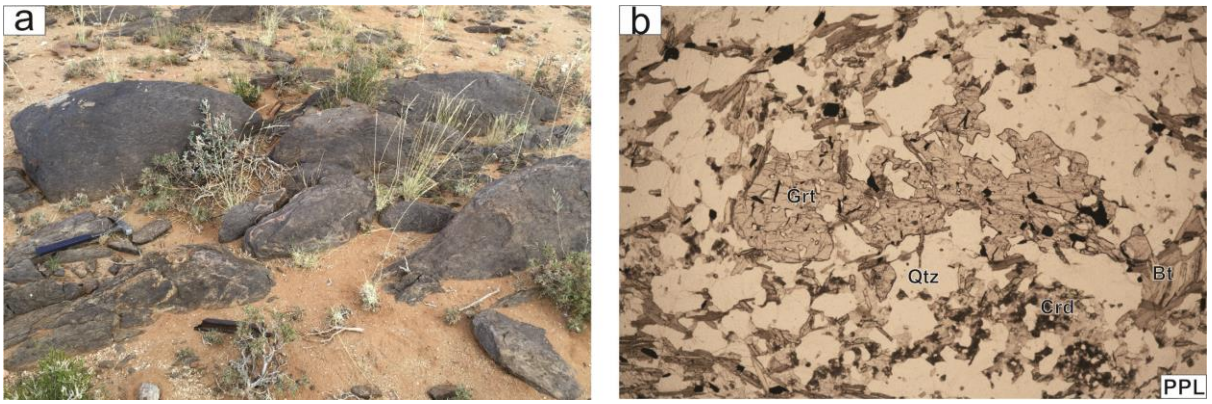

Figure 3-5: (a) Subcropping restitic granulitic pelites in the EC (b) Photomicrograph (FOV= 4.5 mm) showing highly altered and fractures garnet (centre). Biotite is growing within and adjacent to both garnet and cordierite. FOV = Field of view. PPL=plain polarised light.

3.2.4 **Mesocratic Porphyritic Granite**

The mesocratic porphyritic granite is widely distributed throughout the study area (Figure 3-1 and Appendix B) and is usually preserved as (small isolated) koppies and sub-cropping granite pavements (Figure 3-6a and Figure 3-6b). The granite weathers light brown with pink potassium feldspar megacrysts (Figure 3-6 b). The rock texture is porphyritic with euhedral phenocrysts of potassium feldspar and subhedral quartz. Garnet is locally present and disseminated within the matrix. Microcline occurs as megacrysts up to ~5 cm in size (Figure 3-6c). When the granite is strongly sheared potassium feldspar is deformed into augens and rotated porphyroclasts, (Figure 3-6c) and reduced to smaller well-rounded grains (suggesting reworking under grain size reduction conditions) (Figure 3-6d). The modal composition is biotite (~40%), potassium feldspar (30%), quartz (15%) and plagioclase (15%) (Figure 3-6e and Figure 3-6f). The fabric in the rock is defined by biotite wrapping around potassium feldspar and quartz porphyroclasts and by elongated potassium feldspar porphyroclasts (Figure 3-6d and Figure 3-6e).

Stellenbosch University https://scholar.sun.ac.za

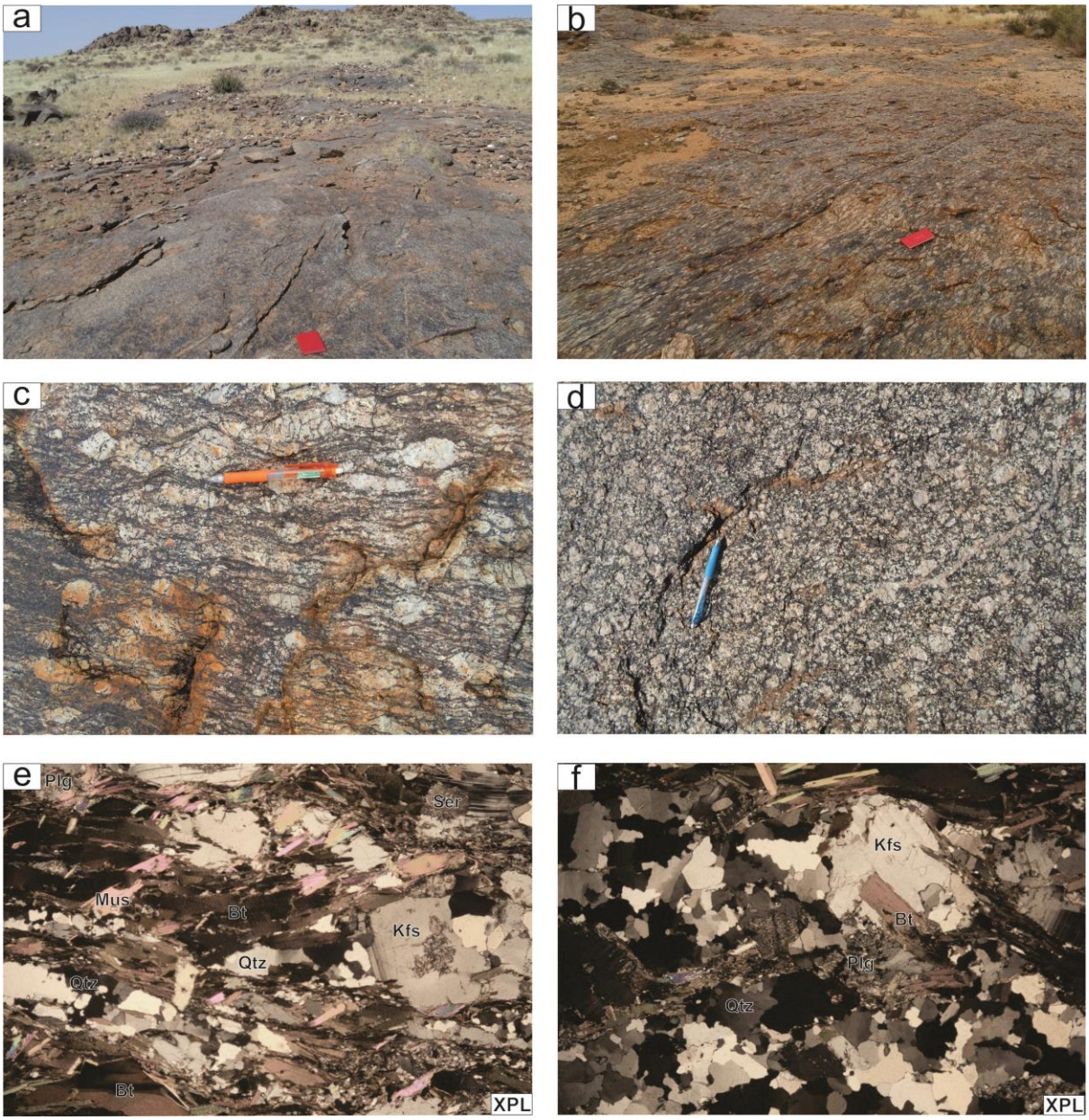

Figure 3-6: Outcrop pictures and photomicrograph of the mesocratic porphyritic granite. (a) Isolated koppies and sub-cropping granite pavement of the mesocratic porphyritic granite. (b) Sub-cropping sheared mega-crystic mesocratic porphrytic granite. The shear fabric in the rock is defined by sub-parallel aligned elongated potassium feldspar porhyroclasts. (c) Hand specimen size photo of the sheared mesocratic porphyritic granite, showing both augen and rotated-sigmoidal shaped potassium feldspar porphyroclast surrounded by biotite and muscovite. (d) Hand specimen size photo of a sheared mesocratic porphyritic granite showing various sizes of sub-rounded to angular shaped potassium feldspar resembling a cataclastic texture in the rock. (e) Photomicrograph (FOV=4.5mm) showing dominant shear fabric (left to right) defined by a preferred orientation of partly sericitized potassium feldspar porphyroclast surrounded by biotite and muscovite. Quartz is deformed into thin elongated grains. Some muscovites (late growth) are growing oblique (bottom left to top right) to the dominant shear fabric. (f) Photomicrograph (FOV=4.5mm), quartz occurs as sub-grain and recrystallized grains with irregular grain boundaries probably associated with grain boundaries migration deformation mechanism. FOV = Field of view. XPL=Cross polarised light.

Stellenbosch University https://scholar.sun.ac.za

3.2.5 **Leucocratic Equigranular Granite and Pegmatites**

3.2.5.1 Leucocratic equigranular granite

The leucocratic equigranular granite occurs as a series of intrusive dykes across the study area (Figure 3-1 and Appendix B) and commonly associated with a series pegmatites dykes (Figure 3-7a). The granite intrudes most of the major rock units (including pegmatites) within the study area (Figure 3-7a). Across the study area, the granite intrudes as a series of discordant and folded dykes (locally up to 200 m thick). A series of intrusive dykes of the leucocratic equigranular granite were observed intruding both sub-parallel and across the D_4 shear zones. In the MRPSZ the granite occurs as a 15km long and up to 100m thick sheared dyke oriented sub-parallel to the NW-SE strike orientation of the MRPSZ (Figure 3-1 and Appendix B).

The leucocratic equigranular granite weathers orange to dark-brown (Figure 3-7b and Figure 3-7c). When fresh the granites have a fine- to medium-grained (overall grain size < 2mm) leucocratic equigranular texture (Figure 3-7b). In some places, a porphyritic variety of this granite was observed (leucocratic porphyritic granite). Phenocrysts are mostly of quartz and microcline within in a groundmass is of sericitized plagioclase. The mineral composition is quartz (~30-35%), microcline (~30%), plagioclase (~ 25%), biotite (~5%), muscovite (~5%) and micro-perthite (~2%) (Figure 3-7d). Although in hand specimen the rock has an equigranular texture (Figure 3-7c), at microscopic scale the majority of the minerals have anhedral to subhedral grain shapes resembling an overall inequigranular polygonal texture (Figure 3-7d and Figure 3-7e). Microcline, plagioclase and biotite are altered to sericite and chlorite. Micro-perthite occurs at the grain boundaries of plagioclase and microcline (Figure 3-7d). Quartz and microcline show strong undulose extinction (Figure 3-7c). Magnetite, zircon, apatite, sphene and opaque minerals are present in accessory amounts.

Stellenbosch University https://scholar.sun.ac.za

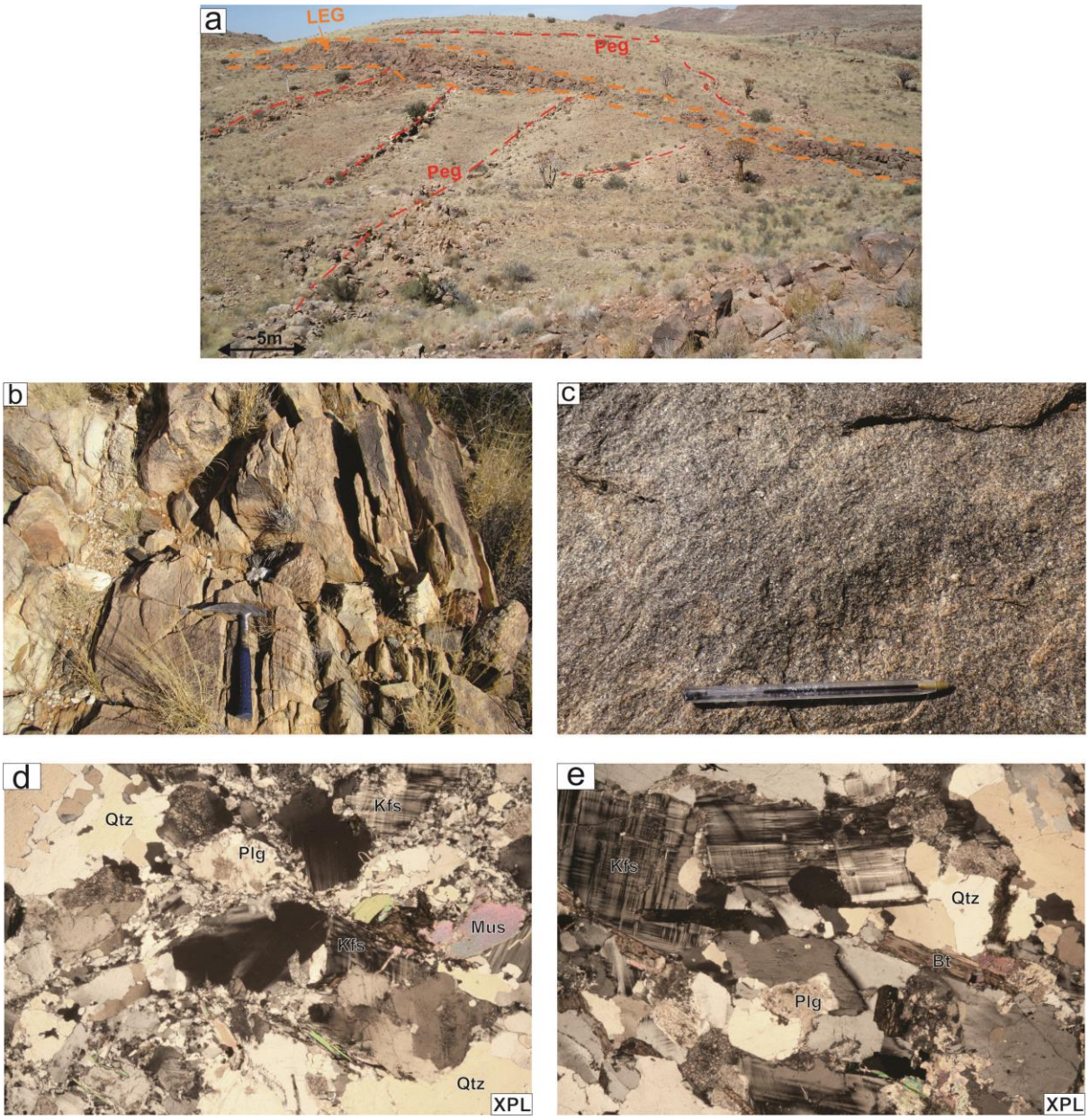

Figure 3-7: Outcrop pictures and photomicrograph of the leucocratic equigranular granite. (a) Sheared dyke of leucocratic equigranular granite (LEG) (Orange dotted lines) cross-cutting sheared pegmatites (Peg) (Red dotted lines). (b) Sheared orange to light brown weathering dyke of the leucocratic equigranular granite. (c) Fine to medium grained texture of the weakly sheared leucocratic equigranular granite. (d) Photomicrograph (FOV=4.5mm) of the leucocratic equigranular granite; Plagioclase and potassium feldspar are altered to sericite and form microperthite texture. Quartz occurs as subgrains with strong with undulouse extinction. Some biotites are altered to muscovite. (e) Photomicrograph (FOV=4.5mm) of the porphyritic variety of the leucocratic equigranular granite with (~4mm) sized potassium feldspar phenocryst (Kfs). FOV = Field of view. XPL=Cross polarised light.

Stellenbosch University https://scholar.sun.ac.za

3.2.5.2 Pegmatites

Pegmatites dykes extensively intruded intruded into the majority of the rocks within the study area (Appendix B). The origin and classification of pegmatites is not part of this study. However, their relationship with the leucocratic equigranular granite and their association with the D_4 shear zone will be considered. In the field, pegmatites occur as light-brown weathering discordant dykes cross-cutting older rocks units (including earlier generation pegmatites dykes) (Figure 3-7a). The pegmatites are commonly coarse-grained (~ 30mm grain size) and composed of potassium feldspar, quartz, plagioclase, biotite, muscovite and minor tourmaline. When sheared, the overall grain size is reduced and they displays cataclastic to mylonitic textures.

3.3 SUMMARY

Broadly, the distribution of the migmatitic banded gneiss, EC and MQ appears to be restricted to specific geographical positions within the study area. The migmatitic banded gneiss is found in the central and southern part of the study area. The northern region of the study area is dominated by the EC and MQ. On the geological map, the two rock packages are mapped as large (km-scale) sets of NW-SE striking slices. Other intrusive rock types, such as mesocratic porphyritic granite, amphibolite dykes, leucocratic equigranular granite and pegmatites are widely distributed across the study area.

The majority of the rock units are intensely sheared and in some places, their protolith and relationship each other cannot be determined with certainty especially along their marginal contacts. Most of the rocks show retrograde metamorphism from amphibolite facies to greenschist facies, dominantly defined by the alteration of feldspars (plagioclase and microcline) to sericite and the replacement of biotite by muscovite and chlorite. Due to shearing intensity, field observation alone was found to be inconclusive in the determination rock relationships especially those between the migmatitic banded gneiss, MQ and EC. Furthermore, the age of the leucocratic equigranular granite and it relationships to D_4 shear zones is not well defined. For this reason geochronology samples for these rock units were collected for U-Pb dating with purpose of determining the their ages (discussed in chapter 4) and hence assist in;

- Determining the potential protolith and emplacement age of migmatitic banded gneiss, MQ and EC and with an aim of defining whether they are derived from the Gordonia Subprovince or Richtersveld Subprovince or both.
- Understanding the significance of the distribution of the three units and the tectonic processes involved.
- Defining the absolute age of the leucocratic equigranular granite, its relationship to pegmatites and timing of D_4 shearing.

Stellenbosch University https://scholar.sun.ac.za

CHAPTER 4: GEOCHRONOLOGY

4.1 INTRODUCTION

The northern part of the study area consists of shear bounded tectonic slices, predominantly hosting rocks of the Eureka Complex (EC) and interlayered quartzo-feldspathic gneiss and amphibolites (MQ) (Figure 3-1). The shearing of the Eureka Shear zone makes it difficult to determine the origin of the rock types. In the absence of the age date, the stratigraphic position of these units has not been well-defined. Moreover, similarities observed in the sheared Eureka grey gneiss of the EC and the migmatitic banded gneiss poses a problem in determining both the distribution and protolith of the two units within the study area. For this reason, age constraints on the selected rock units (1) quartzo-feldspathic gneiss of the MQ, (2) Eureka grey gneiss of the EC, (3) restitic granulitic pelites from the EC and (3) leucocratic equigranular granite (associated with leucocratic equigranular granite) are crucial in establishing the stratigraphic sequence and timing of tectonic processes within the study area.

4.2 METHODOLOGY

Four rock samples weighing approximately 2 kg each were collected for zircon dating. Locality information on sample MA15077, MA15042, MA14062 and MA14027 given in Figure 3-1 and Appendix A. Two of the samples were processed by the Council for Geoscience laboratory in Pretoria (South Africa) and analysed at the Central Analytical Facility (CAF) at Stellenbosch University. The remaining two were prepared at the Department of Earth Sciences, Stellenbosch University. At Stellenbosch University, each sample was cut and a petrographic block was made. The remainder of the rock sample was crushed into <50 mm rock chips with a jaw crusher. The <50 mm rock chips were subsequently milled with a disk mill. The powdered fraction was sieved and re-milled to obtain <350µm powder. The <350µm powder materials were washed and panned to separate heavy and light minerals. The heavy minerals were then removed from the panner with a pipette, placed in a petri dish and dried in an oven for 24 hours. Thereafter, the heavy minerals were run through a magnetic separator to remove the ferro-and para-magnetic from the non-magnetic minerals. Heavy-liquid separation was employed on the non-magnetic portion, to further concentrate the heavy minerals (e.g. zircons). Approximately 100 zircon grains per sample were handpicked with a needle under a light microscope, mounted in epoxy and polished. Zircon shapes and internal structures were determined using backscattered (BS) and cathodoluminescence (CL) imagery acquired with a Zeiss EVO MA15VP SEM and Zeiss Merlin Gemini 2-FI7 at the Central Analytical Facility (Stellenbosch University).

Zircon analysis (U–Pb isotopes) were performed at Central Analytical Facility, Stellenbosch University using a Agilent 7500ce quadrupole laser ablation-inductively–coupled-mass-spectrometry (LA-ICP-MS) system by employing a Thermo-Finnigan Element II mass-spectrometer coupled to a Resonetics Resolution S1 55 excimer/New Wave 213nm laser ablation system. All data were obtained by single-spot analysis on individual zircons grains using a 30 µm and a crater depth of approximately 15-20 µm. The methods applied for analysis followed that described by Frei and Gerdes, (2009) and Meinhold et al.,

Stellenbosch University https://scholar.sun.ac.za

(2010). For accuracy and quality controls of the results; the Plešovice zircon standard (Sláma et al., 2008) were used and the results were consistently in excellent agreements with the published ID-TIMS ages. For zircon interpretation, analyses with 99-100% concordance calculated from 100 x ($^{206}Pb/^{238}U$ age) / ($^{207}Pb/^{206}Pb$ age) are considered concordant. The zircons analyses that fall outside the 99-100% concordance range interpreted to be considered discordant and were excluded from data plotting interpretation. The calculation of Concordia ages and plotting of Concordia diagrams, histograms and probability density plots were performed using Isoplot/Ex 3.75 (Ludwig, 2012). Analytical result tables are attached as Appendix C.

Stellenbosch University https://scholar.sun.ac.za

4.3 RESULTS

4.3.1 MA15077 Eureka Grey Gneiss

4.3.1.1 Sample description

Sample MA15077 is a weakly migmatitic Eureka grey gneiss (Figure 4-1a). The sample was collected within the EC on the eastern side of the Eureka Shear Zone (see chapter 3, section 3.2.3 for full description), approximately 5km southeast of town Warmbad (Figure 3-1). The sample was collected for the purpose of determining the source and depositional age, as well as to decipher ages of the metamorphic events. The rock weathers orange to dark-grey, is moderately sheared (Figure 4-1a) and hosts elongated restitic granulitic pods of pelites. The weakly migmatitic gneissic texture consists of approximately ~10-15% leucosome material (Figure 4-1b). The rock is fine- to medium-grained (<1.5mm), with a modal composition (excluding the leucosome) of quartz (~35-40%), biotite (~30%), plagioclase (~15%), potassium feldspar (~10%) and muscovite (~5%) (Figure 4-1c). Accessory minerals are zircon, sphene and opaque minerals. The heterogeneous compositional banding and its association with restitic granulitic pods of pelites probably suggest that the rock is a paragneiss rather than an orthogneiss.

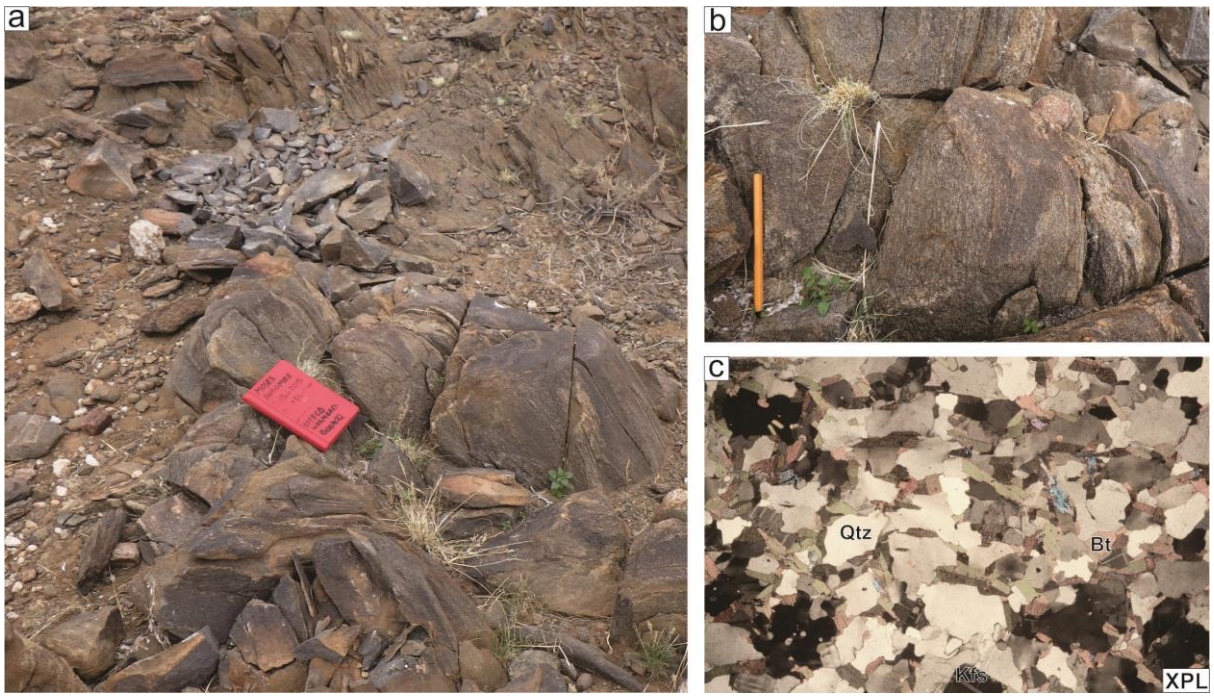

Figure 4-1: (a) Field photograph of the sheared Eureka grey gneiss. (b) Weakly migmatitic texture fine to medium grained texture with centimetre scale leucosomes veins. (c) Photomicrograph (FOV=4.5mm) of the Eureka grey gneiss. Majority of the minerals are approaching equidimentional grain size. Quartz (Qtz) and potassium feldspar (Kfs) have a strong undulose extinction. Biotite (Bt) shows a weak preferred orientation and is replaced by muscovite. FOV = Field of view. XPL=Cross polarised light.

Stellenbosch University https://scholar.sun.ac.za

4.3.1.2 Zircon morphology

Sample MA15077 contains dominantly elongated subhedral zircons with a small population of anhedral zircons (Figure 4-2). Majority of the zircons have fairly rounded edges, abrasions and fractures, more typical of detrital zircons. The zircons have a long axis dimension in the range of ~80-200 µm and an aspect ratio of long axis to short axis between 3:1 and 2:1. Most of the zircons show bright to moderate luminescence, with oscillatory zoned cores surrounded by moderately bright to non-luminescence overgrowth and rims (Figure 4-2). The majority of the zircons have an elongate lop-sided core domain and a few have sub-rounded cores. The rim overgrowths around the core domain is usually characterized by poorly developed uneven oscillatory zoning showing predominantly thick, moderate to no luminescence layers alternating with thin bright luminescence layers.

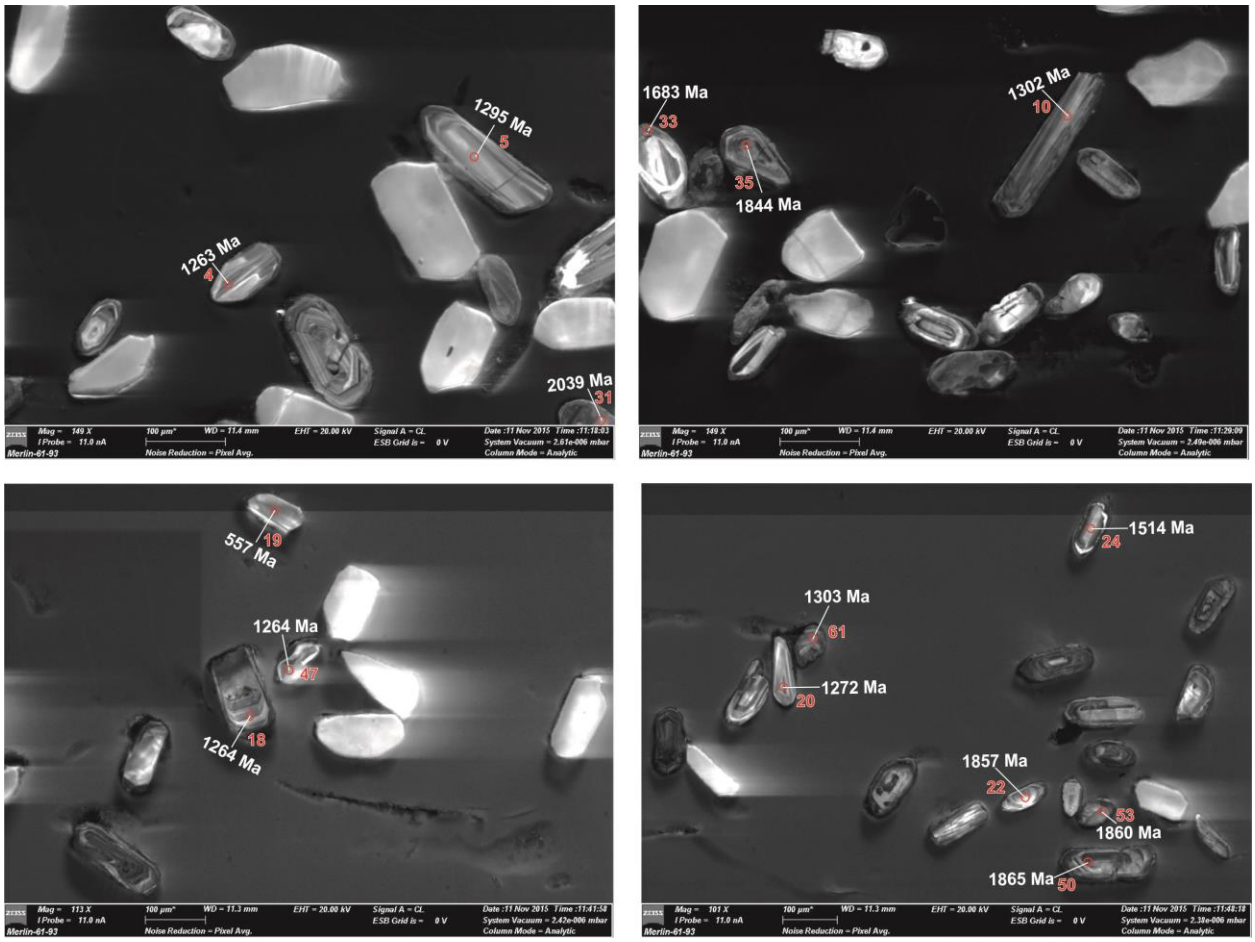

Figure 4-2: Cathodoluminescence (CL) images of representative zircons from sample MA14042. Majority of the medium sized zircons are elongated with a subherdal grain shape. Small sized zircons have anhendral shape. (Red numbers and circle represents the analysis number and spot localities with their corresponding concordant $^{207}Pb/^{206}Pb$ isotopic ages.

Stellenbosch University https://scholar.sun.ac.za

4.3.1.3 U-Pb results

Out of 63 spots analysed on 53 detrital zircons (Appendix C), 22 analysis were 99% and 100% concordant (Figure 4-3a). The concordant results were plotted on a Wetherill Concordia diagram (Figure 4-3a). The remaining values (below 99% and beyond 100%) plotted below the Concordia curve (probably because of Pb loss). These data were considered discordant and were excluded from the analysis. Out of the 22 concordant analyses, four main concordant age population groups were identified. The first age population group is represented by core domains of four small stubby anhedral zircons. This age population group produced a concordant age of 1863 ± 14 Ma (2σ decay-const, errs included, MSWD=0.039 and probability of concordance=0.84) (Figure 4-3b). The second population group of two zircon cores gave a concordant age of 1310 ± 16 Ma (2σ decay-const, errs included, MSWD=0.084 and probability of concordance=0.77) (Figure 4-3c). The third age population group, represented by 6 spots on the cores of elongated euhedral zircons gave a concordant age of 1297 ± 8.5 Ma (2σ decay-const, errs included, MSWD=0.036 and probability of concordance=0.850) (Figure 4-3d).The fourth population group of three spots on the core and oscillatory zoned rims surrounding the core of three sub- to anhedral zircons gave a concordant age of 1262 ± 13 Ma (2σ decay-const, errs included, MSWD and probability of concordance at 0.14 and 0.71, respectively) (Figure 4-3d). The youngest concordant age of 557 Ma came from rim between the core and exterior of a very stubby zircon. The oldest zircon core in the sample gave a concordant age of 2029 Ma (Figure 4-3f). Other individual detrital zircons gave a wide variety of concordant ages: 1264 Ma, 1272 Ma, 1514 Ma, 1683 Ma, 2029 Ma and 2039 Ma (Figure 4-3a and Figure 4-3f).

Stellenbosch University https://scholar.sun.ac.za

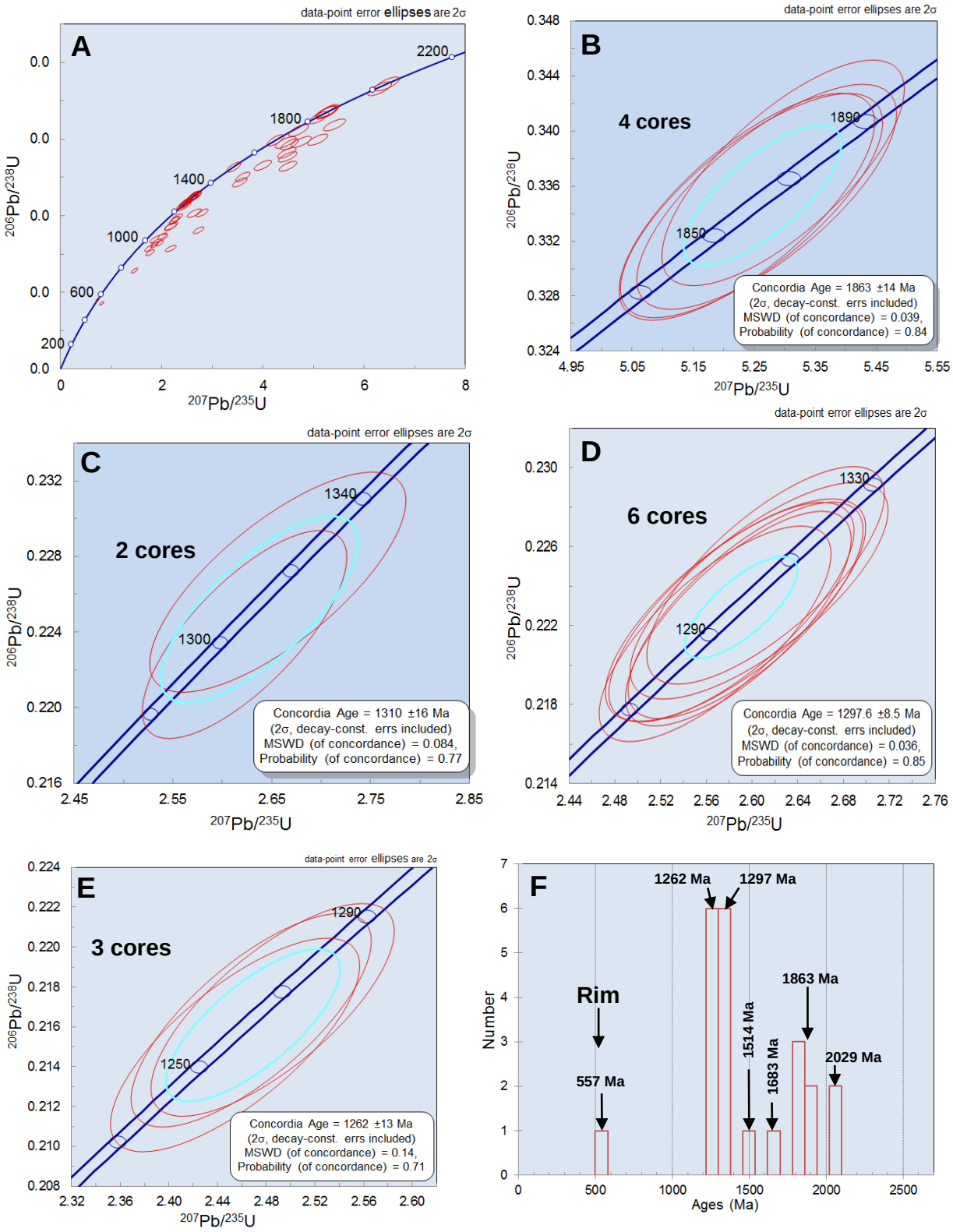

Figure 4-3: (A) $^{206}Pb/^{238}U$ versus $^{207}Pb/^{235}U$ Wetherhill Concordia diagram for LA-ICP-MS U-Pbages data for zircons from sample MA15077, showing all the concordant and discordant ages obtained from 63 spot analysed on 53 zircons. (B, C, D and E) Enlarged LA-ICP-MS U-Pb age plot for dominant detrital zircons (dominantely cores) age groups. (F) Relative probability distribution plots for $^{207}Pb/^{206}Pb$ age data showing the concordant detrital zircons age populations for sample MA15077.

Stellenbosch University https://scholar.sun.ac.za

4.3.2 **MA15042 Restitic granulitic pelite**

4.3.2.1 Sample description

Sample MA15042 was collected from the Eureka Shear Zone, in the top northwestern extension of the EC (Figure 3-1). Similarly to the Eureka grey gneiss, this metasediment (see chapter 3, section 3.2.3.2 for full description) was sampled with the aim of determining its source and depositional age, as well as to decipher the timing of metamorphic overprint. The rock occurs as dark-weathering isolated lithology (Figure 4-4a), in close proximity with sheared sub-cropping mesocratic porphyritic granite and dykes of leucocratic equigranular granite. It has a granophyric to protocataclastic texture, with 40% of the matrix made up of fine-grained sub-rounded to angular fragments quartz, microcline, garnet and sillimanite (Figure 4-4d and Figure 4-4c). The modal composition is quartz (~25%), microcline (~20%), sillimanite (~20%), biotite (15%), garnet (10%), plagioclase (5%) and cordierite (5%). Garnet, sillimanite, cordierite and biotite are porphyroblastic (Figure 4-4c); quartz and potassium feldspar are porphyroclastic. Large crystals are separated by a groundmass of sillimanite bundles associated with finer-grained angular aggregates of quartz, potassium feldspar and garnet (Figure 4-4c). Majority of biotites occurs as eloganted grains along grain boundaries and within fractures of garnet and cordierite. These probably suggest that they are secondary and resulting from the breakdown of garnet and cordierite (Figure 4-4c).

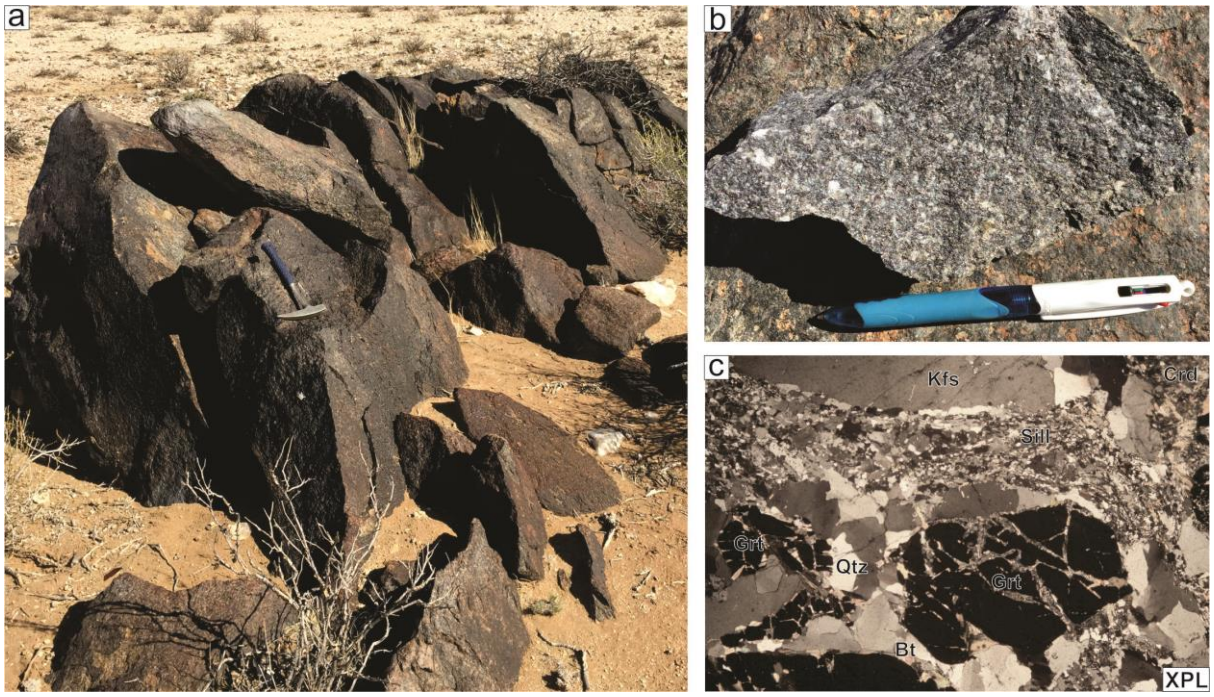

Figure 4-4: (a) Field photograph showing a dark weathering isolated blobs of a restitic granulitic pelite from the EC. (b) Hand specimen photograph showing a granofelic to slightly cataclastic texture. (c) Photomicrograph (FOV=4.5mm) of the metapelite. Both porphyroclasts (quartz and potassium feldspars) and porphyroblasts (garnet (grt), cordiotite (Crd) and biotite are surrounded by a lamellae of sillimanite mixed fine grained aggregates of garnet, quartz and potassium feldspar. FOV = Field of view. XPL= Cross polarised light.

4.3.2.2 Zircon morphology

Three zircons population groups comprised of; (1) prismatic euhedral zircons, (2) and subhedral zircons and (3) stubby anhedral zircons were identified in sample MA15042 (Figure 4-5). Prismatic euhedral zircons are elongated with a long axis diameter in the range of ~60-154µm and aspect ratios over 2:1.

Stellenbosch University https://scholar.sun.ac.za

This zircons group has both small and large cores. Small cores are generally elongated and have a regular bright luminescence core domain. Larger cores are mainly irregular with uneven oscillatory zoning of bright to moderate luminescence. The zircon overgrowth on the cores is dominated by consistently equidimensional oscillatory zoning of bright to no luminescence layers. In a few zircons where oscillatory zoning is uneven, no luminescence zones are prevalent. The second population group consisting of anhedral zircons have subprismatic shape defined by moderately rounded edges on the exterior rims. These zircons have a stubby bright or moderately luminescence cores, but the exterior rims overgrowth shows a sub- to anhedral growth shapes. The zircons have long axis diameters in the range of ~50 and 230 µm and aspect ratios between 2:1 and 3:2. The third population group consisting of stubby rounded zircons have long axis diameters in the range of ~30-70 µm and aspect ratios of 3:2. The cores zones are subrounded and consist of uneven layering of bright to no luminescence. The rims are dominated by unevenly oscillatory zones of thick, moderate to no luminescence layers and thin bright luminescence layers. The wide variety of zircons types in the sample most likely suggest that they are detrital.

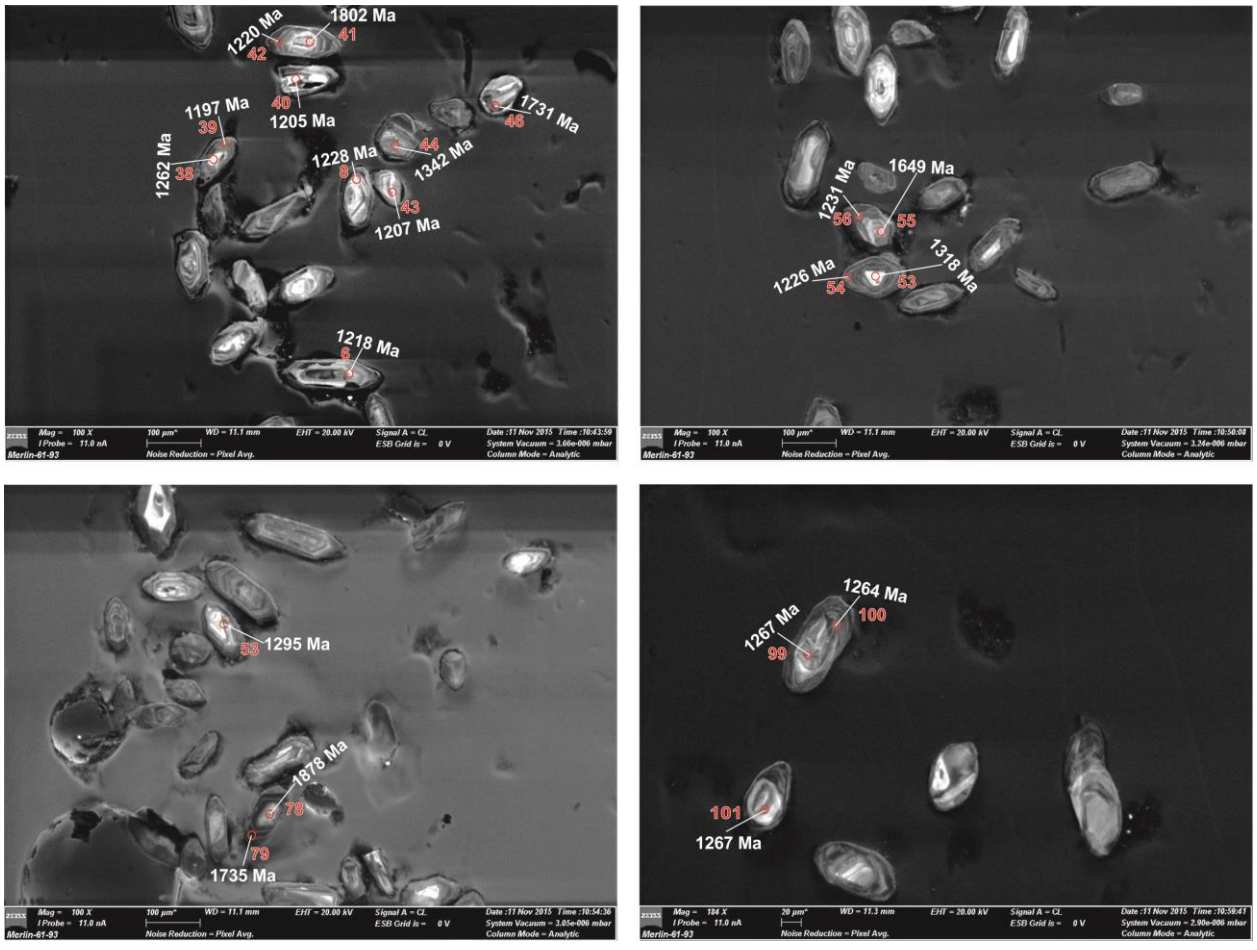

Figure 4-5: Cathodoluminescence (CL) images of representative zircons from Sample MA14042. A1 to A4 shows various zircons shapes with dominant bright luminescence cores and moderate to none luminescence core overgrowth rims. (Red numbers and circle represents the analysis number and spot localities with their corresponding concordant $^{207}Pb/^{206}Pb$ isotopic ages.

Stellenbosch University https://scholar.sun.ac.za

4.3.2.3 U-Pb results

One hundred and two spots were analysed on 82 different detrital zircons (Appendix C). Of these 62 spots gave a 99% and 100% concordance (Figure 4-6a and Appendix C). The results were plotted on a Wetherill Concordia diagram from which 8 concordant age populations ranging between 1212 and 1778 Ma were derived (Figure 4-6a). Four stubby cores of subhedral to anhedral zircons yielded a Concordia age of 1322 ±12 Ma (2σ decay-const, errs included, MSWD=0.31 and probability of concordance=0.58) (Figure 4-6b). Subsequently, the stubby cores of 6 dominantly subhedral zircons provided a Concordia age at 1300 ± 9.2 Ma (2σ decay-const, errs included, MSWD=0.00104 and probability of concordance=0.97) (Figure 4-6c). Nine subhedral zircons cores and overgrowth oscillatory zoned rims around the core provided a concordant age of 1262 ± 7.4 Ma (2σ decay-const, errs included, MSWD=0.24 and probability of concordance=0.62) (Figure 4-6d). Twenty-three spots on the rims of dominantly euhedral zircons represent the dominant age population. These zircons provided a Concordia age at 1212 ± 4.3 Ma (2σ decay-const, errs included, MSWD=0.43 and probability of concordance=0.51) (Figure 4-6e). Two cores of anhedral zircons gave a concordant age of 1778± 19 Ma (2σ decay-const, errs included, MSWD=0.21 and probability of concordance=0.65) (Figure 4-6f). Two anhedral zircons cores generated concordant age of 1736 ± 20 Ma (2σ decay-const, errs included, MSWD=0.086 and probability of concordance=0.77) (Figure 4-6f). The cores from two anhedral zircons gave a concordant age of 1681 ±19 Ma (2σ decay-const, errs included, MSWD=0.0016 and probability of concordance=0.97) (Figure 4-6f). Two subhedral zircons overgrowth rims around the core gave a concordant age of 1243 ± 15Ma (2σ decay-const, errs included, MSWD=0.0082 and probability of concordance=0.93) (Figure 4-6f). Other individual detrital zircons gave concordant ages of; 1878 Ma, 1842 Ma, 1755 Ma, 1700 Ma, 1649 Ma, 1342 Ma, 1289 Ma, 1236 Ma and 1231 Ma (Figure 4-6f). The youngest zircon in a sample provided a concordant rim age of 1197 Ma and the oldest zircon gave a concordant core age of 1999 Ma (Figure 4-6a and Figure 4-6f).

Stellenbosch University https://scholar.sun.ac.za

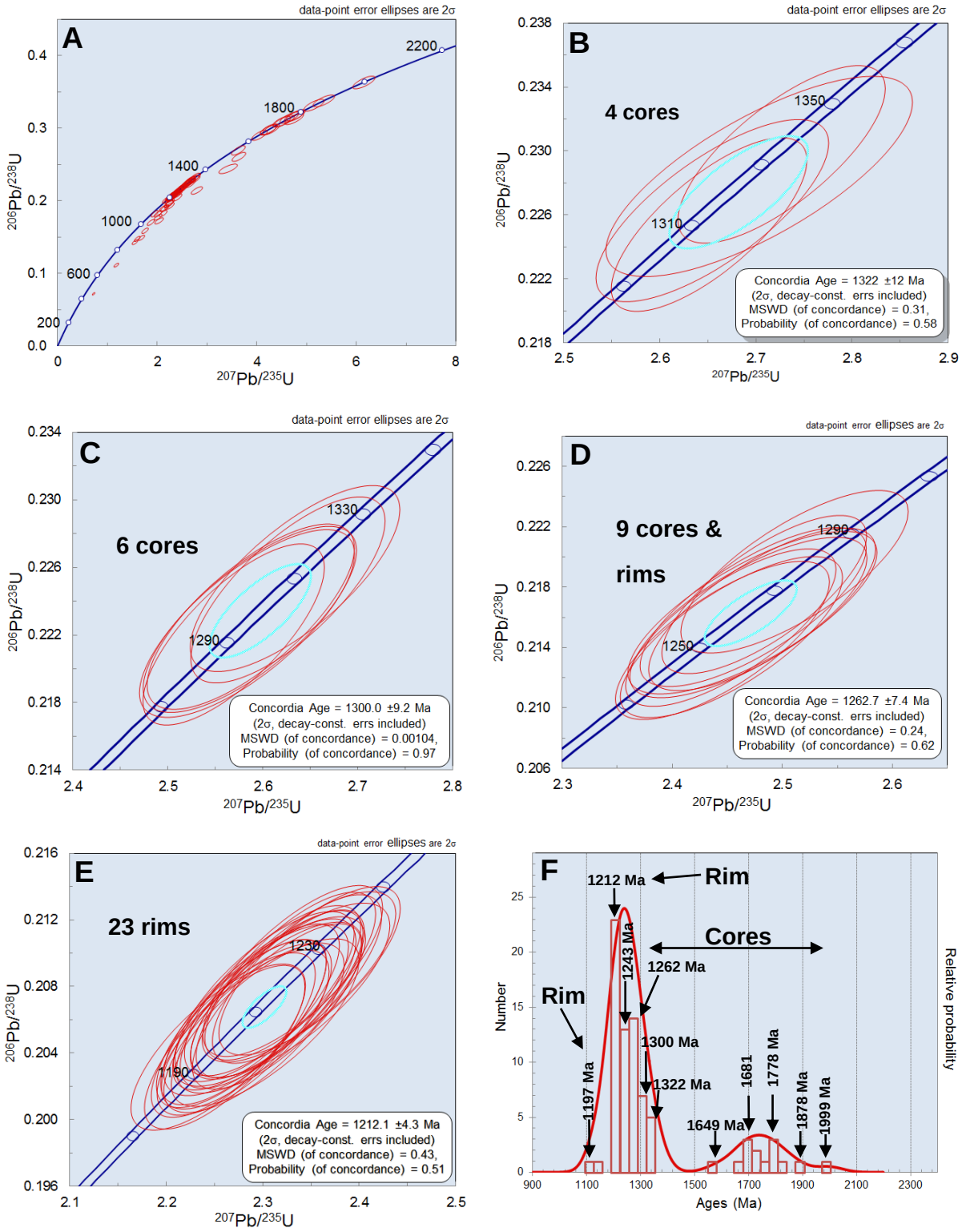

Figure 4-6: A) $^{206}Pb/^{238}U$ versus $^{207}Pb/^{235}U$ Wetherhill Concordia diagram for LA-ICP-MS U-Pb ages data for zircons from sample MA15042, showing all the concordant and discordant ages obtained from 102 spot analysed on 82 zircons. (B, C, D and E) Enlarged LA-ICP-MS U-Pb age plot for dominant detrital zircons age (dominantly cores) groups. (F) Relative probability distribution plots for $^{207}Pb/^{206}Pb$ age data showing the concordant detrital zircons age populations for sample MA15042.

Stellenbosch University https://scholar.sun.ac.za

4.3.3 **MA14069 Quartzo-feldspathic gneiss**

4.3.3.1 Sample description

Sample MA14069 is a quartzo-feldspathic gneiss, collected in the northern central part of the study area (Figure 3-1), within the SE-NW trending package of interlayered amphibolite and quartzo-feldspathic gneiss (MQ) (see chapter 3, section 3.2.2 for full description). The rocks occur as a unique orthogneiss package that is restricted to the northern part of the study area (ESZ). The rock sample was collected with a purpose of determining the inheritance, metamorphic and crystallization age that will be useful in understanding the stratigraphic sequence relationships of the Eureka shear zone host rocks. The quartzo-feldspathic gneiss is usually sheared (Figure 4-7a) and is commonly found interlayered with amphibolites. The rock is leucocratic and fine to medium grained (grain size ~0.5-1.0mm) (Figure 4-7b). The dominant minerals are quartz (~20-25%), microcline (~20-25%), sericitized plagioclase (~20%), biotite (20%), muscovite and chlorite (10%) (Figure 4-7c). Quartz and microcline are recrystallized and have strong undulose extinction (Figure 4-7c).

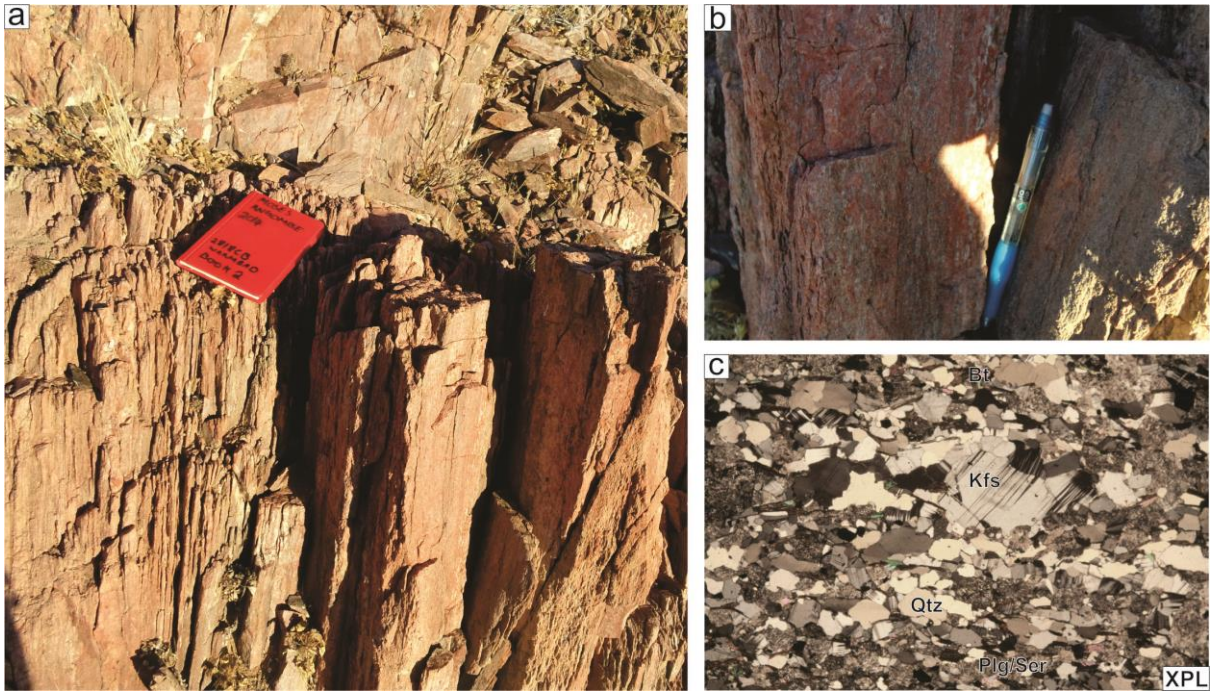

Figure 4-7: (a) Strongly lineated and foliated quartzo-feldspathic gneiss in the ESZ. (b) Potassium feldspar dominated leucocratic equigranular texture in the quartzo-feldspathic gneiss. (c) Photomicrograph (FOV=4.5mm) of the quartzo-feldspathic gneiss showing equidimentional aggregates of microcline, biotite and quartz within a ground mass of sericitized plagioclase. Biotite are elongated and partly altered to muscovite. Chlorite is minor and occurs as an alteration product of sericitized plagioclase, biotite and muscovite. FOV = Field of view. XPL=Cross polarised light.

4.3.3.2 Zircon morphology

Zircons in sample MA14069 are dominantly medium-sized elongated subhedral shaped, while small sized stubby subrounded zircons are a minority (Figure 4-8). Elongated subhedral zircons have sizes in the range of (100 to 250 µm) and aspect ratios over 2:1. Majority of the elongated sub-hedral have elongated bright and no luminescence cores. The overgrowth rims around the cores and outer rims have unevenly distributed oscillatory zoning comprised of dominant thick bright luminescence layers alternating with

Stellenbosch University https://scholar.sun.ac.za

minor thin moderate to no luminescence layers. The smaller stubby zircons have sizes in range of 30-90 µm. The cores are sub-rounded with moderate luminescence and weakly pronounced oscillatory zones. The overgrowth rims around the cores also show weakly developed oscillatory zoning dominated by thin layers of moderate luminescence and thick bright luminescence layers.

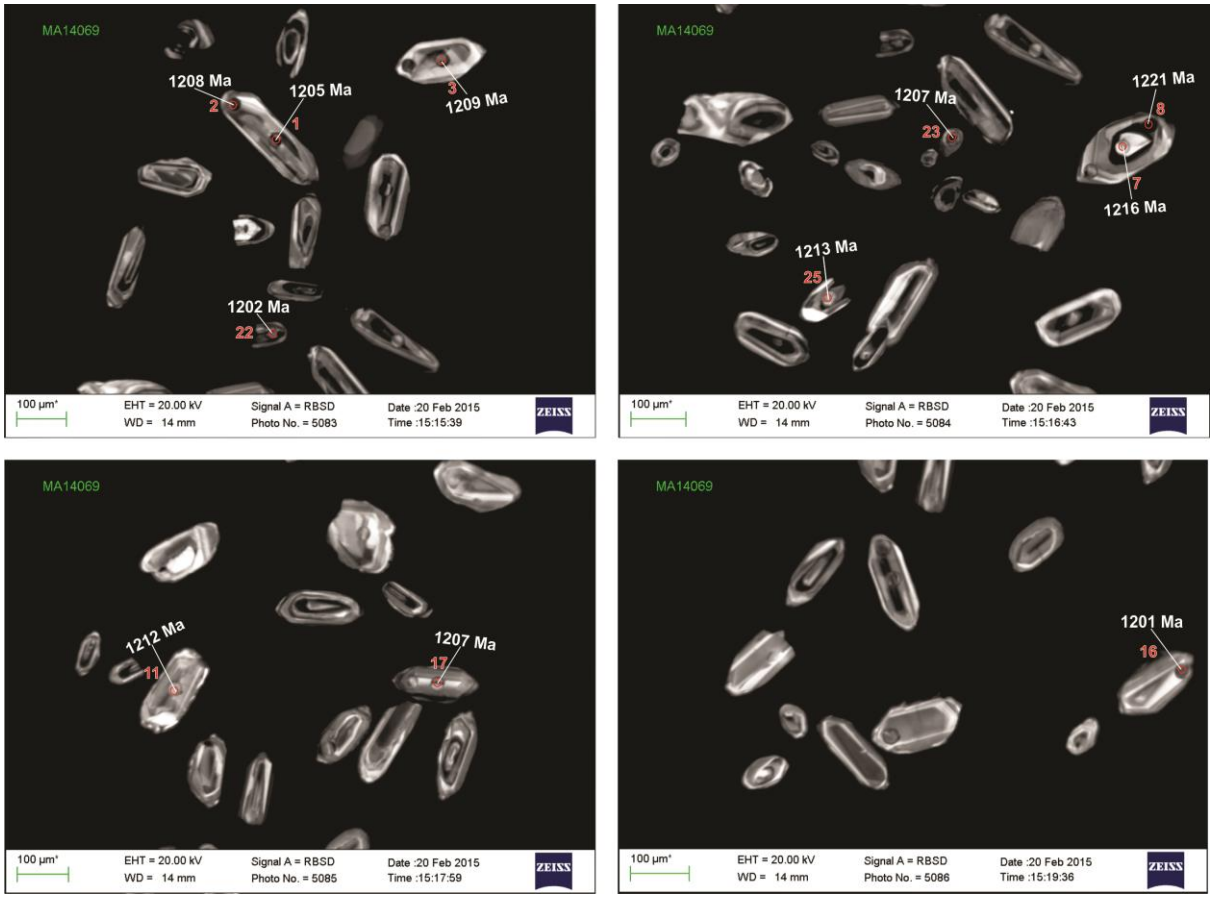

Figure 4-8: Cathodoluminescence (CL) images of representative zircons from sample MA14042, showing both elongated subhedral (medium sized) and anhedral (small sized) shaped zircons. Majority of the zircons shows elongated thin cores of moderate to none luminescence and an exterior overgrowth rim of thick bright luminescence (Red numbers and circle represents the analysis number and spot localities with their corresponding concordant $^{207}Pb/^{206}Pb$ isotopic ages.

4.3.3.3 U-Pb results

In Sample MA14069, 11 out of 27 zircons grains analysed (Appendix C) plotted on the Concordia curve with concordance between 99 and 100% (Figure 4-9a). The remaining values plots below the Concordia curve were probably due to Pb loss (Figure 4-9a). All 11 concordant ages gave a concordant core age of 1207 ± 6.9 Ma (2σ decay-const, errs included, MSWD=0.024 and probability of concordance=0.88), interpreted as age of crystallization of the rock (Figure 4-9b and Figure 4-9c). The oldest near concordant zircon (94% concordant) gave an inheritance age of 1564 Ma (Figure 4-9a). The results plotted on the Discordia diagram gave the upper Discordia curve intercepts at 1206±12 Ma and the lower Discordia curve intercepts at 550±130 Ma (Figure 4-9d).

Stellenbosch University https://scholar.sun.ac.za

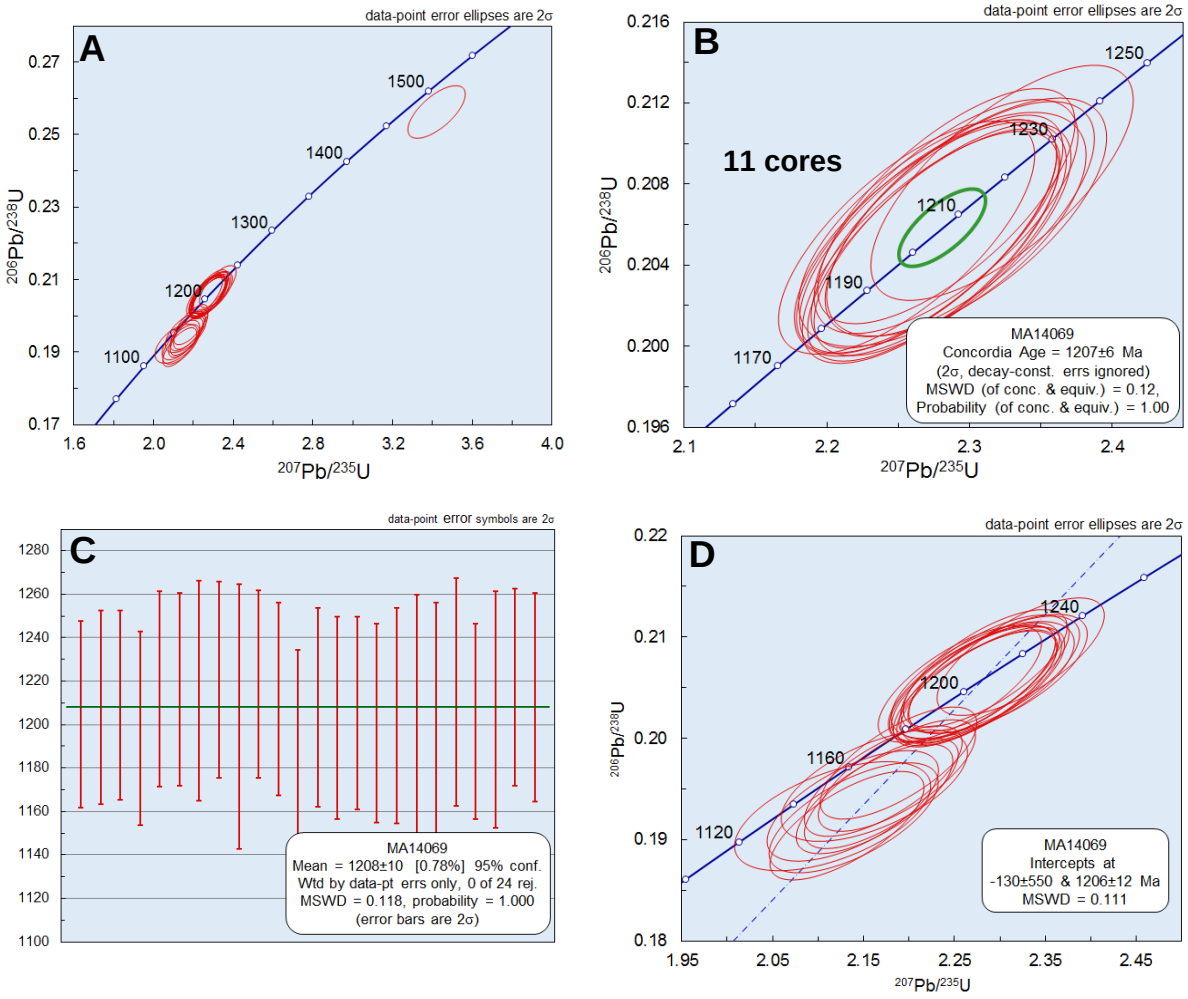

Figure 4-9: (A) $^{206}Pb/^{238}U$ versus $^{207}Pb/^{235}U$ Wetherhill Concordia diagram for LA-ICP-MS U-Pb ages data for zircons analysed from sample MA15042, showing all the concordant and discordant ages obtained from 27 spot analysed on 27 zircons. (B) Enlarged LA-ICP-MS U-Pb concordant plot for 11 zircons cores yielding a concordant age 1207 Ma. (C) Weighted average concordant plot showing a calculated mean average concordant age at 1208 Ma. (D) Discordia diagram showing both concordant and discordant data; the upper Discordia line intercepts at 1206 Ma and lower Discordia line intercepts at 550 Ma.

4.3.4 **MA14027 Leucocratic equigranular granite**

4.3.4.1 Sample description

Sample MA14027B is a weakly sheared leucocratic equigranular granite (Figure 4-10a). The sample was collected in the central northern part of the study area, where the granite is folded as a mega W-E trending open syn-D_4 fold with fold limbs truncated by D_4- shear zone (Figure 3-1). A series of leucocratic equigranular granite intrudes and cross-cut some of the early syn-D_4 shearing pegmatite and is also cut by the D_4 shear zone in both the, MRPSZ and ESZ (see chapter 3, section 3.2.5 for full description). For that reason, a sample of the granite was collected with the intention constraining timing of shearing in the Eureka shear zone. The rock weathers dark brown to orange with a porphyritic texture defined by microcline and quartz phenocrysts in the size range of (3-5mm) (Figure 4-10b). Potassium feldspars phenocrysts are oriented sub-parallel to each other and define a flow foliation in the rock (Figure 4-10b). The groundmass is made of seritized plagioclase. Mineralogically the rock is composed of 30% microcline, 25% quartz, 20% plagioclase, 15% biotite and 10% muscovite (Figure 4-10c).

Stellenbosch University https://scholar.sun.ac.za

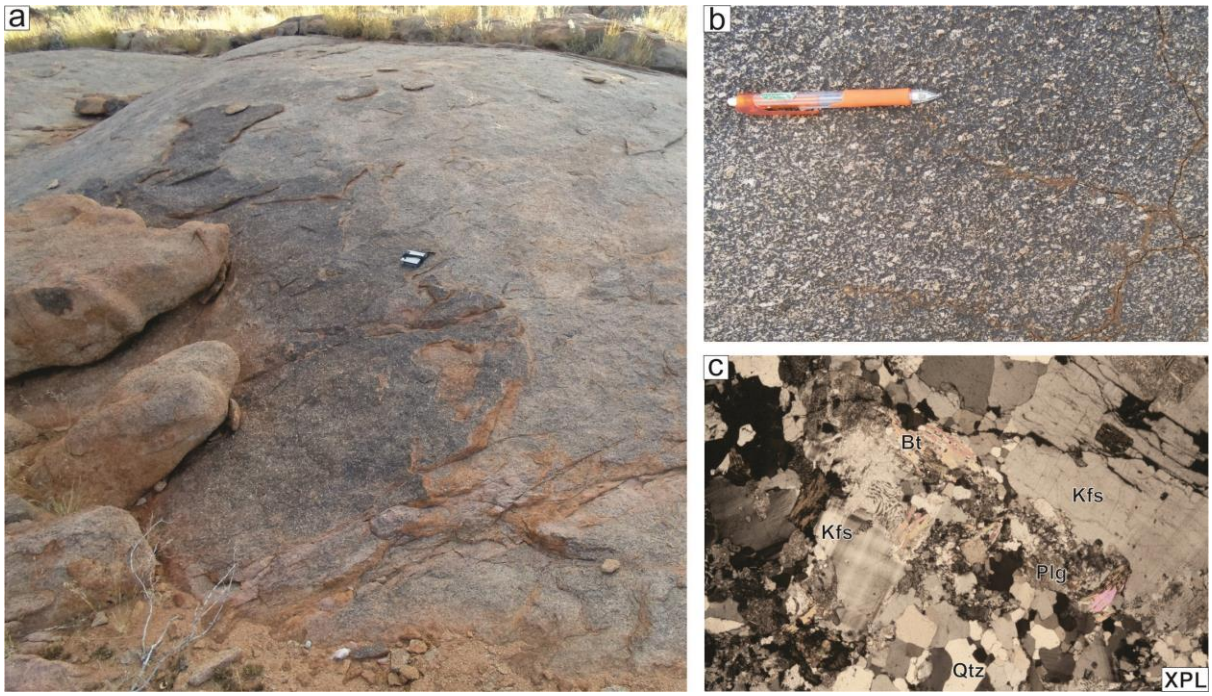

Figure 4-10:(a) Field photograph of the weakly sheared porphyritic variety of the leucocratic equigranular granite dyke. (b) Medium grained porphyritic texture (Potassium feldspar phenocrysts greater than 3 mm) with a flow foliation indicated by the preffered orientation of potassium feldspar (microcline) phenocrysts. (c) Photomicrograph (FOV=4.5mm) of the leucocratic porphyritic granite. The rock is mostly unsheared and majority of the minerals lacks any preffered orientation. FOV = Field of view. XPL=Cross polarised light

4.3.4.2 Zircon morphology

Sample MA15027 shows two zircon populations. The first is comprised of medium sized subhedral shaped and fractured zircons with a long axis diameter in the range of ~125-250 µm and aspect ratios between 2.1 and 3:2 (Figure 4-11). These zircons on the CL image appear to have both bright and none luminescence in their cores and rims structures. They also have a poorly developed oscillatory zoning. Their cores are difficult to see due to either intense brightness or no luminescence. However, 6 zircons are sub-rounded with an uneven proportion bright and no luminescence layers. The second zircon population is comprised of smaller sized anhedral sub-rounded zircons with long axis diameter in the range of ~83-120 µm. These zircons have an overall moderate to no luminescence, with few zircons showing small bright cores. The overgrowth rims around the cores shows oscillatory zoning defined by alternating thick no luminescence and thin moderate luminescence layers. Seven zircons occur as smaller angular broken pieces.

Stellenbosch University https://scholar.sun.ac.za

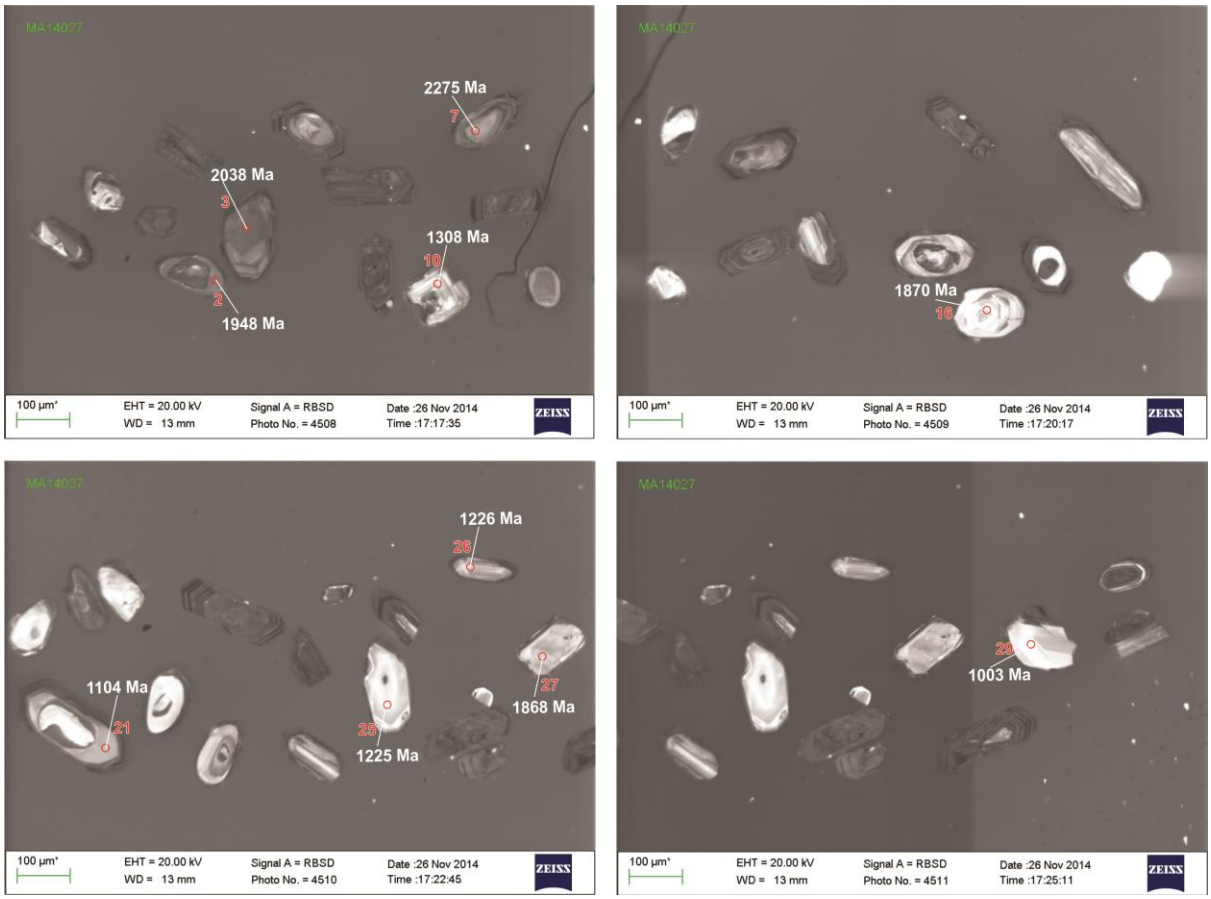

Figure 4-11: Cathodoluminescence (CL) images of representative zircons from sample MA14027. CL imagery shows both subhedral and anhedral shaped zircons associated with some angular zircons fragments. (Red numbers and circle represents the analysis number and spot localities with their corresponding concordant $^{207}Pb/^{206}Pb$ isotopic ages.

4.3.4.3 U-Pb results

Twenty-seven zircons grains were analysed, of which 15 grains were between 98 and 100% concordant (Appendix C). The 12 analyses that plotted below the Concordia line (possibly due to Pb loss) were excluded from the concordant plot. The analysed concordant spots shows a wide range of ages between 1003 and 2275 Ma (Figure 4-12a), with 2 main population peak at 1862 and 1299 Ma. Four zircons cores made up a dominant concordant age population of 1862 ± 15 Ma (2σ decay-const, errs included, MSWD=0.024 and probability of concordance=0.88) (Figure 4-12b). The second age population composed of two zircons cores gave a concordant age of 1227 ± 18 Ma (2σ decay-const, errs included, MSWD=0.0055 and probability of concordance=0.94) (Figure 4-12c). The 2275 to 1227 Ma ages are interpreted to be inherited ages. A single zircon rims gave a concordant age of 1104 and the oldest zircon core is recorded at 2275. The youngest zircon core recorded was 1003 Ma probably indicating the crystallization age of the granite (Figure 4-12d).

Stellenbosch University https://scholar.sun.ac.za

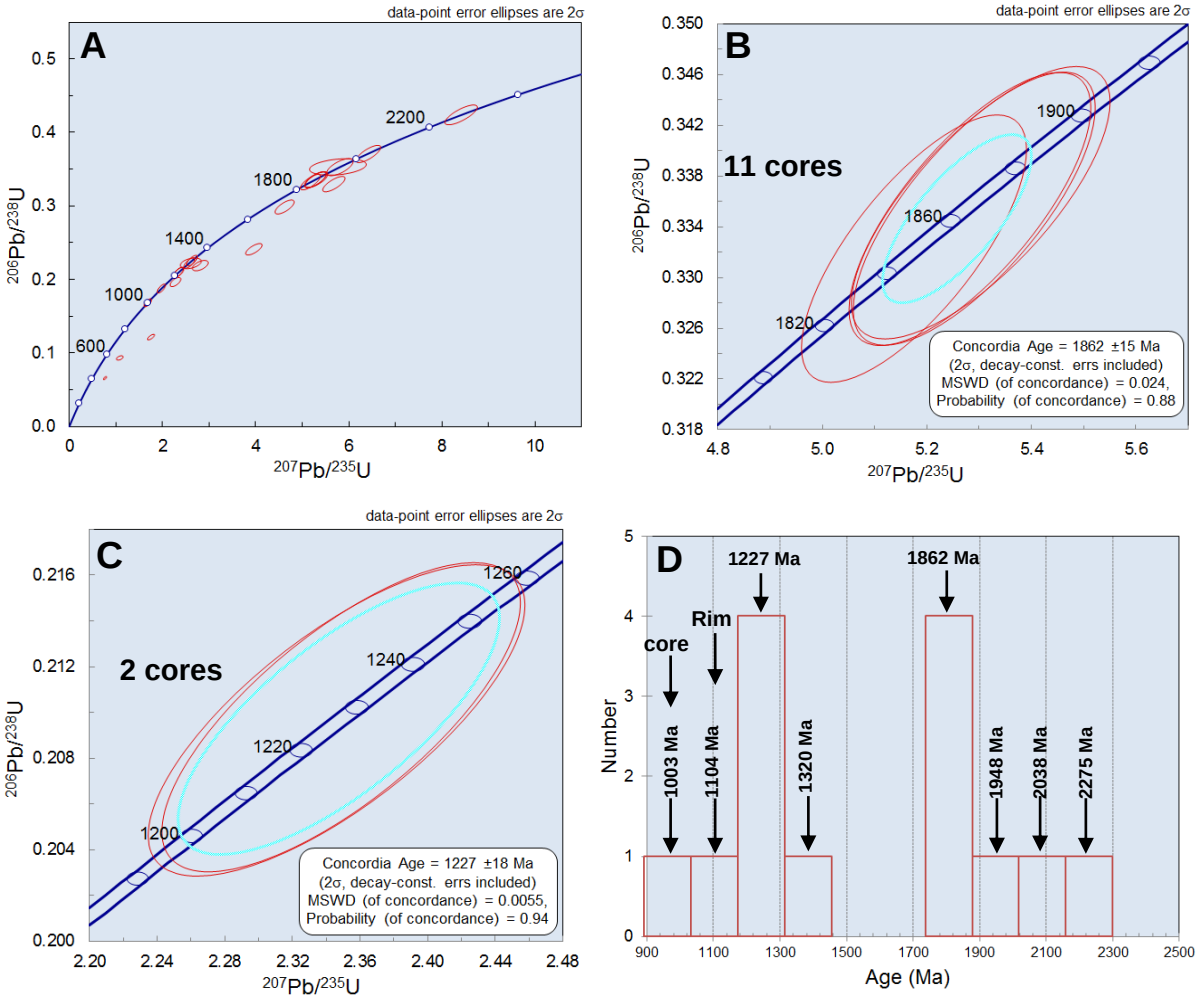

Figure 4-12: (A) $^{206}Pb/^{238}U$ versus $^{207}Pb/^{235}U$ Wetherhill Concordia diagram for LA-ICP-MS U-Pb ages data for zircons from sample MA15042, showing all the concordant and discordant ages obtained from 102 spot analysed on 82 zircons (C) Enlarged LA-ICP-MS U-Pb concordant plot for detrital zircons age population of 1862 Ma. (D) Enlarged LA-ICP-MS U-Pb concordant plot for detrital zircons age population of 1227 Ma. (F) Relative probability distribution plots for $^{207}Pb/^{206}Pb$ age data showing the concordant detrital zircons age populations for sample MA15042.

4.4 SUMMARY

A summary of the results of the four samples were collected from the Eureka Shear Zone are as follows:

- **MA15077 Eureka grey gneiss**

In the Eureka grey gneiss, different variety of zircons (euhedral to anhedral type) gave a wide spectrum of concordant ages between 2029 and 1262 Ma. The zircons are interpreted to be detrital and suggest that Eureka grey gneiss formed through sedimentary processes. The dominant concordant age population is recorded at 1297 ± 8.5 Ma. One zircon gave the youngest concordant rim age of 557 Ma and oldest inheritance age in a sample is recorded on zircon core at 2029 Ma.

Stellenbosch University https://scholar.sun.ac.za

- **MA15042 Restitic granulitic pelite**

A variety of detrital ages between 1999 Ma and 1197 Ma are recorded in this unit. The dominant detrital zircon population is represented by dominantly euhedral to subhedral zircon cores; core overgrowth rims gave a concordant age population of 1212 ± 4.3 Ma. Series of other age populations are recorded at 1262 ± 7.4 Ma, 1300 ± 9.2 Ma, 1322 ± 12 Ma, 1243 ± 15 Ma, 1681 ± 19 Ma and 1778 ± 19.

- **MA14069 Quartzo-feldspathic gneiss**

Eleven zircon grains in the quartzo-feldspathic gneiss (MA15069) gave a single concordant age peak at 1207 ± 6.9 Ma. This age is interpreted to be crystallization age of this unit.

- **MA14027 Leucocratic porphyritic granite**

The youngest concordant age in a sample is recorded at 1003 Ma. The age was obtained from the zircon core and was interpreted to represent the crystallization age of the granite. The leucocratic equigranular granite (MA14027) intrudes syn-D_4 shearing and the crystallization age of granite will be useful is determining the timing of shearing.

Stellenbosch University https://scholar.sun.ac.za

CHAPTER 5: STRUCTURE

5.1 INTRODUCTION

Deformation (D_4) shearing in the study area is considered to have affected an area of up to 25 km wide, extending from the Marshall Rocks-Pofadder Shear Zone (MRPSZ) in the south and up noth to the Eureka Shear zone (ESZ) (Figure 5-1). Within this area, the structural elements and boundaries of the ESZ have not previously been defined. In order to outline the structure of the ESZ and delineate the boundaries of ESZ, a brief study was also carried out on the MRPSZ. Due to the complexity of the structures, the study area was subdivided into three structural domains based on litho-tectonic units and orientation of shear fabrics in order to compare and contrast the structural elements of the two shear zones. The three main structural domains identified are (1) the Eureka Shear Zone (ESZ), (2) the Intermediate (ISZ) and (3) the Marshall Rocks-Pofadder Shear Zone (MRPSZ) domains (Figure 5-1).

The ESZ domain is situated in the northern part of the study area and is characterized by a ~15 km wide region of dominantly WNW to NW striking shear fabric and large distinct shear bounded lithotectonic slices hosting the strongly sheared EC and MQ (Figure 5-1). The ISZ domain is represented as a 4 km wide zone that lies between the ESZ and the MRPSZ domains (Figure 5-1). This domain is characterised by a main NW-SE striking shear fabric and large intrusive bodies of variably sheared leucocratic equigranular granite dyke and mesocratic porphyritic granite that resting within a strongly deformed migmatitic banded gneiss (Figure 5-1). The MRPSZ is the southernmost domain of the study area and covers up to ~6vkm wide and WNW-striking MRPSZ *sensu stricto*. This chapter will mainly focuses on the D_4 structural elements of the ESZ domain (described in detail in section 5.3). These are later compared to those found in the MRPSZ and ISZ domins (described in detail in section 5.5).

The ESZ domain is further subdivided into two structural subdomains, i.e. the Eureka Complex (EC) and the interlayered amphibolites and quartzo-feldspathic gneiss (MQ) subdomains (Figure 5-8a). The reasons for these subdivision are: 1) each subdomain domain contains unique lithologies with distinctive rheological properties, 2) the orientations of the shear fabrics varies greatly across the main ESZ domain and within both the EC and MQ subdomains (Figure 5-8a) and 3) the contact between the rocks EC and MQ subdomains are characterized by phyllonite bearing zones that are considered as cryptic thrusts due to the difference age and structural cut-off between the two packages (discussed later in chapter 6). Since each subdomain contains significant variation in the style of S_4, L_4 and F_4 fabrics, this chapter will describe (in this order) the structural components and microstructure (presented in section 5.3) and spatial variation of these fabrics elements using stereonets plots, with reference to selected geographical locations within the subdomains (section 5.4). Cross-sections are drawn across the structural domain were there are good rock outcrop exposure (section 5.4). The structure of the Intermediate and MRPSZ domains are described briefly in section 5.5 and section 5.6 describes significant post D_4 shearing structures observed in the ESZ domain and across the study area. Prior to the description of D_4 structural elements of the ESZ domain, the existing D_4 structural nomenclature of the area is outlined in section 5.2.

Stellenbosch University https://scholar.sun.ac.za

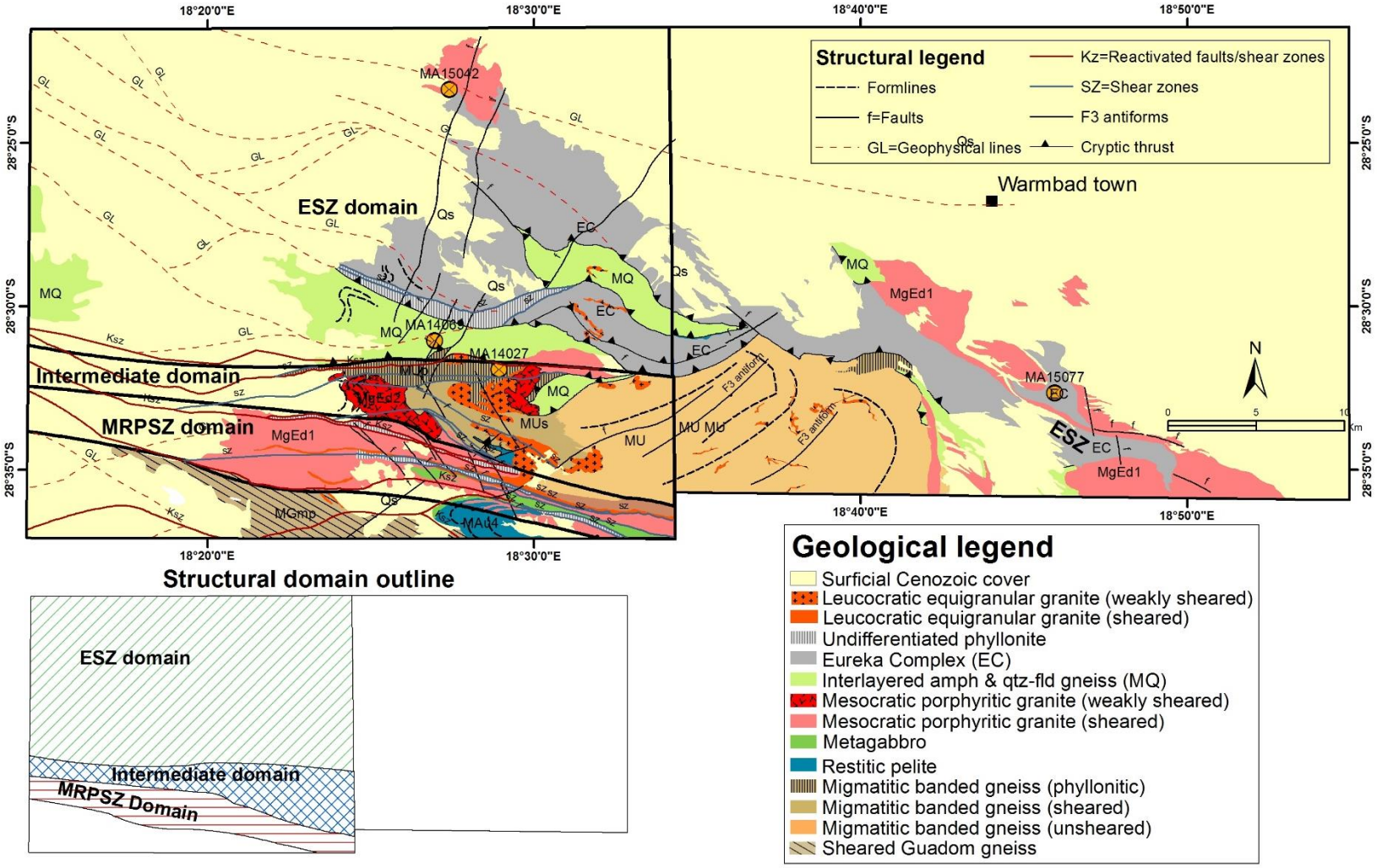

Figure 5-1: Simplified geological map of the study area showing three structural domains; Eureka shear zone (ESZ), Intermediate domain (ISZ) and Marshall Rocks-Pofadder Shear Zone (MRPSZ) domain.

Stellenbosch University https://scholar.sun.ac.za

5.2 STRUCTURAL NOMENCLATURE

In the study area, the main deformation episode D_4 (described in detail in Chapter 2; section 2.3) is subdivided into four deformation stages D_{4a}, D_{4b}, D_{4c} and D_{4d} that overlap and cross-cut in time during progressive shearing as summarised in Table 5-1. In the MRPSZ, the structural imprints imposed by these deformations stages covers a region of approximately 1-5 km north and south of the MRPSZ core zone (Figure 5-1) (Colliston et al., 2014; Lambert, 2013; Macey et al., 2015).

In this study, these deformation stages are not fully recognized. The reasons for this are: (1) in the field area, the MRPSZ is much wider, with moderate rock outcrop exposures that are extensively intruded by leucocratic equigranular granites and pegmatites and making it difficult to map out and identify D_{4a}, D_{4b}, D_{4c} and D_{4d} domains separately at a scale of 1:50 000. (2) Although the timing of shearing relationship in both the ESZ and MRPSZ is interpreted to be similar based on the age relationship between the leucocratic equigranular granites (discussed in Chapter 6, section 6.5). The nature and style of the structural components observed in the ESZ do not entirely fit with those previously observed and/or documented in the MRPSZ. Therefore, this study will in general consider the D_4 fabric in the ESZ and MRPSZ to be both characterized by a foliation (S_4), mineral stretching lineation (L_4) and folding (F_4), but character and style of structural components of the ESZ domain will be described in detail and compared to those found in the MRPSZ.

Stellenbosch University https://scholar.sun.ac.za

Table 5-1: Summary of the D4 deformation subdivisions in the study area. Compiled using data from: (Colliston and Schoch, 2013; Lambert, 2013; Macey et al., 2015)

EARLY NEOPROTEROZOIC	**D4 SHEARING (MARSHALL ROCKS-POFADDER, SHEAR ZONE ~1000-950 Ma)**	**D_4**	D_{4d}	Late brittle deformation overprinting D_{4a} D_{4b} D_{4c} fabrics	Mylonitized-brittle breccia domains overprinting D_{4c} ultramylonites	PROGRESSIVE DEVELOPMENT OF F4 (OPEN-TIGHT ISOCINAL FOLDS)
			D_{4c}	Accommodation of progressive deformation	Oblique high strain deformation associated with discrete mylonites and ultramylonites overprinting earlier D_{4a} and D_{4b} fabrics	
			D_{4b}	Shear zone core development brittle-ductile deformation (amphibolite-greenschist facies)	Development of S_{4b} and L_{4b} fabrics due to the strain increments into the shear zone	
			D_{4a}	Initial shear zone formation ductile deformation & drag of wall rocks (amphibolite facies)	Ductile rotation and folding of the pre-existing planar (S_2/S_4) and linear fabrics (L_2/L_4) of the gneissic wall rocks into the shear zone	

Stellenbosch University https://scholar.sun.ac.za

5.3 THE STRUCTURAL COMPONENTS OF THE EUREKA SHEAR ZONE DOMAIN

Deformation D_4 in the ESZ is characterized by the development of a dominant NW-SE striking foliation (S_4) (section 5.3.1), mineral stretching lineation L_4 (section 5.3.2) and a folding event F_4 (section 5.3.3). This section will discuss the S_4, L_4 and F_4 fabrics found in the ESZ domain. These fabrics are locally associated with the development phyllonitic, cataclasite and mylonitic textures within the host rocks. As a result, in order to study the conditions of shearing of the ESZ domain, microstructures from oriented samples of strongly sheared fault rocks of the ESZ domain are also described in section 5.3.4. However, due to the large variation in the geometry of structural components within the ESZ domains, their distribution and style will only be discussed in section 5.4.

5.3.1 S_4

In the ESZ domain, S_4 is characterized by a strong penetrative planar foliation. At a mega scale, the foliation fabric in the ESZ record as ~20 km-wide and NW-SE lineaments (Figure 5-2). Although the foliation appears to be a dominantly striking NW-SE at aerial view, in the field, there are significant variations to this geometry. In the northwestern part of the ESZ domain the foliation strike toward the NNW (~340°) (Figure 5-2), whereas southwest of the ESZ domain the foliation strike closely toward the NW (~325°) (Figure 5-2). The only major deviation in the geometry of the foliation is observed at the southeastern part of the domain where foliation form a mega NE trending bent structure (Figure 5-2). At outcrop scale, the foliation generally varies from: (1) decametre-scale wide and shallow to subvertical penetrative fabric in moderately deformed domains and (2) localised discrete steeply dipping (>70°) penetrative fabric in strongly deformed domains. The latter, is usually found wrapping around the margins of the former and forming large scale moderately sheared lozenges surrounded by strongly sheared rocks at the margins. In moderately deformed domains, majority rock units tend to have a gneissocity texture that locally grades into a phyllonitic texture (Figure 5-3a). In strongly deformed domains the foliation is discrete and is usually associated with the development of cataclasites, phyllonites and few localized outcrop scale cataclastic-mylonitic textures (Figure 5-3a). The differences in foliation intensity recorded on the rocks of the ESZ (dominantly the Eureka grey gneiss, mesocratic porphyritic granite, quartzo-feldspathic gneiss and amphibolites) are described as following.

Stellenbosch University https://scholar.sun.ac.za

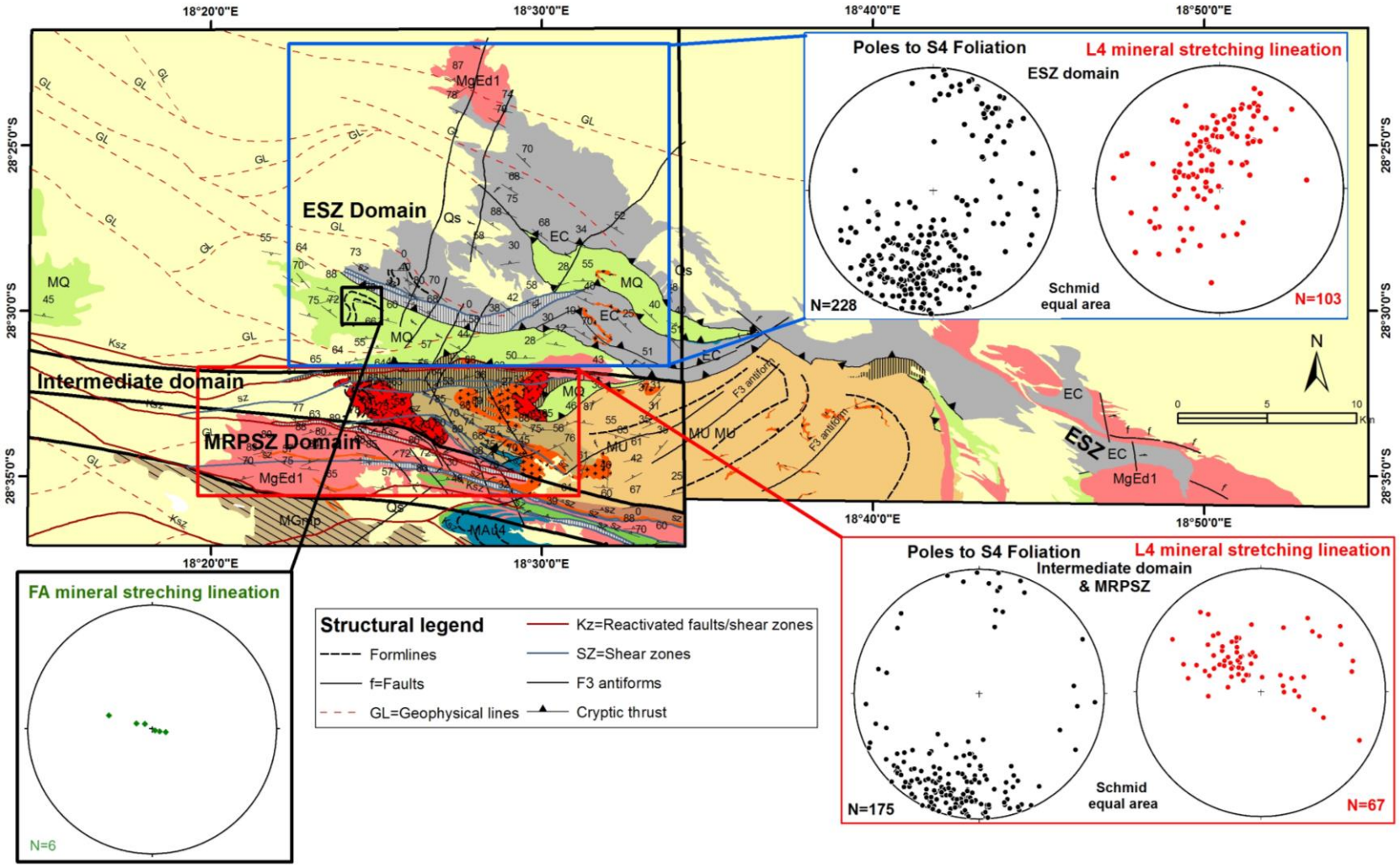

Figure 5-2: Simplified geological map of the study area, showing geometries of the D_4 fabric in the ESZ, MRPSZ and Intermediate domain.

Stellenbosch University https://scholar.sun.ac.za

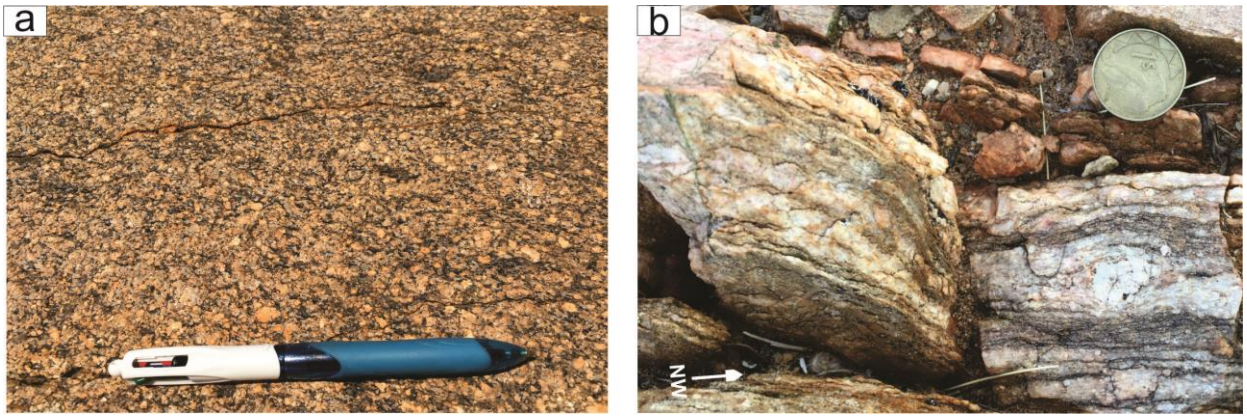

Figure 5-3: (a) Cataclasites of the leucocratic equigranular granite (b) Outcrop localized cataclasite and mylonite of the quartzo-feldspathic gneiss.

In strongly deformed domains of the meta-psammitic rocks (for example the Eureka grey gneiss), the foliation at meso-scale is usually distorted and associated with either chaotic folds or truncated by anatomising discrete shear zones (Figure 5-4a). The discrete shear zones are commonly hydrothermally altered and dominated by chlorite, white mica (sericite), potassium metasomatism, epidote and diopside. (Figure 5-4b). In some localities, were biotite and muscovite rich layers are present, kink folds (Figure 5-4c) and crenulation cleavage are developed. Crenulation cleavage usually have a foliation planes sub-parallel to the fold axis of biotite and muscovite micro-folds. When this textures are found the protolith could not be deduced and the unit is considered to be a phyllonite. In localities were they are phyllonitic zones are wide enough; they are mapped out as undifferentiated phyllonite belts (Figure 5-8). In petrographic section, mica domains (biotite, muscovite and chlorite) are usually observed growing subparallel to each other (Figure 5-4d) and defining the foliation (syn-deformation growth), but few grains grows oblique to it (late to post deformation growth). Sericite, epidote diopside are disseminated across the textures and probably represent a post D_4 alteration. Retrograde metamorphism at upper to mid greenschist facies is defined by a replacement of biotite to muscovite and subsequently, muscovite to chlorite (Figure 5-4d).

In the mesocratic porphyritic granite and quartzo-feldspathic gneiss, the foliation in moderately deformed domains at outcrop scale is characterized by a sub-parallel alignment of augen to sigmoidal microcline porpyroclasts that are separated and surrounded by biotite domains (Figure 5-4e). In strongly deformed domains, microcline porphyroclasts are deformed into delta and sigma clasts, associated with various smaller sized sub-rounded to angular porphyroclasts (Figure 5-4f). In the mafic rocks (amphibolite and metagabbro), the foliation is represented by sub-parallel alignment of hornblende separating elongated quartz grains.

In summary, S_4 is dominantly defined by a NW-SE striking, moderate to steeply dipping foliation accompanied by mid to upper greenschist facies retrogressed assemblages and by the development of cataclasite to mylonitic textures. The foliation observed in the ESZ domain is shows some resemblances to S_{4b} of the MRPSZ domain (discussed in section 5.5.1). However, stereonets plots in Figure 5-2 shows that foliation in the ESZ domain is dominantly striking NW-SE and dipping moderately to steeply toward the NE and SW. This geometry differs from the S_4 of the MRPSZ and Intermediate domain that is

Stellenbosch University https://scholar.sun.ac.za

dominantly striking WNW-ESE and dipping steeply to the NNE and SSW (Figure 5-2) and hence, making the orientation of the foliation ESZ domain unique from that of the MRPSZ and intermediate domain (Figure 5-2).

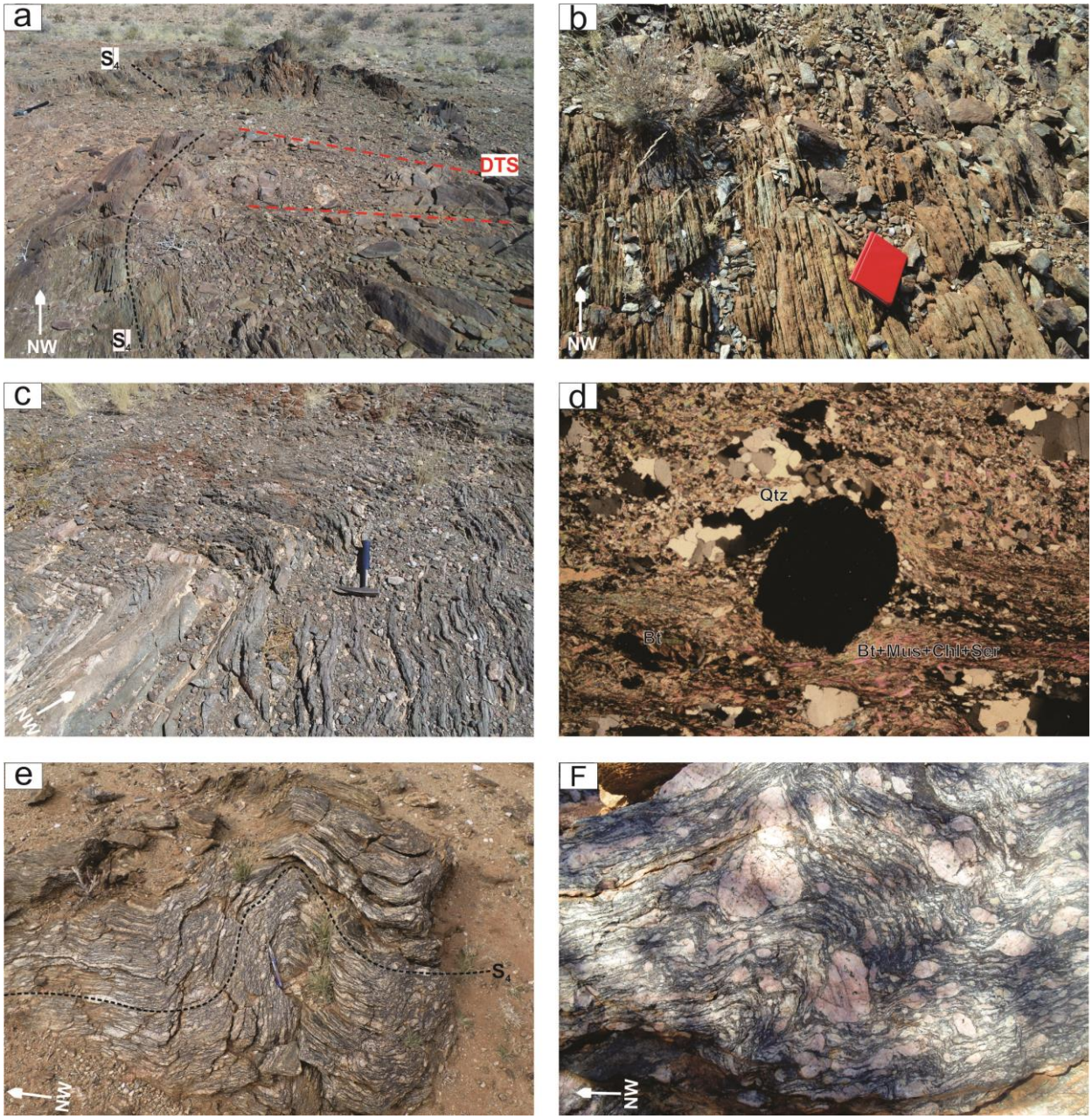

Figure 5-4: (a) S_4 shear foliation in phyllonites of the ESZ domain transposed by outcrop scale discrete truncating shear zones (DTS). (b) Chlorite and sericite rich phyllonites, hydrothermal altered and retrogressed at greenschist facies. (c) Kink folds associated with crenulation cleavage in a biotite-muscovite rich phyllonite. (d) Photomicrograph (FOV=2 mm) of a garnet-quartz-muscovite-biotite phyllonite form the sourthern margin of the ESZ Domain. The phyllonite groundmass is dominated by lamellae of biotite, muscovite, sericite and chlorite. Muscovite is growing within biotite. Sericite and chlorite are disseminated within the rock matrix. Garnet occurs as mantled sigma porphyroblast. Some quartz and biotite are dynamically recrystallized and confined to the tails of the garnet porphyroblast. FOV = Field of view. XPL=Cross polarised light. (e) Near isoclinal tight folding in the sheared mesocratic porphyritic granite. Potassium feldspar porphyroclasts are stretched and separated by biotite. (f) Proto-mylonite texture in the mesocratic porphyritic granite. Potassium feldspar porphyroclasts are sheared into rotated delta and sigma porphyroclasts. Biotite and quartz are deformed into a dark fine grained aggregates (phyllite) wrapping around potassium feldspar prophyroclasts. Progressive shearing in the pronto-mylonite texture was probably accompanied by the development of asymmetrical kink folds (Field of view=~25 cm).

Stellenbosch University https://scholar.sun.ac.za

5.3.2 L_4

Mineral stretching lineation (L_4) in the study area is defined by a strong penetrative stretching of the quartz and potassium feldspar minerals on the S_4 surfaces (Figure 5-5a and Figure 5-5b) as well as in hinge lines of various asymmetrical folds. The trend and plunge of L_4 varies across the ESZ domain (Figure 5-2) and will be discussed in section 5.4. In the quartzo feldspathic gneiss, quartz is usually stretched into sets of elongate aggregates or occurs as elongated ribbons. Potassium feldspars occurs as streaky aggregates alternating with micas (commonly biotite). In the fold hinge zone, a linear stretching of potassium feldspar is usually common and oriented subparallel to the fold axis (Figure 5-5c). In low grade mylonites (cataclasites-proto-mylonite) of the quartzo-feldspathic gneiss, L_4 occurs as cataclasite lineation defined by a linear alignment and stretching of sub-rounded to elongated potassium feldspar alternating with quartz ribbons on the foliation surface (Figure 5-5d). In the amphibolites, L_4 is rarely seen but in some localities; it occurs as elongated lumps or clustering of hornblende and actinotite on the S_4 surface.

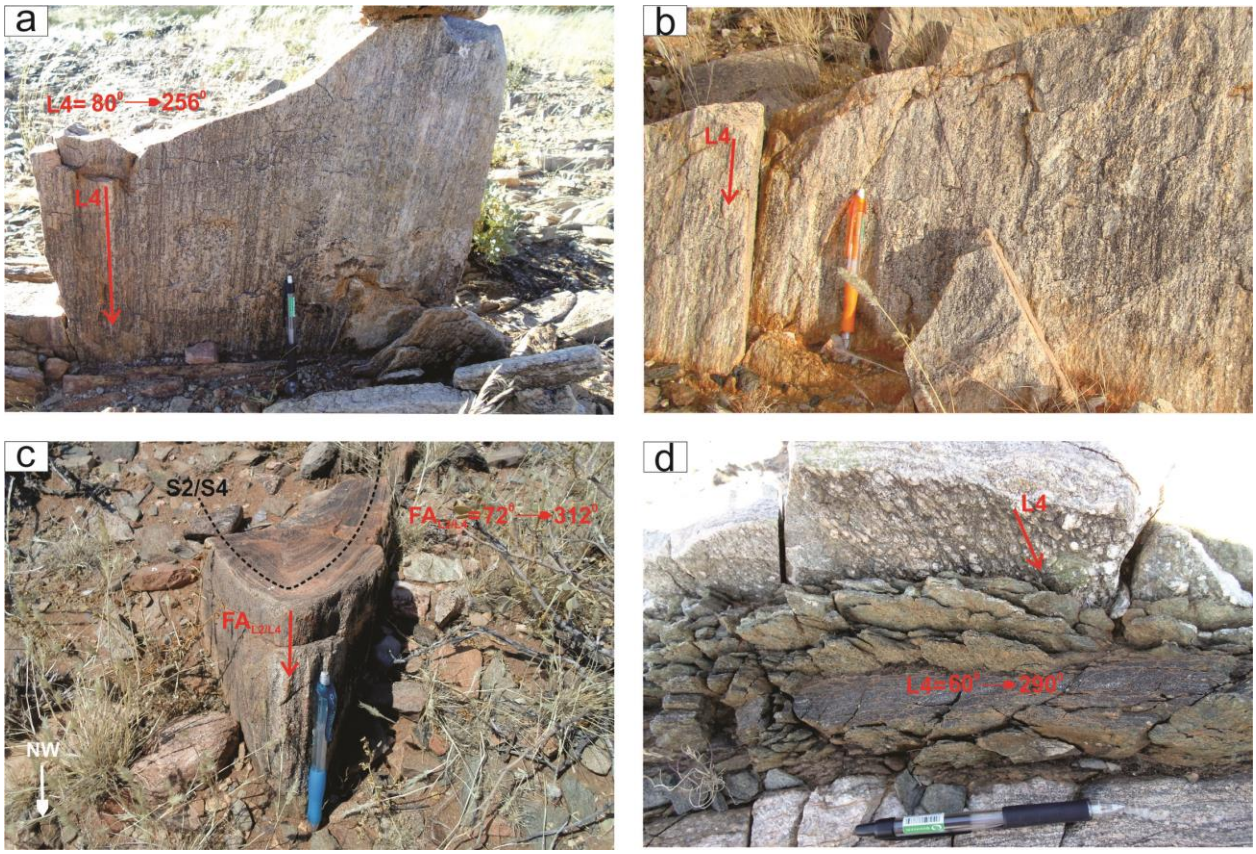

Figure 5-5: (a and b) Near vertical plunging stretching lineation (L_4) in the quartzo feldspathic gneiss dominantly defined by a series of linear elongated threads of potassium feldspar (c) L_4 characterized by the elongation of potassium feldspar in the hinge zone of a NW steeply plunging asymmetrical fold within the quartzo-feldspathic gneiss (FAL_4). (d) Cataclastic lineation, shown by both sets of parallel linear aligned/stretched of sub-rounded to elongated potassium feldspar porphyroclasts in the low-grade mylonites of the quartzo-feldspathic gneiss.

Stellenbosch University https://scholar.sun.ac.za

5.3.3 **Folding**

The majority of folds observed in the ESZ domain occur within the MQ package. The folds are mostly asymmetrical, SW verging, NW trending and associated with various S and Z type parasitic intrafolial folds (Figure 5-6a). The generation of the folds is poorly understood, but they are considered to have developed as a function drag folding of earlier developed S_4 fabrics and/or inherited S_2 fabrics (termed: S_2/S_4 in this study). In some localities, fold limbs are also transposed by the D_4 shear zones at different scales, making it difficult to link and reconstruct the overall main folding domains (Figure 5-6a). Depending of the shearing intensity the interlimb angle varies from close in moderately sheared domains to tight in highly strained domains (Figure 5-6b). The folds normally show stretching/extension in direction sub-parallel to the S_4 (NW-SE strike orientation) and are accompanied by shortening in the NE-SW direction. Although steeply NW steeply plunging are folds are common, few shallow plunging NW trending folds are observed in some localities (Figure 5-6c). Discrete S_4 is usually oriented sub-parallel to the fold axis (Figure 5-6c) and in places re-orientating and transposing the limbs of the pre-existing S_2 or earlier S_4 fold generation.

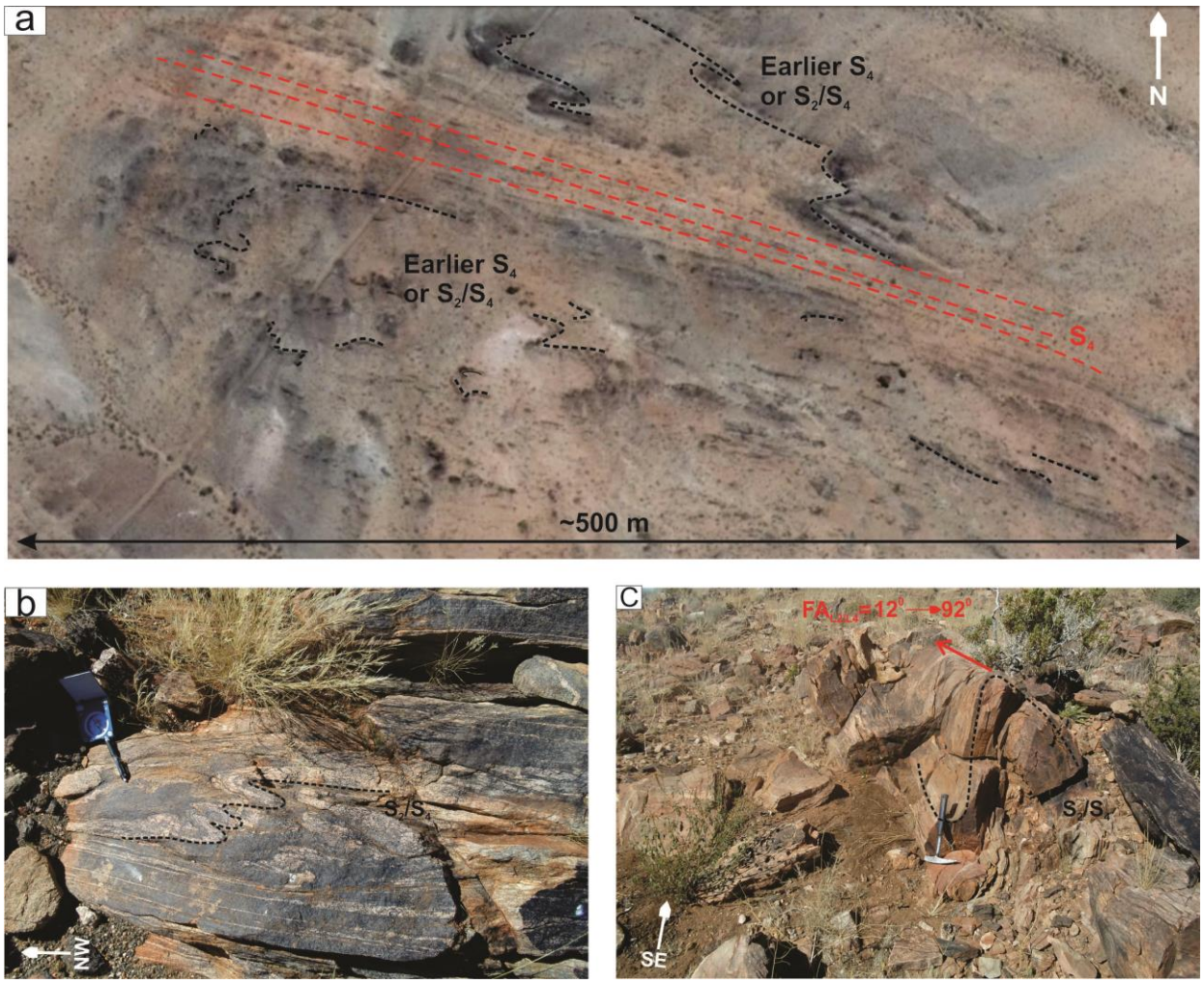

Figure 5-6: Google earth image showing asymmetrical folded amphibolite marker horizons in the ESZ domain. Folds are tightened and their limbs are transposed by the D_4 shear zones. (b) Folded leucosome layer of the Eureka grey gneiss showing the typical steeply dipping SW-verging intrafolial asymmetric folds in the ESZ domain. (c) ESE trending, shallow plunging and tight asymmetrical folded quartzo-feldspathic gneiss.

Stellenbosch University https://scholar.sun.ac.za

5.3.4 **Microstructure**

Various structural oriented thin section from strongly deformed rocks were studied to determine the kinematics and shearing condition (brittle or ductile or both) in the ESZ domain. These are comprised of samples from the mesocratic porphyritic granite (Figure 5-7a), quartzo-feldspathic gneiss (Figure 5-7b), amphibolite (Figure 5-7c) and leucocratic equigranular granite (Figure 5-7d). In the field, these rocks showed a strong fabric with rotated potassium feldspar and quartz porphyroclasts, both resting and wrapped around by a fine grained matrix. L_4 is usually well pronounced on the foliation surface. However, at microscopic scale majority of the textures showed a matrix grain size textures with irregular grain boundaries that is often overprinted by brittle fractures propably related to D_5 deformation. Thus, making it difficult to identify various microfabrics and shear sense indicators. Detailed microstructure description structural oriented thin sections are as following.

The mesocratic porphyritic granite (Figure 5-7a), shows a strong intercystalline deformation and recrystallization texture; indicated by strong undulose extinction and irregular grain boundaries in various grain sizes of quartz and potassium feldspar (Figure 5-7a). Quartz is preserved as small fine grained polycrystalline grains (<1.5 mm). Potassium feldspars (microcline) porphyroclasts are irregular shaped, altered to sericite and have few internal grain microfractures. However, some larger potassium feldspar grains (> 2mm) appear flatted and elongated subparallel to L_4 (Figure 5-7a). Potassium feldspars are separated and/or wrapped around by a muscovite dominant and few biotite mica domains. Mica domains have a complex internal structure, comprised of biotite truncated by discrete sub-parallel microscale shear zones (Figure 5-7a).

In the quartzo-feldspathic gneiss (Figure 5-7b), micas are scarce and the shear fabric is defined by lenses of recrystallized and sericitized feldspars separated by elongated recrystallized quartz veins (Figure 5-7b). Quartz veins have strong undulose extinction, extremely elongated and extending across the petrographic section field of view (FOV= 4.5 mm) (Figure 5-7b). The elongated quartz veins have straight grain boundaries, uniformly layered in the rock texture and aligned sub-parallel to the L_4 (Figure 5-7b). The overall groundmass matrix shows variable grain sizes of both quartz and altered potassium feldspars with irregular grain boundaries (Figure 5-7b).

Amphibolites (Figure 5-7c), shows reticular brown hornblende resting in the groundmass of sericitized plagioclase associated with some epidote/chlorite alteration. The Leucocratic equigranular granite (Figure 5-7d), shows strong undulose extinction of quartz and potassium feldspar with irregular grain boundaries. The rock texture is fragmented and overprinted by a E-W trending fault breccia (D_5) filled with ±chlorite, diopside and epidote. In summary, all microstructures display evidence for ductile structures that are in places overprinted by D_5 fault breccia. No significant shear sense indicators are observed from the microstructures of the ESZ domain.

Stellenbosch University https://scholar.sun.ac.za

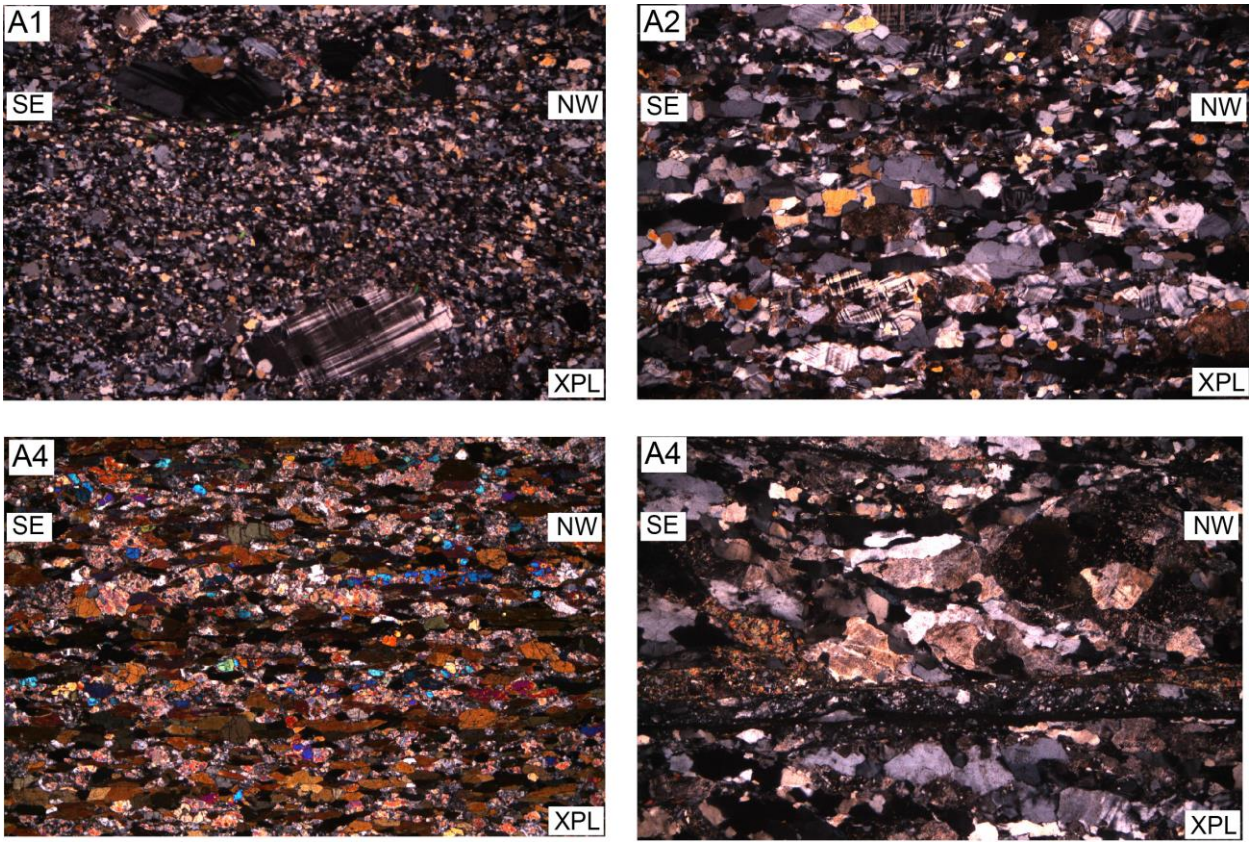

Figure 5-7: Photomicrograph of oriented structural samples from strongly sheared rocks of the ESZ: (A1) mesocratic porphyritic granite. (A2) quartzo-feldspathic gneiss, (A3) Amphibolite, and (A4) leucocratic equigranular granite. (FOV =4.5mm). FOV = Field of view. XPL=Cross polarised light. See text for description.

Stellenbosch University https://scholar.sun.ac.za

5.4 DISTRIBUTION AND STYLE OF THE STRUCTURAL COMPONENTS

The ESZ domain is subdivided into two structural subdomains, i.e. the Eureka Complex (EC) and the interlayered amphibolites and quartzo-feldspathic gneiss (MQ) subdomains (Figure 5-8a). This section describe in detail the distributions and styles of the S_4, L_4 and F_4 fabrics within the ESZ domain. The structural data plotted in stereonets is grouped into several areas (EC1, EC2, EC3, EC4, MQ1 MQ2 MQ3 and MQ4) that dominantly shows common similarities in geometry and rock types (Figure 5-8a). The orientations of the fabrics are described with the help of the stereonets plots and are further strengthened by field observation.

5.4.1 **Eureka Complex Subdomain**

The EC subdomain is restricted to the northern part of the ESZ domain and is characterised by the lithotectonic package hosting the rocks of the EC. This section will describe the orientation of the S_4 and L_4 and F_4 within the EC-subdomain. In the northwestern extension of the EC subdomain (Figure 5-8a, area: EC1) the dominant S_4 strike is WNW-ESE and dips steeply between 65˚ and 80˚ (Figure 5-8a, area: EC1). The stretching lineation was not observed due to poor rock outcrop exposure. Toward the southeast (Figure 5-8a, area: EC2) rock exposure is poor and S_4 maintains a WNW-ESE strike and moderate to subvertical dip. The stretching lineation (L_4) dominantly plunges shallowly toward the WNW. Further south-east (Figure 5-8a, area: EC4), the rocks of the EC and MQ are interfolded by a NE trending, shallow to moderate plunging mega-scale fold covering an area of approximately 30 km^2 (Figure 5-8a, area: EC4). Within the mega fold zone, S_4 gently rotates from; 1) NE dip in the eastern limb, N dip in the mega fold hinge zone and NNW dip in the western limb (Figure 5-8a, area: EC4). The dip angle is dominantly moderate and L_4 is dominanly down dip and plunges between NNE and NNW. Fold axis lineation (FAL_4) measured on the parasitic intrafolial folds of the mega fold in this area plunges moderately too steep toward the N and NE direction (Figure 5-8a, area: EC4). The orientation of FAL_4 in this area (Figure 5-8a, area: EC4) reflects the attitude of the mega-scale fold hinge zone. In the mega fold hinge zone, intrusive dykes of moderately sheared leucocratic-equigranular granite (up to 100m thick) are folded as NW trending, slightly SW verging, tight folded dykes. The folds sizes measured on the intrusive dykes display a wavelength in the range 250 m to 500m with an amplitude of 460m and 900m, respectively (Figure 5-8a, area: EC4 and Figure 5-8b, cross-section profile: a-b).

Stellenbosch University https://scholar.sun.ac.za

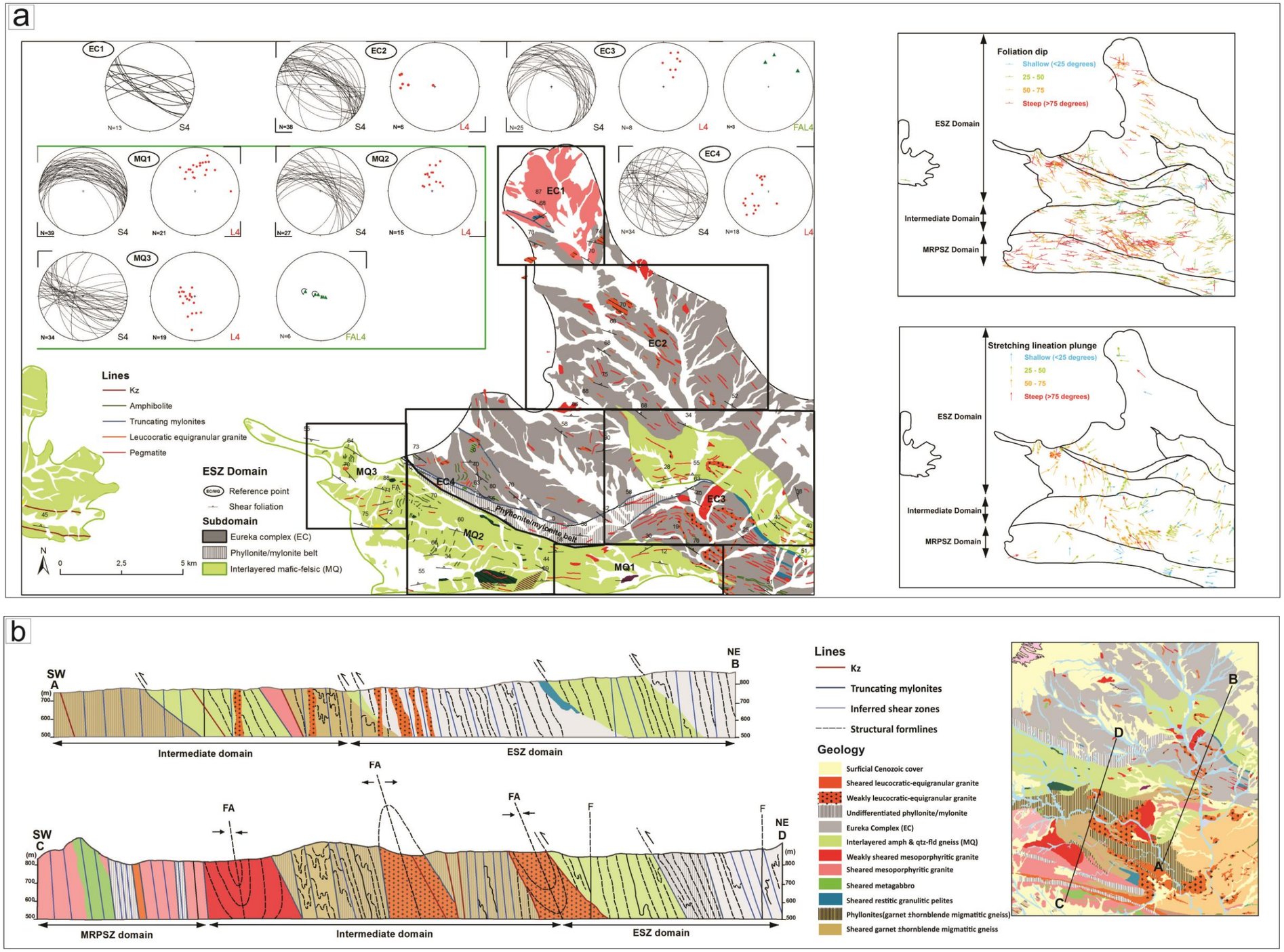

Figure 5-8: (a) Map showing overall lateral extent and geometry of the shear fabric in the ESZ domain. Map also shows the sigmoid shaped litho-tectonic slices of the MQ (Green) and EC (grey) in the ESZ domain. The streonets plots are plotted for both foliation and lineation with reference to specific geographic location. The overall geometries of foliation and lineation for all structural dominas is also dislplayed on two thematic maps (top right). (b) Schematic cross-sections are drawn along the profile A-B and C-D. The formlines on the cross-sections shows that the majority of the asymetrical folds in the ESZ are dominately pluging near vertical. Steeply dipping foliations are commonly recorded along the discrete shear zones. See the text for detailed description.

Stellenbosch University https://scholar.sun.ac.za

5.4.2 The Contact between the Eureka Complex and Interlayered Amphibolites and Quartzo-Feldspathic Gneiss Subdomains

In the west (Figure 5-8a, area: EC4), the contact between the rocks of the EC and MQ subdomain is gradational and marked by a continuous NW-trending (~1km thick) high strain belt (phyllonite-mylonite belt) that sheared the majority of the units from both subdomains into phyllonites, cataclasite and protomylonites (Figure 5-8a, Figure 5-8b and Figure 5-9a). S_4 along the high strain belt strike NW at a moderate to steep dip (50^0-80^0). Some foliation show a variety of shallow to steep dip toward the north, west and east (Figure 5-8 a, area: EC4 and Figure 5-9a). This orientation is consistent with the field observation that some of marker horizons (dykes of leucocratic-equigranular granite, pegmatites and amphibolites) appears to be rotated and drag folded into parallelism with NW striking phyllonite belt (Figure 5-8a, area: EC4 and Figure 5-9 a). L_4 stereonet plot show some L_4 plunging steeply to the NW in the phyllonite belt and others plunging moderately toward the W and SW in the wallrocks of the EC subdomain (Figure 5-8a, area: EC4). In the field, strongly sheared dykes of leucocratic granite and pegmatites are oriented sub-parallel to the NW-striking shear foliation. These dykes are cross-cut by oblique younger generation of weakly sheared leucocratic granite dykes and pegmatites oriented in the direction sub-parallel to the late-post D_4 discrete sinistral shear zone (described in section 5.6) (Figure 5-9a) The overall shear motion in this area at mega scale reflect a dextral-strike slip. However, most of the L_4 are down dip and probably imply a vertical slip component associated with a top to the SW transpressional motion.

Stellenbosch University https://scholar.sun.ac.za

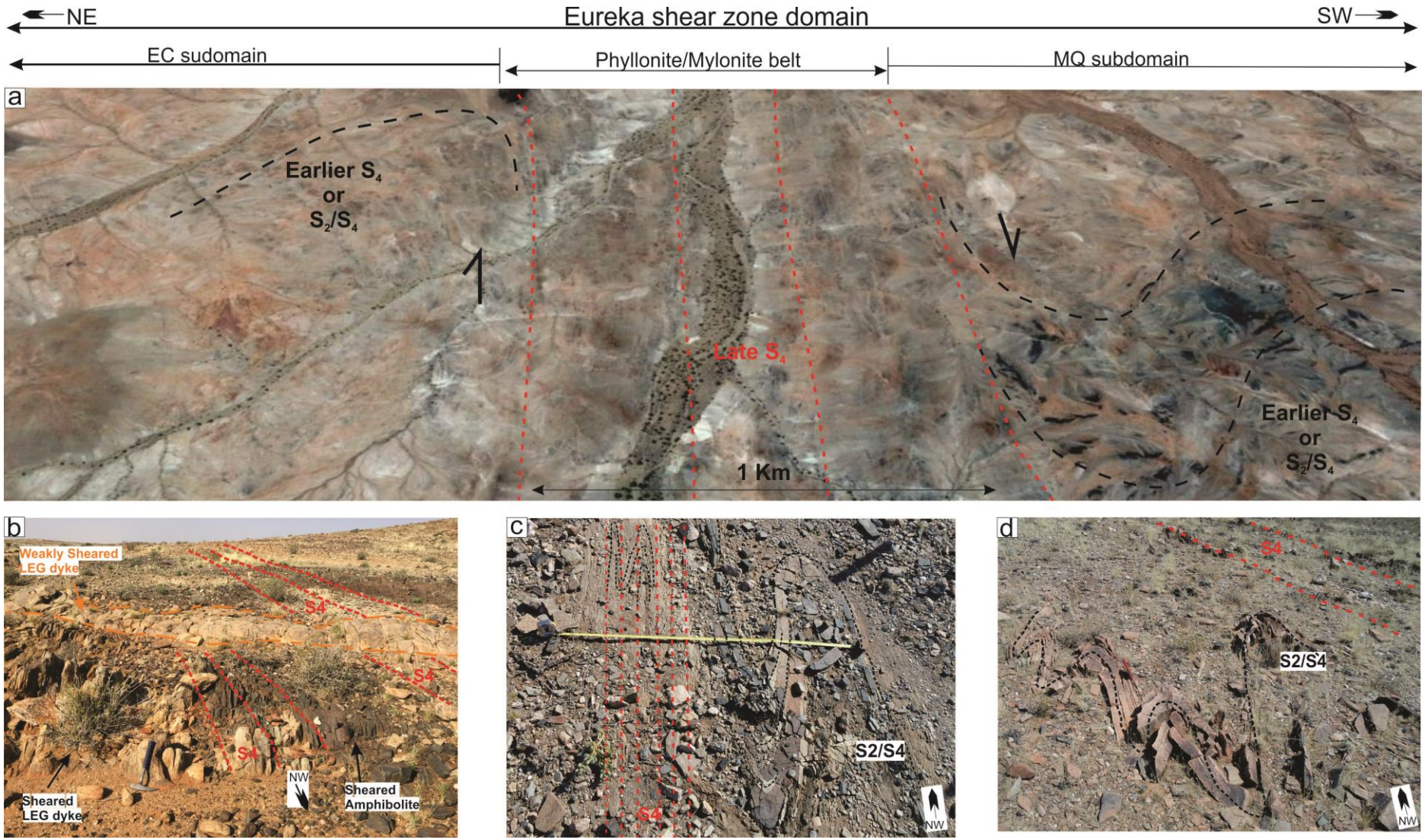

Figure 5-9: (a) Google earth image showing the rotation of the earlier shear foliation into the phyllonite-mylonite belt. The sense of shearing deduced from the drag-fold is consistant with a dextral sense of movement. (b) Foliation subparallel strongly sheared leucocratic equigranular granite (LEG) (ealier syn-shearing generation) and amphibolites, intruded and cross-cut by an oblique weakly sheared dyke (late-shearing generation). (c) Steeply dipping WNW-ESE trending, tight and slightly SW verging asymmetric folds in the MQ. Fold axis of the asymmetric folds are oriented sub-parallel to S_4. (d) S-type asymmetric folds at the southern margin of MQ subdomain.

Stellenbosch University https://scholar.sun.ac.za

5.4.3 Interlayered Amphibolites and Quartzo-feldspathic Gneiss (MQ) Subdomain

The MQ subdomain characterised by the lithotectonic package hosting the rocks of the MQ, is situated south of the EC subdomain and separated from it by a NW-striking phyllonite-mylonite belt (Figure 5-8a and Figure 5-9a). Other sigmoid shaped MQ units are also mapped in the vicinity. In the east (Figure 5-8, area: MQ1), S_4 strike between WNW and NW direction and dips moderately to steeply (35°-75°) . L_4 is down dip and plunging toward the N and NE. In the central part of MQ subdomain (Figure 5-8a, area: MQ2), a series of amphibolites dykes form NW trending asymmetrical folds that are dragged and have their nothren limb transposed at the southern margin of the phyllonite-mylonite belt (Figure 5-9a). S_4 strike WNW and dip steeply along the discrete S_4 zones that transpose the rotated (NW to N striking) S_4 or S_2/S_4 (Figure 5-8a, area: MQ2).

In the northwest (Figure 5-8a, area MQ3), the majority of the rocks are strongly sheared into phyllonites comprising of asymmetric folds with cataclastic and prontomylonitic textures. The asymmetrical folds are WNW-ESE trending, tight and verging toward SW (Figure 5-9c and Figure 5-9d). The size of the folds varies on outcrop scale, but a representative fold was measured with a wavelength and amplitude at (~50cm) and (~30cm), respectively (Figure 5-9c). Lithological units banding contrast between amphibolites and quartzo-feldspathic gneiss units within the folds domain range in the thickness of ~1 to 10 cm (Figure 5-9c). The fold axis are steep and trending WSW to W sub-parallel to the WNW-ESE striking S_4 (Figure 5-8a, area MQ3, Figure 5-9c and Figure 5-9d). S_4 dips subvertical and strike mostly WNW-ESE. The stretching lineations are dominantly down dip (Figure 5-8a, area: MQ3).

In summary, the ESZ domain display evidence for intense shearing with a foliation that varies between WNW and NW. Nevertheless, shearing is partitioned within the domain and intense shearing is dominantly limited to the contact between the rocks of the EC and MQ subdomain (Figure 5-8b, cross-section profile: a-b and c-d and Figure 5-9a). In the south, the rocks of MQ sub domain are in contact with the migmatitic banded gneiss (intermediate domain). This contact is also characterized by a zone of intense shearing. S_4 at the marginal contact dip both shallow and steeply toward the NNE direction with a dominant down dip plunging L_4.

5.5 MARSHALL ROCKS-POFADDER SHEAR ZONE AND INTERMEDIATE DOMAIN

5.5.1 Marshall Rocks-Pofadder Shear Zone Domain

In the MRPSZ domain, the deformation recognised correlates with D_{4b} (summarised in Table 5.1). Strain recorded in this domain is dominantly high and localised in thick layers of phyllonites and/or discrete (~10m thick) layers of mylonite and ultramylonite (Figure 5-10a and Figure 5-11). The fault rocks are strongly altered and coated with epidote, diopside and chlorite consistent with retrograde metamorphism at greenshist facies (Figure 5-10a). The mylonitic foliation (S_{4b}) is extensively intruded by syn-D_4-shearing pegmatites and leucocratic-equigranular granite dykes, both oriented sub-parallel to S_{4b}. A ~100 m thick and ~15 km long sheared leucocratic-equigranular granite dyke (Figure 5-11) intruded the central part

Stellenbosch University https://scholar.sun.ac.za

(core) of the MRPSZ in this part of the area. The shear foliation (S_{4b}) strikes WNW-ESE and dips at a moderate to steep angle (Figure 5-11, area; MRPSZ). The steeply dipping foliations are recorded along truncating mylonite and discrete shear zones (Figure 5-8b, cross-section profile: c-d).The stretching lineation (L_{4b}) varies; some L_{4b} plunge moderately to shallowly toward the ESE and NW direction and a few are plunging shallowly toward the NE direction (Figure 5-11, area; MRPSZ). The NW and SE plunging lineation were commonly recorded on the discrete mylonite zone that are dominantly restricted to the core (Figure 5-10a). The thickness of the MRPSZ domain increases from 3 km in the east to 5 km in the west. Furthermore, the field observation shown a decrease in shearing intensity from east to west shown by the abundance of thick discrete mylonite and ultramylonite layers in the east compared to the west along the shear zone (Figure 5-11).

5.5.2 **Intermediate Domain**

The intermediate domain is characterized by NW thinning zone between the MRPSZ and ESZ domain (Figure 5-11). Intense shearing was mainly recorded within the migmatitic banded gneiss. The shear foliation mostly strike mostly NW-SE, splaying from the MRPSZ domain and anatomised around the moderately weakly sheared mesocratic porphyritic granite (Figure 5-11). The S_4 in the intermediate domain is slightly oblique to the dominant shear (WNW-ESE striking foliation) of MRPSZ and ESZ domain. In the east, intermediate domain is considered to have preserved D_2 L-S fabric, which is the oldest fabric, recognised within the study area. Toward the west D_2 fabrics are dragged and completely transposed into D_4 by shearing (Figure 5-11). In the central part, the intermediate domain is characterized by a two sets of mega-scale, close to tight, NW-SE-trending, SW verging isoclinal folds of variably strained leucocratic-equigranular granite sitting within a highly sheared migmatitic banded gneiss (Figure 5-11). In the west, the domain pinch out where the shear fabric form-lines of the ESZ domain and MRPSZ are rotated toward each other (Figure 5-11).

In the east (Figure 5-11, area: INT1), the amphibolite facies grade shear fabric S_2/S_4 in the migmatitic banded gneiss are dragged and rotated toward the MRPSZ into D_{4a} in the wall rocks and later to a greenschist facies D_{4b} within the core of the MRPSZ. In this region, the foliation (S_2/S_4) strikes NE-SW and the lineation (L_2/L_4) dominantly plunge moderate to shallowly toward the NE direction. In the central part (Figure 5-11, area: INT2), S_2/S_4 is completely transposed and only greenschist facies (retrogressed) S_4 fabric is recognised. In this area, the northern limb of the leucocratic granite fold is truncated by high strained zone that sheared the majority of the rocks into phyllonites (Figure 5-11, area: INT2). The shear foliation strike between SSW and WNW with a shallow to moderate dip. The steeply north dipping foliation was measured on curvilinear late discrete shear zones. The stretching lineation is sub-horizontally toward both NE to ENE and WNW to SW. The fold axis stretching lineation on isoclinal folds (Figure 5-10b) plunge shallowly to moderately toward the WNW (Figure 5-11, area: INT2 and Figure 5-8b). Toward the south and closer to the MRPSZ domain (Figure 5-11, area: INT3) shear foliation has a near-vertical dip and NW-SE strike orientation which is slightly oblique to the WNW-ESE strike orientation of the MRPSZ domain. The stretching lineation are plunging moderately too steep toward the NW. The fold axis stretching lineation varies from shallow to steeply plunging and trend WNW-ESE (Figure 5-10b). In this area, various intrusive dykes (up to 200m thick) of variably sheared leucocratic-equigranular

Stellenbosch University https://scholar.sun.ac.za

granite intrudes both sub-parallel and across the shear foliation. The angle between the orientation of late intrusive sheared dykes and earlier shear fabric is less than ~30^0 (Figure 5-10c). In west (Figure 5-11, Area: INT4) the shear foliation wraps around weakly sheared and folded mesoprophyritic granite (Figure 5-11 and Figure 5-8b, cross-section profile: c-d). The shear foliation is dominantly striking WNW-SE and dipping steeply to N and NE direction. The stretching lineation (L_4) moderately plugging between the NW and NE direction. Amphibolite horizons markers displays an S-type drag fold defined by a top NE rotation at the southern margin of the ESZ domain and bottom SW rotation into the MRPSZ domain.

Mylonites from both the intermediate and MRPSZ domain show good preservation of potassium feldspar rotated porphyroclasts (Figure 5-10d). In the mylonite texture, mica shear bands are made up of biotite that is partly altered to muscovite and chlorite. Few large biotite grains are deformed into biotite fish. Potassium feldspar prophyroclasts are deformed into both sigma and delta clasts (Figure 5-10d). Kinematics deduced from the biotite fish and potassium feldspar shows a dominant dextral sense of shearing (Figure 5-10d).

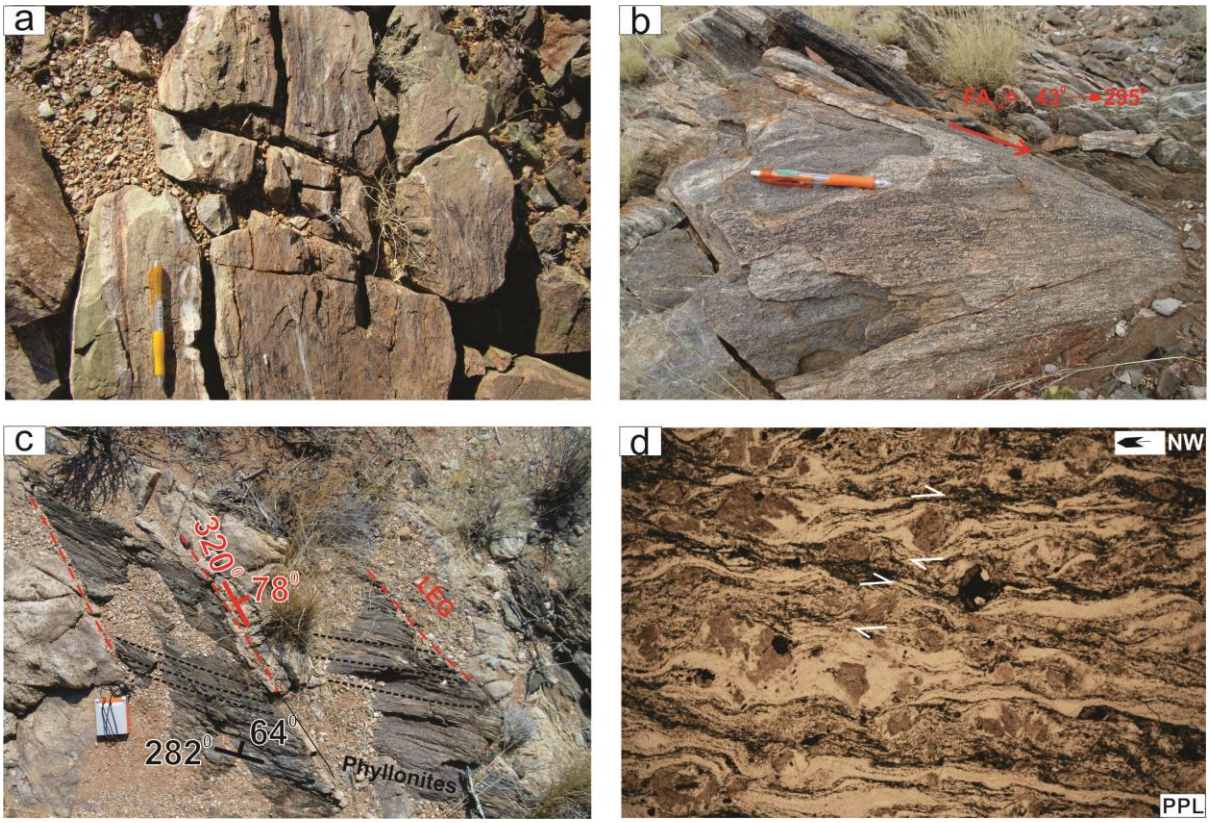

Figure 5-10: a) Outcrop photo of the quartz-feldspar mylonites in the MRPSZ domain. Fault rock texture altered by chlorite, epitode and diopside. (b) Strongly sheared and folded leucocratic equigranular granite. Granite is folded as a close, NW-SE-trending, SW verging and moderately plunging isoclinal fold in the intermediate domain. (c) Undifferentiated phyllonites representing an earlier S_4 shear fabric (black dotted line) cut-off by late D_4 shear zone (black dotted line) that is associated with the intrusion of the leucocratic equigranular granite within the intermediate domain. (d) Representative quartz-feldspar ultramylonites photomicrograph (FOV =4.5mm) with rotated potassium porphyroclasts showing a dominant dextral sense of shearing.

Stellenbosch University https://scholar.sun.ac.za

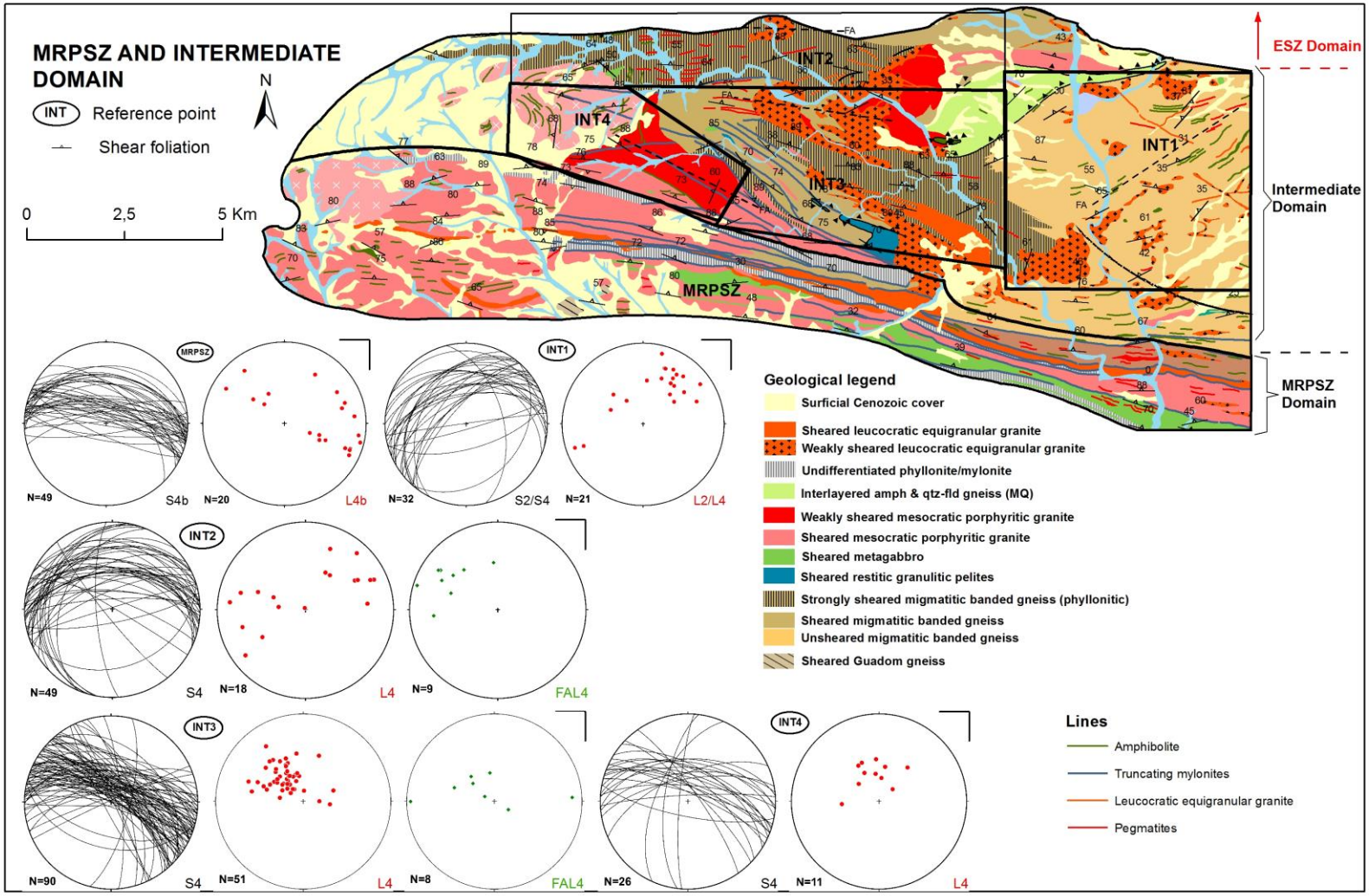

Figure 5-11: Map showing geometries of the L-S fabric in the MRPSZ and Intermediate domain. The stereonets plots are plotted for both foliation and lineation with references to specified geographic locations point. The overall geometries of foliation and lineation for all structural domains is also displayed on two thematic maps in Figure 5-8. See the text for detailed description.

Stellenbosch University https://scholar.sun.ac.za

5.6 POST D_4 STRUCTURES

Locally, two discrete shear zones are observed cross-cutting and overprinting S_4. One is a cm-scale NE-SE trending shear zone associated with a sinistral sense of shearing “late discrete sinistral shear zones,” and the other one is a long (km-scale) W to WNW trending curvilinear potassium-metasomatised high strain zone “curvilinear late discrete shear zones.” These two shear zones are considered as post D_4 deformation rather than D_5 deformation because they are accompanied with both ductile and brittle textures. Unlike D_5 which is dominantly characterized by brittle fracturing.

5.6.1 **Late discrete sinistral shear zones**

Late discrete sinistral shear zones were clearly observed cutting the mesocratic porphyritic granite in the northwestern part of the ESZ domain (Figure 5-12a). They occurs as ~10 cm thick quartz-feldspar-biotite proto-mylonite zone (Figure 5-12a and Figure 5-12b), striking NE-SW and dipping steeply at (~65^0 to 80^0) (Figure 5-12a). Along the late discrete mylonite zones, the earlier S_4 in the mesocratic porphyritic granite wall rocks is dragged and rotated into parallelism with a NE-SE striking discrete shear zone (Figure 5-12a and Figure 5-12b). In the mylonite zone, pre-existing potassium feldspar (microcline) megacrystic porphyroclast (~5cm) are deformed into both small elongate sub-rounded porphyroclast (<2mm) and fine-grained aggregates of quartz, potassium feldspar biotite and sericite indicating shearing at greenschist facies metamorphic conditions. The majority of biotite domains warps around potassium feldspar porphyroclasts and few are transposed by small shear zones into S-C` shear bands. The kinematics indicators on S-C` shear bands and the drag fold of the earlier S_4 in the wall rocks are consistent with a sinistral sense of movements. Few subrounded to angular fragments of microcline (Figure 5-12c) probably represent a cataclastic texture overprint. The matrix is also overprinted by brittle fractures, oriented both randomly and sub-parallel to the mylonitic fabric (Figure 5-12c).

Stellenbosch University https://scholar.sun.ac.za

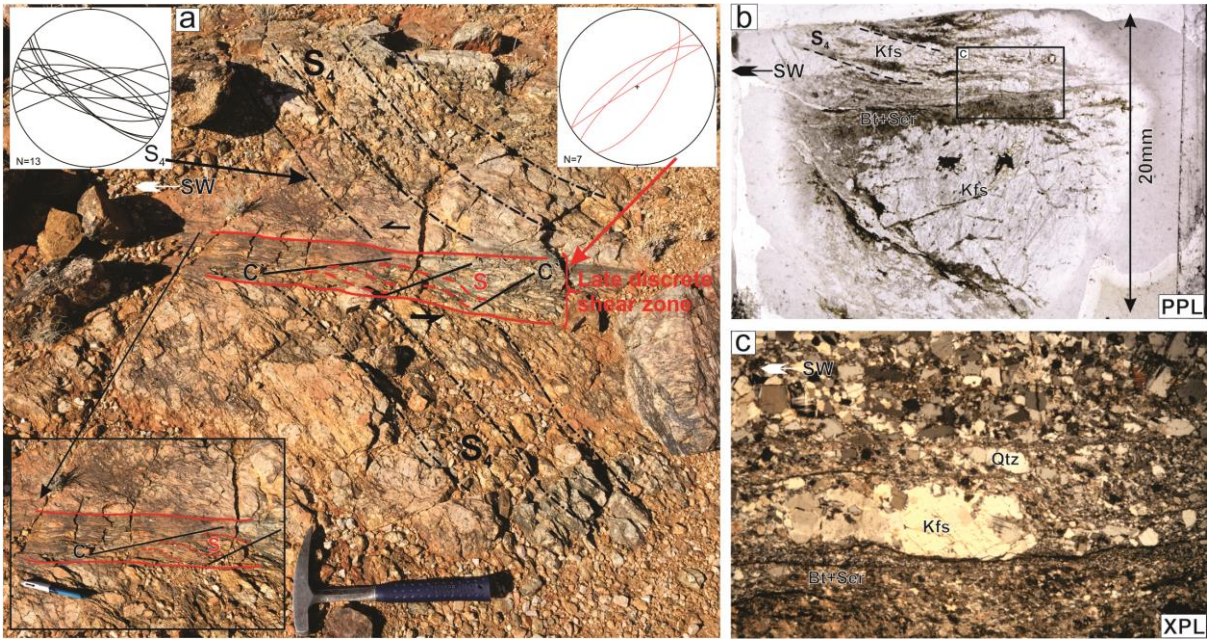

Figure 5-12: A representative field photograph of the mesocratic porphyritic granite and stereonets plots showing the late discrete sinistral shear zone. The Late NE-SE striking discrete ductile shear zone (red line) within a sheared mesocratic porphyritic granite drag fold and rotates the pre-existing WNW-ESE S_4 fabric. Within the mylonite zone, biotite domains are transposed by small-scale shears zones into forming S-C` shear bands. (b) Thin section slide scan of the oriented petrographic section showing microscopic fabric along the discrete mylonite zone. S_4 is rotated and cut-off by a discrete mylonite zone. Potassium feldspar (microcline) porpyroclast are separated by biotite and sericite. (Black box C = Photomicrograph position). (c) Photomicrograph (FOV=4.5 mm) of the mylonite zone within a mesocratic porphyritic granite recrystallized fragments of both quartz and microcline are resting within a groundmass of sericite and biotite. FOV = Field of view. XPL=Cross polarised light. PPL=plain polarised light.

5.6.2 **Curvilinear late discrete shear zones (Kz)**

The curvilinear late discrete shear zone are mostly brittle, heterogeneous along strike and are represented by a series of W-E and WNW-ESE trending linear to curvilinear interconnected shears zones (Figure 5-13). In field, these discrete shear zones where commonly observed at southern margins of the ESZ domain and southward to MRPSZ. They extend several kilometres along strike and with a maximum thickness of ~10 m. Where exposed, they are mapped out mapped out as “Kz” zones on the geological map (Appendix B), can be traced as elevated hills on the weathered regolith (Appendix B) and underneath the Cenozoic cover (geophysical lines=GL) on the high resolution magnetic data (Figure 5-13). Shearing/deformation usually intense and unevenly distributed along the discrete shear zone compared to the marginal wall rocks. Potassium alteration is prominent along these zones and usually associated with micaceous coating of white mica (muscovite and sericite), chlorite and epidote. Separating curvilinear discrete late shear zones (Kz) from D_5 fracture is not always easy especially east of ESZ domain were the curvilinear discrete late shear zones extend into a incohesive fault breccias (Figure 5-13) that separate the strongly strained MQ (in the north) from the unsheared migmatitic banded gneiss (In the south). Rock textures observed along strike range from: (1) chaotically folded phyllonites intruded by sheared pegmatites (Figure 5-14a), (2) strongly foliated and lineated discrete sheet of quartz vein (Figure 5-14b), (3) incohesive fault breccia filled by quartz vein (Figure 5-14c) and (4) cohesive fault breccia overprinting discrete phyllonites (Figure 5-14d).

Stellenbosch University https://scholar.sun.ac.za

In the eastern part of the ESZ, pseudotachylyte (Figure 5-14e) were observed on strongly heterogeneously deformed/fractured outcrop bearing similar characteristic as the one described above. The main central vein of the pseudotachylte is partly preserved and oriented perpendicular to three injection veins with diameters in the range of ~1 to 10 mm (Figure 5-14e).

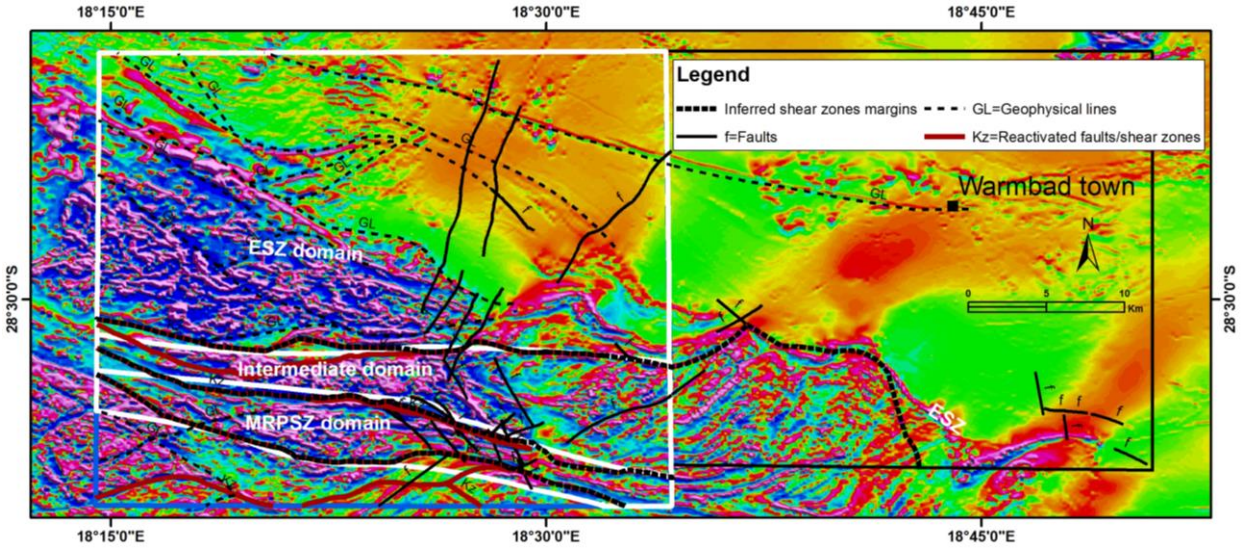

Figure 5-13: 1st vertical derivative of the high-resolution airborne magnetic data showing major post D_4 structures of the study area.

5.6.3 D_5

Deformation episode (D_5) represents the last deformation event recorded in the study area. This deformation is represented by a series of km-scale long NW and NE trending brittle incohesive fault breccia and fracture filled with quartz veins (faults=f) (Figure 5-13) that cross-cut the D_4 shear fabric across all the structural domains. In the Intermediate and MRPSZ domains majority of the D_5 structures trend NW-SE. In the ESZ domain, they trend dominantly NE-SW (Figure 5-13 and Appendix B). Some of the D_5 fault breccia are found interconnected and extending into the curvilinear late discrete shear zone making it difficult in some instances separate the two in the field (Figure 5-13 and Appendix B).

Stellenbosch University https://scholar.sun.ac.za

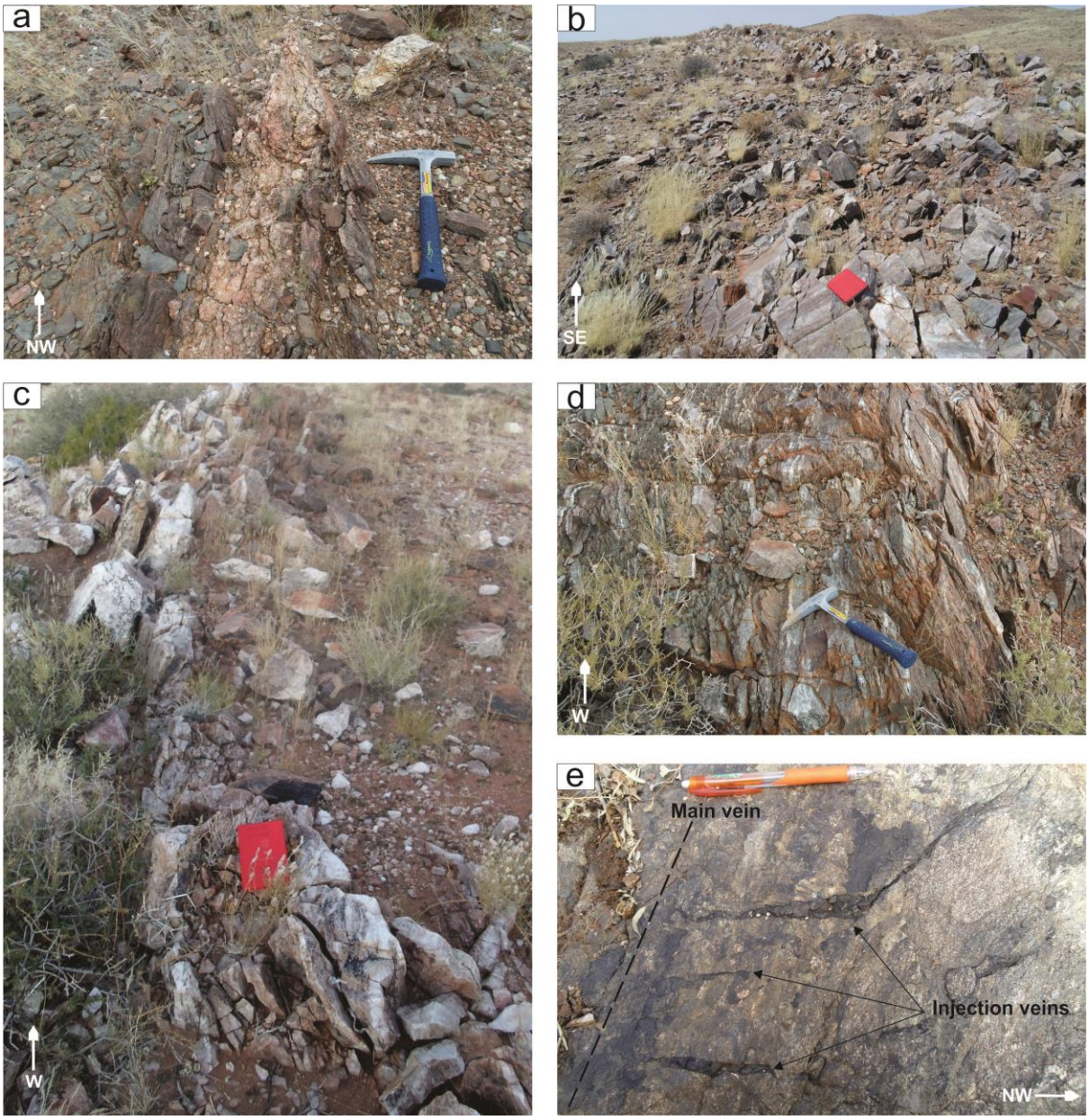

Figure 5-14: Field photograph of various E-W trending fault rocks observed along Kz zones at the southern margins of the ESZ domain. (a) Sheared amphibolite intruded by sheared pegmatite (center) and altered by potassium rich fluid. (b) Ridge of sheared quartz vein that intruded along Kz zones. (c) Unsheared quartz vein intruded along along the Kz fault plane. (d) Cohesive brittle fault overprinting the pre-existing highly strained phyllonites. (e) Pseudotachylytes showing three injection veins connected to the poorly preserved central vein. The injection veins are filled with black fine grained materials.

Stellenbosch University https://scholar.sun.ac.za

5.7 SUMMARY

In this chapter, the structure of the ESZ domain is described along with that of intermediate and MRPSZ domain. The ESZ domain forms a 15 km wide zone of intense shearing situated north of the intermediate and MRPSZ domains. Lithologically, the ESZ mostly hosts rocks of the gneissic EC and MQ.The contacts between these two units are marked by strongly deformed zones that transformed the host rocks into proto-mylonites, phyllonites and cataclasites. The southern margin of the ESZ is marked by a lithological contact between the migmatitic banded gneiss and interlayered amphibolite and quartzo-feldspathic gneiss. The northern margin of the ESZ is not defined due to poor outcrop exposure. The shear foliation (S_4) in ESZ domain varies from a widespread strong penetrative planar foliation to a discrete intensive shear fabric that anatomising around less deformed rocks. Secondary minerals assemblages observed in sheared host rocks are usually a combination of ±biotite+muscovite+chlorite (syn to late D_4 shearing) and sericite+epidote+diopside (post D_4 shearing). The shear fabric in the ESZ shows a cataclastic and phyllonitic texture dominant with few localized mylonite texture. The folds observed in the ESZ domain at various scales as NW-trending and SW verging asymmetric folds that are dominantly restricted to the MQ.

The isolation and correlation of pre-existing, inherited and newly developed fabrics in the study area has been problematic. These are merely due to: (1) poor rock exposure, making it difficult to isolate a set of unique fabrics with a definite rock unit and trace it along the shear zone; (2) dominant rock units such as (interlayered quartzo feldspathic gneiss and amphibolite, mesocratic porphyritic granite) are intensively intruded by pegmatites and leucocratic-equigranular granite; (3) majority rock units are retrogressed to greenschist facies; and (4) some of the rock units are chaotically folded and strongly strained beyond recognition. The overall orientation, metamorphic grade and fault rock textures of the S_4/L_4 fabrics are more variable in ESZ domain compared to the MRPSZ and Intermediate domains, but they show some similarities with S_{4b}/L_{4b} fabrics that are found in the MRPSZ domain. The D_4 fabrics in the ESZ is cross-cut by late discrete sinistral and curvilinear discrete shear zones and all fabrics in the study area are cross-cut by D_5 structures.

Stellenbosch University https://scholar.sun.ac.za

CHAPTER 6: DISCUSSION

6.1 LITHOLOGICAL PROTOLITHS

This study identified a variety of sheared rock units in the study area as presented in chapter 3. Disregarding the obviously intrusive rocks such as the mesocratic porphyritic granite, metagabbros, leucocratic equigranular granite and pegmatites, the fundamental units of the study area are; migmatitic banded gneiss, interlayered amphibolite and quartzo-feldspathic gneiss (MQ) and Eureka Complex (EC). This section will focus on the three fundamental units and will discuss their potential origin, relationship to the other lithologies documented in the adjacent area and their potential relative tectonic domains.

6.1.1 **Migmatitic Banded Gneiss**

The migmatitic banded gneiss is restricted to the intermediate domain and the northern part of the MRPSZ domain. The heterogeneous compositional banding of thin cm-scale layering of amphibolites, quartzo-feldspathic, quartz-hornblende gneiss and quartz-biotite gneiss correlates with Beukes (1973), Blignault et al. (1983) and Macey et al. (2015)'s description of the migmatitic volcanoclastic porphyroclastic unit that belong to the Umeis gneiss of the Pella Domain of the Richtersveld Subprovince. Furthermore, the geographical position of the migmatitic banded gneiss is consistent with the occurrence of the Umeis gneiss mapped by Macey et al. (2015) in the area east and adjacent to the study area. The L-S fabrics in the migmatitic gneiss in the eastern part of the intermediate domain are accompanied by a high grade amphibolite facies metamorphism and are interpreted to be due to D_2 deformation rather than D_4 shearing. These fabrics are probably related to the D_2 Namaqua Orogeny deformation and link this unit into the Pella Domain rather than the Vioolsdrif domain of Richtersveld Subprovince. Moreover, the occurrence of garnet and andalusite bearing layers interbanded with hornblende-biotite-quartz-feldspar gneiss and amphiblotite layers in some localities suggest that a the rock is comprised of both pelitic supercrustal materials and volcanoclastic sequences as previously suggested by (Beukes, 1973; Blignault et al., 1983; Macey et al., 2015). U-Pb zircon dating done on two samples of the Umeis Orange River Group by Macey et al. (2015) gave a rock formation age at 1875 ±6 Ma for a sample collected below the Lower-Fish River-Onseepkans Thrust (LFROT) far east of the study area and 1876 ±5 Ma for the sample collected just 20 km east of the study area and 5 km north west of the Tantalite Valley Massif.

6.1.2 **Interlayered Amphibolite and Quartzo-feldspathic Gneiss**

U-Pb dating on the quartzo-feldspathic gneiss gave a magmatic zircon cores and rims age at 1207 ±6 Ma. This age is interpreted as crystallization age of the quartzo-feldspathic gneiss. The interlayering field relationship between the quartzo-feldspathic gneiss and amphibolite suggest that both rock types probably formed around the same time. The protolithic and stratigraphic correlation (based on age and field description) of this unit does not fit in with those of the Pella and Kakamas domains. However, they could be linked to the bimodal interlayered mafic-felsic gneisses that intruded in the LFROTZ and adjacent Pella (footwall) and Kakamas (hanging wall) domains as suggested by Macey et al. (2015). Macey et al. (2015) documented and dated the package of interlayered quartzo-feldspathic gneiss and

Stellenbosch University https://scholar.sun.ac.za

amphibolites (Oupvlakte Complex) at 1215 ±9 Ma in the LFROTZ in the Onseepkans area (Southern eastern border region of Namibia) (Figure 6-3). Other packages of rock units mapped in closed proximity with the LFROTZ are Witwater gneiss, Velloordrift schist and Grass River Gneiss (Figure 6-3) (Macey et al., 2015). Similarly, Blignault (1977) documented a package of interlayeried quartzo-feldspathic gneiss and amphibolites along the LFROTZ in the Ai-ais area. The author visted this area and confirmed the existence of this rock unit. Macey et al. (2015) and Blignault (1977) description and age of the units correlate with that obtained in this study and hence, suggest that both units are probably co-genetic and the LFROTZ represents a belt extending over 200 km from the Onseepkans area (southeast) to the Ai-ais area (northwest). The LFROTZ is also associated with a series of intrusive rock units such as: the Orange falls suite granite (1210-1120Ma) (Bial et al., 2015a; Macey et al., 2015); Eendoorn Suite (1250-1190 Ma); and mafics of the Kum Kum suite (1225-1210 Ma) (Macey et al., 2015).

6.1.3 **Eureka Complex**

Rocks of the EC make up northern part of the ESZ domain and are differentiated from other litho-tectonic units by 1) having a lesser amount of amphibolite dykes and 3) hosting the Eureka grey gneiss along with remnants pods of restitic granulitic pelites. U-Pb zircon dating of Eureka grey gneiss and restitic pelite produced a wide variety of detrital zircon core ages that show similar inherited age peaks (Figure 6-1). The shared core age peaks in both rocks were recorded at; ~2049 Ma, ~1842 Ma, ~1700 Ma, ~1300 Ma and ~1262 Ma (Figure 6-1). The similarities in the inherited ages suggest that both rocks where derived from the same source between 2049 and 1262 Ma.

The zircon core ages between 1842 and 2049 Ma recorded in both rock units represent the oldest inherited in both rocks and were probably derived from the Orange River Group of the Richtersveld Subprovince (2.0-1.8 Ga) (Blignault, 1977; Macey et al., 2015; Reid, 1997). The ages in the range of ~1262 Ma, 1300 and ~1322 Ma corresponds with the ages of the Kakamas Domain, Konkiep Subprovince and Areachab terrane of the Gordonia Subprovince (Eglington, 2006). They most likely imply the presence of sediments sourced from these terranes/domains. In the restitic granulitic pelite the cores and oscillatory overgrowth rims around the cores of euhedral to subhedral shaped zircons gave dominant population peak at 1212 ± 4.3 Ma (Figure 6-1). These zircons appears to be magmatic and their resultant age most likely suggest a migmatization event and/or an inheritance from various intrusive rocks such as the Kum Kum Suite (1225-1215 Ma), Eendoorn Suite (1250-1190 Ma) and MQ (~1215-1207 Ma) (Macey et al., 2015; this study) that are associated with the formation of the LFROTZ around ~1200Ma (Macey et al., 2015). The absence of the ~1200 Ma inheritance ages in the Eureka grey gneiss (Figure 6-1) could imply that the Eureka grey gneiss and restitic granulitic pelite where not in the same vicinity around ~1200 Ma. The 1262 Ma age probably deposited the last sediment in Eureka grey gneiss and suggest that rock was already formed before ~1200 Ma. The complex detrital zircons pattern of the EC is consistent with sediments sourced from both Kakamas Domain of Gordonia Subprovince and Pella Domain of Richtersveld Subprovince. Similar detrital inheritance ages are recorded in the rocks Narries Group and Arus Gneiss of Kakamas Domain.

Stellenbosch University https://scholar.sun.ac.za

The youngest zircon rim age of 1197 Ma in the restitic granulitic pelite is linked to metamorphic event probably related terminal phase of LFROT at 1195 Ma (Macey et al., 2015) (Figure 6-1). The 557 Ma rim age in the Eureka grey gneiss (Figure 6-1) can be interpreted to have occurred due to a metamorphic or migmatization overprint rather than inheritance. This age probably suggest a reactivation episode perhaps related to the Pan African event were a series of mobile belts were formed during the assembly of supercontinent Gondwana (Eglington, 2006). However, as only one grain with this age was recorded it is difficult to attribute too much significance to it and more work would be needed to assess its possible significance.

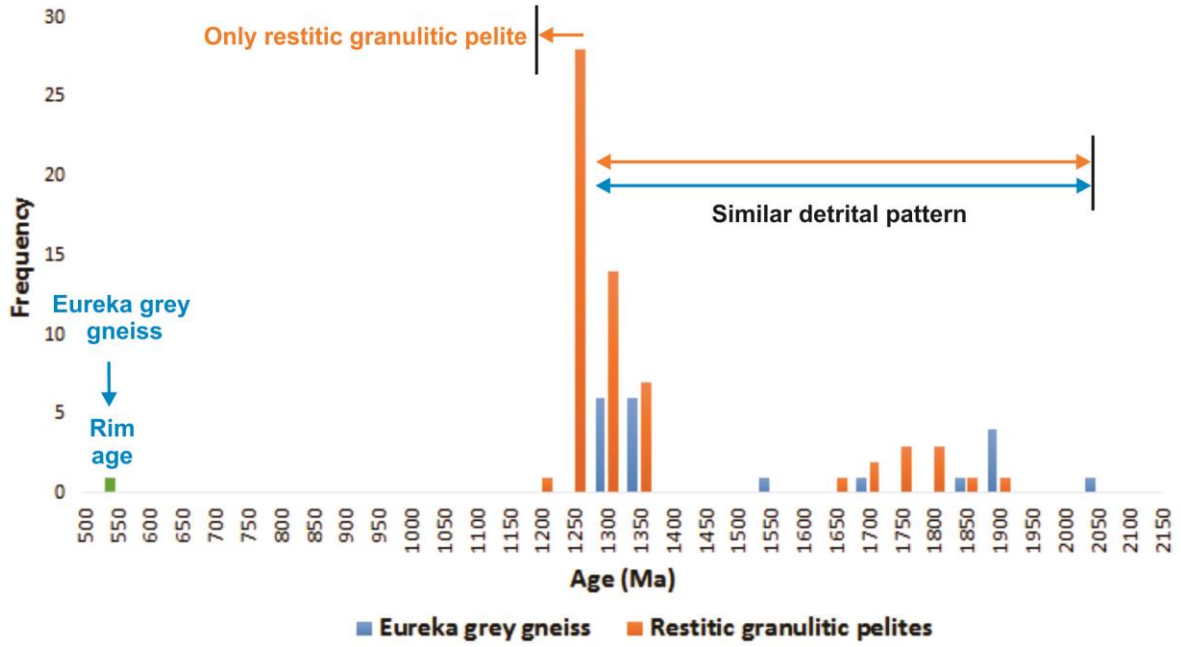

Figure 6-1: Relative probability distribution plots for $^{207}Pb/^{206}Pb$ ages of Eureka grey gneiss and restitic granulitic pelite of the EC. The data show similar detrital zircons ages between 1262 Ma and 2049 Ma in both rock units. The youngest rim ages are recorded at 1197 Ma in the restitic granulitic pelite and 557 Ma in the Eureka grey gneiss.

6.2 METAMORPHIC CONDITIONS OF THE HOST ROCKS.

Proterozoic metamorphic terrains are often associated with complex structural and metamorphic history. The use of mineral parageneises alone in the reconstruction of PTt-paths is usually not conclusive since older mineral assemblages are often re-equilibrated by younger deformation and metamorphic events (Passchier et al., 1990). However, the supplementary use of macro-and microfabric elements is considered useful since they are not easily obliterated or re-equilibrated by later events (Passchier and Trouw, 2005; Passchier et al., 1990). During D_2 Namaqua Orogeny, peak metamorphic condition is recorded at 660 ^{0}C and 4 kbar (low precision estimate) in the amphibolite facies rocks of the Pella Domain in the Richtersveld Subprovince (Macey et al., 2015). In the granulite facies rocks of the Gordonia Subprovince, peak metamorphic conditions are recorded at 780 ^{0}C and 5.5 kbar (low precision estimate) (Macey et al., 2015). Majority of sheared rocks recorded in the study area show an upper to mid greenschist facies metamorphic retrogressed condition indicated by the presence of greenshist facies mineral assemblages ±biotite+muscovite+chlorite (syn-D_4 shearing) and sericite+epidote+diopside (late to post D_4 shearing).

Stellenbosch University https://scholar.sun.ac.za

The migmatitic banded gneiss and MQ peak metamorphic conditions are interpreted at amphibolite grade due to the presence of hornblende (Deer et al., 1992; Winter, 2001). Peak metamorphic facies assemblages in the restitic granulitic pelites were recorded at upper amphibolite to granulite facies and are indicated by the presence of ±sillimanite+cordierite+garnet. These assemblages where probably achieved during the early Kibaran stage anatexis at 1351 to 1299 Ma (Bial et al., 2015b) or during the regional metamorphic event around ~1220 Ma (Bial et al., 2015a, 2015b; Eglington, 2006; Macey et al., 2015). The restitic character of the pelites suggest that peak metamorphic condition was most likely accompanied with subsequent loss of melt (Bial et al., 2015b; Macey et al., 2015; this study).

However, majority of the petrographic section observed in this study shows that most of the peak mineral assemblages discussed above are retrogressed to mid-upper greenschist facies (growth of syn-D_4 biotite). The breakdown of cordierite and garnet to biotite and potassium feldspar to sericite suggest a rehydration associated retrograde metamorphism at greenschist facies probably at temperature below 450 ^{0}C (Baltatzis, 1979; Deer et al., 1992). The growth and alignment of secondary minerals such as biotite and muscovite aligned both parallel and oblique to the D_4 shear fabric in the majority of the rock textures indicates that retrograde metamorphism occurred syn-to post D_4 shearing.

6.3 RELATIONSHIP TO THE REGIONAL LITHOLOGICAL FRAMEWORK

The migmatitic banded gneiss is correlated to the Umeis gneiss of the Pella Domain (~1.9-2.0 Ga) of the Richtersveld Subprovince that marks the footwall of the LFROTZ and represents the oldest rock unit in the study area. The MQ formed at 1207 ±6 Ma, an age similar to a range of intrusive voluminous bimodal magmatism that are found closely associated with the LFROTZ. The ages similar to those obtained by Macey et al., (2015) from the Interlayered amphibolite and qtz-fsp gneiss (1215 ±9 Ma) of Oupvlakte Complex found in the LFROTZ. The Eureka grey gneiss and restitic granulitic pelites correlates with the rock of the Narries Group and Arus Gneiss of Kakamas Domain and represents the hanging wall unit that is separated from the Pella Domain footwall by the LFROTZ (Macey et al., 2015; this study). In the ESZ, both the migmatitic banded gneiss, MQ and EC are strongly reworked by the D_4-shearing event, and most likely suggest that the ESZ cut through the LFROTZ and part of the Pella and Kakamas domains (Figure 6-3).

6.4 SHEARING NATURE AND KINEMATICS

6.4.1 Lateral Extent and Geometry of the Shear Fabric

The ESZ forms a ~2 to 15 km wide and 50 km long WNW-striking shear zone. The thickness of the shear zone (where exposed) decrease significantly from the northwest to the southeast. In the study area (west), the shear zone broadens up to approximately 15 km before the younger Karoo sedimentary cover conceals it. In the east; 10 km north east of the Tantalite Valley Massif Complex, the shear zone narrow to the thickness of less than 2 km before it disperse underneath the Eendoorn Suite and Cenozoic cover (Macey et al., 2015). The orientation of the shear fabric in ESZ domain is closely aligned with the occurrence of the MQ and EC lithotectonic units. The southern boundary of the ESZ is marked by a transitional high strain zone that separate the strongly sheared (MQ and EC) in the north from the variably

Stellenbosch University https://scholar.sun.ac.za

sheared migmatitic banded gneiss in the south. The contacts between these three packages are interpreted as cryptic thrust zones on the basis that they have separate and cut-off thick lithotectonic units (migmatitic banded gneiss, MQ and EC) that have different ages and are correlated to different tectonic domains (Pella, LFROTZ and Kakamas) (Macey et al., 2015) as discussed in section 6.3. The northern boundary of the ESZ is not defined due to poor rock exposure.

Despite a general WNW strike of moderately to steeply dipping foliation, the ESZ domain preserves a series of complex asymmetrical interconnected structures (Figure 5-8a). Steronets plots and field observation shows that the S_4/L_4 fabrics in the ESZ varies due to a combination of the following factors: (1) km-scale phyllonite dominant shear zones separating less strained lithotectonic domains; (2) series of discrete m-scale shear zones both oriented sub-parallel and oblique to the dominant WNW strike shear foliation; (3) late brittle fractures and faults overprinting the earlier D_4 shear fabrics; and (4) drag folded (amphibolites, pegmatites and leucocratic equigranular granite) that stand out as marker horizons across the ESZ domain (Figure 5-8a).

The ESZ domain is also associated with various WNW-ESE trending, tight and SW verging asymmetrical folds (Figure 5-6a). Majority of the folds shows a steeply pluging fold axis to the NW, NE and SW that are locally oriented subparallel to L_4. These folds probably formed during shearing as large complete asymmetrical folds associated with various S, M and Z type parasitic intrafolial folds. Progressive shearing probably tightened the fold interlimb angle and transposed limbs of the main folds containing S and Z type's intrafolial folds. Thus, leaving the M type intrafolial folds preserved in the hinge zones (Figure 5-6a). The stretching of the folds limbs and the rotation of their hinge zones appears dextral and is in line with the NW-SE shear strike orientation. Shortening appears to be directed along NE-SW direction (Figure 5-6a). The preservation asymmetry of these folds is consistent with Carreras et al., (2005) model of fold development in high mechanical anisotropy under simple shear conditions. Under this conditions intense shearing is accommodated along the fold limbs and the fold hinge zones are rotated dextrally as a rigid body along the NW-SE shear transport direction (Carreras et al., 2005). Down dip lineation's on some of the limbs (Figure 5-8a) probably suggest transpressional shearing associated with a top (NE) to the SW transport motion.

Large variations in the geometries of the D_4 L-S fabrics within the ESZ domain (described in chapter 5; section 5.4) is not fully understood. However, these variations could have been aided by a number factors such as: (1) the development, orientation and exploitation of the both pre-existing D_2 and earlier D_4 fabrics; (2) anatomising shear foliation probably due to compositional anisotropy (Carreras, 2001; Carreras et al., 2005; Passchier, 1984; Ponce et al., 2013), generally between the strongly competent MQ and less competent EC and within their respective rock units; and (3) high strain accumulation in some part of the shear zone (along discrete phyllonites-mylonite zones and late discrete sinistral shear zones) which transpose the limb of folds and rotate the pre-existing D_2 and earlier D_4 shear fabrics into NW-SE striking parallelism during progressive shear zone (Carreras, 2001; Fusseis et al., 2006; Lambert, 2013; Ramsay, 1980; this study).

Stellenbosch University https://scholar.sun.ac.za

6.4.2 **Strain Partitioning and Fault Rock Textures**

Strain in km-scale shear zones localize due to a number of factors such as; strength anisotropy, pre-existing viscous fabric, compositional anisotropy, grain size and retrogression (Carreras et al., 2013; Handy, 1989; Platt and Behr, 2011; Rennie et al., 2013; Stewart et al., 2000). In the study area, high strain is interpreted localized along thick km-scale long phyllonites-mylonite zones, cm-scale wide late discrete sinistral shear zones and curvilinear discrete shear zones that separate lesser-strained domains. The heterogeneity and co-existence of variably sheared intrusives (variety of sheared and unsheared generation of pegmatites and quartz veins) phyllonites, pseudotachylyte and fault breccias recorded along the long curvilinear late discrete shear zones probably represent a later D_5 episode exploiting of a pre- existing D_4 structure.

In the field, shearing in the ESZ domain appears to be characterized by a low grade (upper-mid greenschist facies), phyllonite-cataclasite dominant shear fabric associated with few localized discrete mylonites. However, microstructure from the ESZ domain show evidence for ductile deormation indicated by the presence of matrix grain sizes, irregular grain boundaries shapes, annealed and dynamically recrystallized potassium feldspar and quartz (Figure 5-7). The cataclasitic feldspar observed across the ESZ domain suggests that shearing was accompanied by some brittle reduction in grain in size (Rennie et al., 2013; Simpson, 1985; Stewart et al., 2000). The co-existence of few cataclasitic potassium feldspars and ductile microstructure is some rock textures is interpreted to suggest a dominant plastic deformation condition (Simpson, 1985; Stipp and Kunze, 2008; Stipp et al., 2002). However, the overall microstructure textures are consistant with grain boundaries sliding deformation mechanism (Lagoeiro and Fueten, 2008; Wightman et al., 2006).

The abundance of (phyllonite and fault breccias) and the absence of ductile rotated potassium feldspar in the rocks of the ESZ domain compared to the Intermediate and MRPSZ domains suggest that the deformation in the ESZ domain occurred at much colder condition and/or probably experienced a strong-late (D_5) brittle overprint. Furthermore, large quantities of phyllonite fault rocks in the ESZ domain could imply a long term fluid induced weakening (Jefferies et al., 2006). Fault rocks that formed under brittle deformation are more susceptible to erosion (Stewart et al., 2000) and hence; this could explain why the fault rocks of the ESZ domain are poorly preserved compared to those of the MRPSZ. In summary, unlike the MRPSZ domain, the ESZ domain is more heterogeneously sheared at all scales, more brittle sheared and lacks a dextral drag fold of the less strained wall rocks and a core zone. The shear fabrics (S_4/L_4) of the ESZ domain are linked to the deformation episode D_{4b} found in the MRPSZ, and they probably developed during D_4 progressive shearing as previously documented by (Lambert, 2013; Macey et al., 2015).

Stellenbosch University https://scholar.sun.ac.za

6.4.3 **Kinematics of Shearing**

6.4.3.1 Eureka Shear Zone domain

Shear sense indicators were not commonly observed in the ESZ at both meso-and microscopic-scale. At meso-scale the kinematics could not be deduced due to poor outcrop exposure, making it difficult to locate both the shear sense indicators and a mineral stretching lineation on the same rock surface. At At mega scale the rotation of the fold hinge and limbs shows a dextal sense of shearing (Figure 5-9a). At microscopic scale the the overall fabric and potassium feldspar phenocrysts appears more flattened and rotated potassium feldspar porphyroclasts were not commonly observed (Figure 5-7a). However, meso-scale S-C' shear fabric on the late discrete sinistral shear zones were consistent with a sinistral sense of shearing (Figure 5-12).

6.4.3.2 Intermediate and MRPSZ domain

In these two domains, the shear sense indicators at the meso-scale are indicated by the drag folding of the limbs of the folds that are displaced by fold axis sub-parallel discrete shears. At microscopic scale, the shear sense indicators are preserved as biotite fish and potassium feldspar sigma and delta clasts (Figure 5-10d). In all cases, the dominant sense of shearing is interpreted to be dextral. The stretching lineation (L_4) on both surface plunges moderately to steeply, suggesting an oblique lateral dextral movements accompanied by a moderate to steep dip slip slide. The kinematic interpretation is consistent with the kinematic interpretation of both Colliston and Schoch, (2013), Macey et al., (2015) and Lambert, (2013) kinematic interpretation of the MRPSZ.

6.5 TIMING AND DURATION OF SHEARING

Evidence for progressive and strain variation during D_4 shearing are observed along the mega-scale folded dykes of leucocratic equigranular granite that extends from the southern margin of the ESZ, across the intermediate domain and into the MRPSZ domain. The existence of high and low strain localization along the mega-scale leucocratic equigranular granite dyke suggest that strain is both localized in some vicinities and at the same time variable across the structural domains. The sub-parallel orientation of the moderately to strongly sheared leucocratic equigranular granite and pegmatites dykes to the D_4 shear zones implies that the two intruded syn- D_4 shearing (Clifford et al., 1974; Lambert, 2013; Macey et al., 2015; this study) and were variably progressively sheared. The weakly to unsheared leucocratic equigranular granite dykes and pegmatites are usually oriented oblique to the D_4 and probably represent a different younger generation granite dykes that intruded late to post D_4 shearing.

U-Pb zircon dating of a sample collected from syn-tectonic porphyritic leucocratic equigranular granite at the southern margin of the ESZ domain gave a youngest magmatic core zircon age of 1003 Ma (Figure 6-2). This age is interpreted as the crystallization age of the leucocratic equigranular granite. The 1003 Ma imply that shearing had already started before 1003 Ma. In the relation to age of the sheared and unsheared pegmatites (~1005 Ma and 958 Ma) dated by Lambert, (2013), the leucocratic equigranular granite both pre-dates and post-dates some of the pegmatites and field observation also confirms these

Stellenbosch University https://scholar.sun.ac.za

relationships. Field relationship between the leucocratic equigranular granite, pegmatites and D_4 shear zones advocate that the both syn-tectonic pegmatites and leucocratic equigranular granite dyke swarms that intruded both the MRPSZ domain and ESZ domain are probably similar. Thus, constraining the timing of shearing in both shear zones during and after the intrusion of pegmatites and leucocratic-equigranular granite between 1005 to 958 Ma (Lambert, 2013).

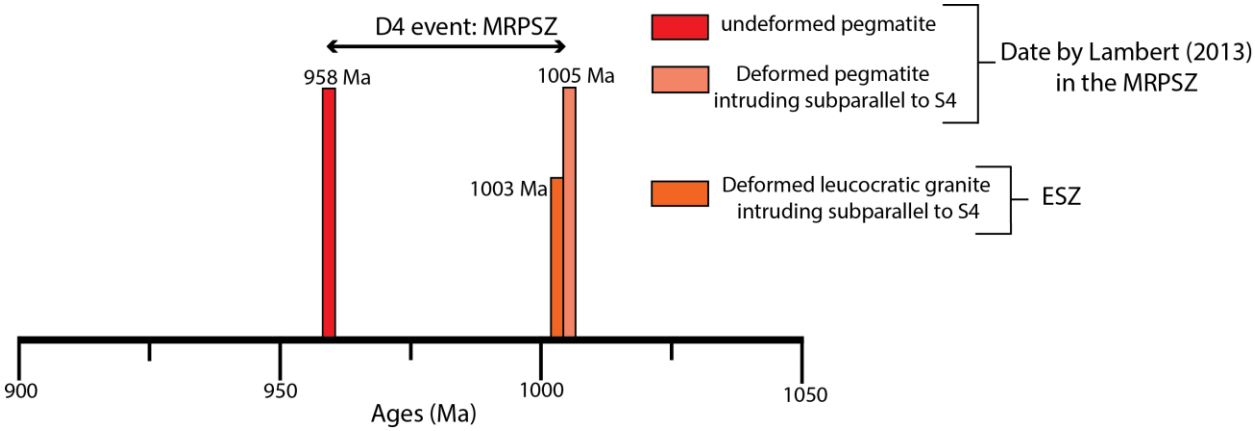

Figure 6-2: Age relationship between undeformed and deformed pegmaitites of the MRPSZ and the deformed leucocratic granite of the ESZ.

6.6 WHAT IS THE EUREKA SHEAR ZONE

6.6.1 Present Lithological and Structural Framework

The ESZ shows a complex lithological, metamorphic and structural history. The ESZ can be differentiated from the MRPSZ by: 1) its association sigmoidal shaped lithotectonic slices of the MQ and EC and 2) having a greenshist facies cataclasite-brittle dominant shear fabric. The southern margins of the ESZ (mostly in east) is marked by a contact between the low strained migmatitic banded gneiss of the Pella Domain in south and high strained MQ and EC in the north (Figure 6-4) (Macey et al., 2015; this study). The northern margin of the ESZ domain was not delineated due to poor outcrop exposure. The field relationship and ages of MQ and EC that occurs as large cut-off tectonic slices within the ESZ are somehow similar to those mapped by Macey et al., 2015 in the LFROTZ and probably indicate the presence of this originally D_2 imbricated thrust zone (LFROTZ) (Figure 6-3) (Macey et al., 2015; this study). Structural and kinematic evidence for D_2 thrusting are not observerd in the ESZ, probably due to D_4-shearing overprint. However, the correlation ESZ rock types into regional tectonic domains suggests an existence of the: 1) Pella Domain footwall on the southern margin of the ESZ (marked by migmatitic banded gneiss), 2) the LFROTZ intrusive (marked by MQ) and the Kakamas Domain (Eureka grey gneiss and restitic granulitic pelite supracrustal). These rocks are currently strongly and variably sheared by the ESZ and intruded by variety of sheared to unsheared pegmatites and leucocratic equigranular granite (Figure 6-4) (Beukes, 1973; Blignault et al., 1983; Macey et al., 2015; this study).

Stellenbosch University https://scholar.sun.ac.za

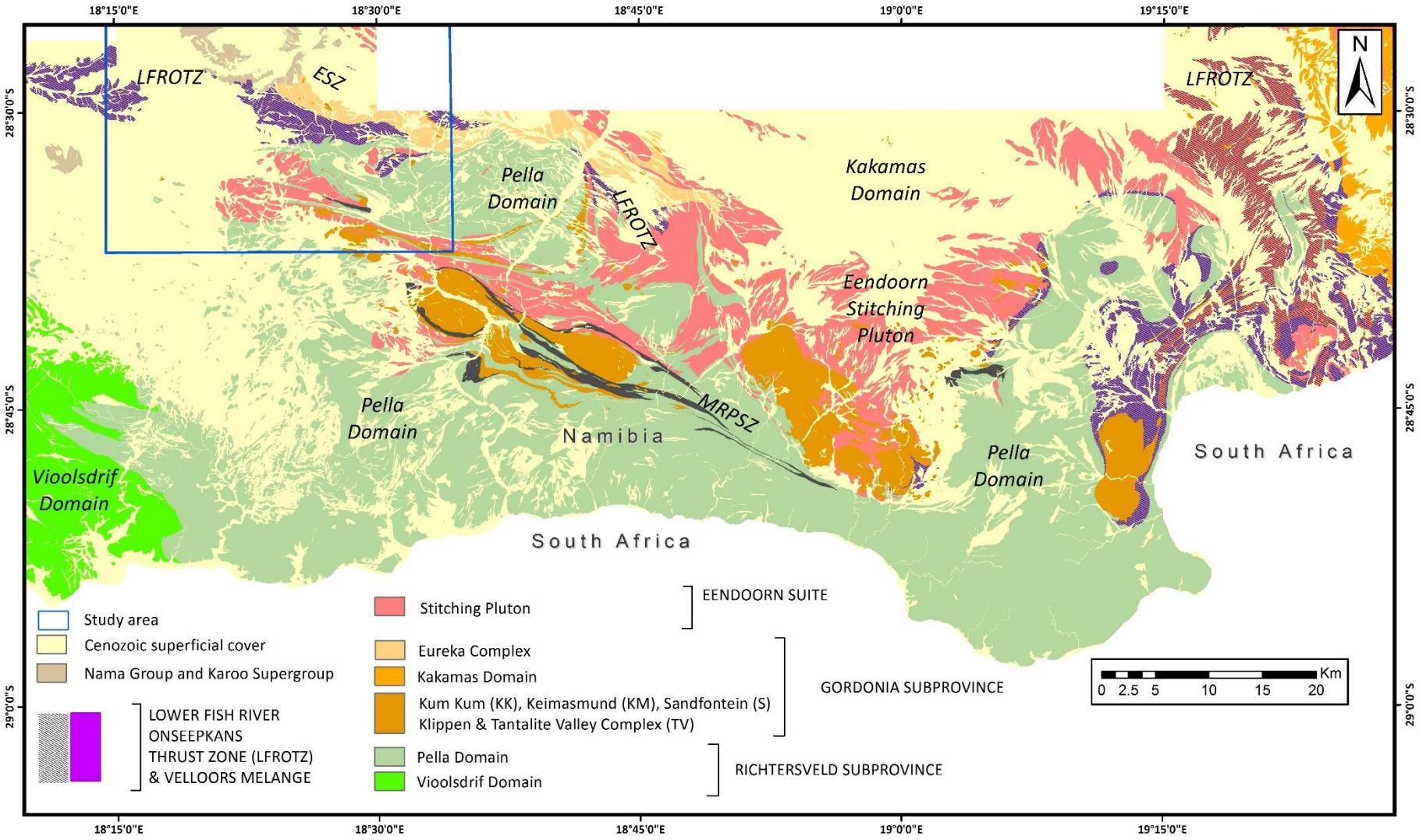

Figure 6-3: Tectonostratigraphic map of the study area (southern Namibia) showing the distribution of the LFROTZ in the study area and the areas adjacent to it (modified after Macey et al. (2015)*).*

Stellenbosch University https://scholar.sun.ac.za

6.6.2 **Evolution**

Prior to D_4 shearing the rocks of the ESZ probably occurred as melange of imbricated thrust slices that were thrusted on top of the migmatitic banded gneiss of the Pella Domain by the LFROTZ (Figure 6-4). During D_2, the multistage thrusting event (LFROTZ) was probably accompanied by the intrusion of the MQ (Oupvlakte complex), Eendoorn suite (mesocratic porphyritic granite) and metagabbros of the Kum kum Suite (Macey et al., 2015; this study). Shearing in the MRPSZ evolved as ductile amphibolite facies grade deformation that progressively developed into a brittle-ductile and finally brittle deformation between 1005 Ma and 960 Ma (Lambert, 2013; Macey et al., 2015). Generally, the orientation and metamorphic grade conditions of shearing in the ESZ is similar to that of the MRSPZ. However, shearing in the ESZ appears to have occurred at much colder conditions compared to the MRPSZ. Moreover, the lack of shear sense indicators in the ESZ probably suggest the ESZ did not experience a strong regional strike slip deformation as the MRPSZ, but rather a localized shearing, accompanied by flattening that is probably by the fluids and/or nature of the lithology (phyllonite) found in the ESZ. In the west, the shear fabric of the MRPSZ and ESZ deduced from the high-resolution airborne magnetic data shows a series of interconnected lineaments merging into one another (Figure 5-13). This spatial geometrical relationship probably suggest that the ESZ originated as a splay-type shear of the MRPSZ that is exploiting a weaker existing terrane boundary between the Kakamas Domain and Pella Domain.

Evidence for progressive shearing and strain variability in both the ESZ and MRPSZ are recorded are on the syn-D_4 shearing leucocratic equigranular granite and pegmatites dated at ~1000 Ma (Figure 6-2) (Lambert, 2013; this study). The sheared and unsheared syn to post D_4 shearing pegmatites that intruded both ESZ and MRPSZ constrains the timing of both shear zones between 1005 to 958 Ma (Lambert, 2013). A 550 Ma single zircon rims age obtained from the Eureka grey gneiss suggest that the ESZ was probably reactivated at a later stage.

Stellenbosch University https://scholar.sun.ac.za

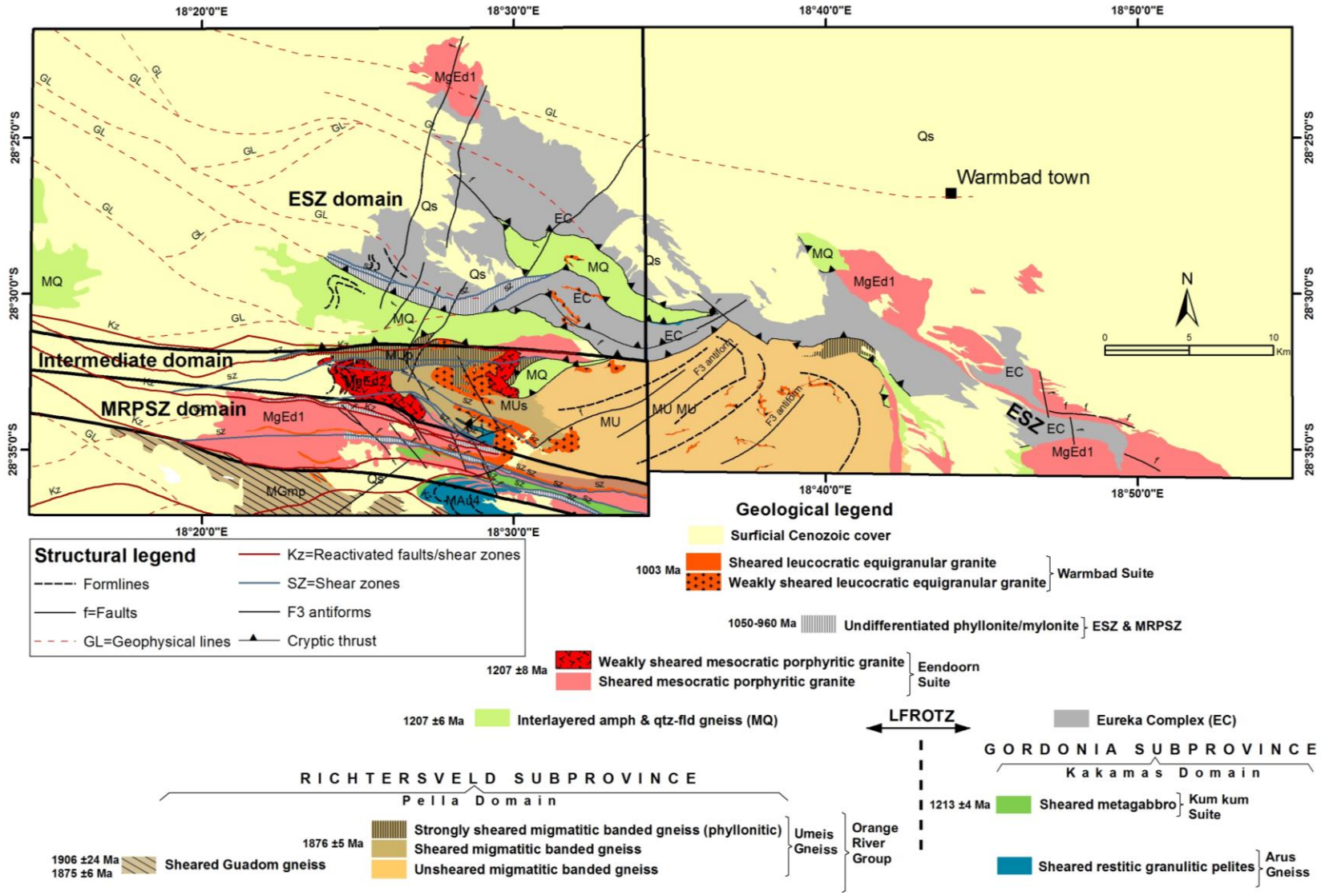

Figure 6-4: Tectonostratigraphic map of the study area and the western extension of the MRPSZ and ESZ. Some of the age data obtained from (Lambert, 2013; Macey et al., 2015).

Stellenbosch University https://scholar.sun.ac.za

CHAPTER 7: CONCLUSION

New data presented in this study shows that the Eureka shear zone (ESZ) comprises of two distinct lithotectonic units. These are: (1) Eureka Complex (EC); and (2) interlayered quartzo-feldspathic gneiss and amphibolite (MQ). The EC is situated in the north and is characterized by a heterogeneous collection of sheared gneisses dominated by garnet-quartz-feldspar biotite paragneiss associated with isolated remnants potassium feldspar-garnet-sillimanite-cordierite granulititic pelites. The EC shows peak metamorphic minerals assemblages at granulite facies and records both Palaeoproterozoic and Mesoproterozoic inheritance ages derived from both the Pella Domain of the Richtersveld Subprovince and Kakamas Domain of the Gordonia Subprovince. The MQ occur fault/thrust bounded sigmoidal shaped bimodal mafic-felsic orthogneiss within the EC that formed at (1215 ±9 Ma) in the LFROTZ. South of the MQ and EC, the ESZ reworked the migmatitic volcanoclastic porphyroclastic rocks of the Pella Domain. The contact between sheared the migmatitic volcanoclastic porphyroclastic, EC and MQ are obscure, marked by high strained zones and interpreted to represent cryptic imbricated thrusts zones of the LFROTZ. A magmatic U-Pb age peak between 1227-1197 Ma in the rocks of the ESZ correlates with the regional Meosproterozoic D_2 Namaqua Orogeny that is linked to the formation of the LFROTZ and juxtapositioning of the Kakamas Domain on top of the Pella Domain. The ESZ is distinct from the MRPSZ and LFROTZ, and contains no unique rock types different from those found in the MRPSZ and LFROTZ. Therefore, this study suggests that the ESZ represents a subvertical late Namaqua D4 shearing event reworking the older (D_2) tectonic boundary between the Mesoproterozoic Gordonia Subprovince (Kakamas Domain) and Palaeoproterozoic Richtersveld Subprovince (Pella Domain).

Shearing in the ESZ is characterized by mid-upper greenschist facies deformation associated with the development of cataclasite-phyllonite (dominant) and mylonitic textures within the host rocks. The shearing nature and fabrics elements of the ESZ are similar to those of the deformation stage D_{4b} found in the MRPSZ. A series of syn to post tectonic sheet-like pegmatites and leucocratic equigranular granite dykes that intruded the ESZ and MRPSZ constrains the time of shearing in both shear zones between 1005 to 960 Ma. The ESZ is poorly exposed, have a complex lithological and structural evolution and hence, it the mechanism driving its formation is still not clear. This study further recommends a comprehensive structural, geochronological and geophysical study on both the ESZ, MRPSZ and LFROTZ to fully understand the dynamics of the three during the amalgamation of the Namaqua Sector of the NNMP

Stellenbosch University https://scholar.sun.ac.za

REFERENCES

Allemendinger, R.W., Cardozo, N.C., Fisher, D., 2012. Structural Geology Algorithms: Vectors & Tensors, Cambridge University Press. Cambridge, England, England.

Bailie, R., Gutzmer, J., Rajesh, H.M., 2011. Petrography, geochemistry and geochronology of the metavolcanic rocks of the mesoproterozoic Leerkrans Formation, Wilgenhoutsdrif Group, South Africa - back-arc basin to the Areachap volcanic arc. South African Journal of Geology 114, 167–194.

Baltatzis, E., 1979. Distribution of Fe and Mg between garnet and biotite in Scottish Barrovian metamorphic zones. Mineralogical Magazine 43, 155–7.

Becker, T., Schreiber, U., Kampunzu, A.B., Armstrong, R., 2006. Mesoproterozoic rocks of Namibia and their plate tectonic setting. Journal of African Earth Sciences 46, 112–140.

Beukes, G.J., 1973. 'n Geologiese ondersoek van die gebied suid van Warmbad, Suidwes-Afrika, met spesiale verwysing na die metamorf-magmatiese assosiasies van die Voorkambriese gesteentes. D.Sc. Thesis, University of the Orange Free state, Bloemfontein, p. 333. Bloemfontein.

Bial, J., Büttner, S.H., Frei, D., 2015a. Formation and emplacement of two contrasting late-Mesoproterozoic magma types in the central Namaqua Metamorphic Complex (South Africa, Namibia): Evidence from geochemistry and geochronology. Lithos 224-225, 272–294.

Bial, J., Büttner, S.H., Schenk, V., Appel, P., 2015b. The long-term high-temperature history of the central Namaqua Metamorphic Complex: Evidence for a Mesoproterozoic continental back-arc in southern Africa. Precambrian Research 268, 243–278.

Blignault, H.J., 1977. Structural-metamorphic imprint on the part of the Namaqua mobile belt in South West Africa. Bulletin, Precambrian research, University of Cape Town 23, 197.

Blignault, H.J., Van Aswegen, G., Van Der Merwe, S.W., Colliston, W.P., 1983. The Namaqualand geotransverse and environs: part of the proterozoic Namaqua mobile belt. Geological Society of South Africa, Special Publication 10, 1–29.

Cardozo, N., Allmendinger, R.W., 2013. Spherical projection with OSXStereonet. Computer & Geosciences 51, 193–205.

Carreras, J., 2001. Zooming on Northern Cap de Creus shear zones. Journal of Structural Geology 23, 1457–1486.

Carreras, J., Cosgrove, J.., Druguet, E., 2013. Strain partitioning in banded and/or anisotropic rocks : Implications for inferring tectonic regimes. Journal of Structural Geology 50, 7–21. doi:10.1016/j.jsg.2012.12.003

Carreras, J., Druguet, E., Griera, A., 2005. Shear zone-related folds. Journal of Structural Geology 27, 1229–1251. doi:10.1016/j.jsg.2004.08.004

Clifford, T.N., Gronow, D.C., Rex, C., Burger, T., 1974. Geochronological and Petrogenetic studies of

Stellenbosch University https://scholar.sun.ac.za

high-grade metamorphic rocks and intrusives in the Namaqualand, South Africa. Journal of Petrology 16, 154–188.

Colliston, W.P., Schoch, A.E., 2013. Wrench-shearing during the Namaqua Orogenesis-Mesoproterozoic late stage deformation effects during Rodinia assembly. Precambrian Research 232, 44–58.

Colliston, W.P., Schoch, A.E., 2002. The structural development of the Aggeneys Hills, Namaqua Metamorphic Complex. South African Journal of Geology 105, 301–324.

Colliston, W.P., Schoch, A.E., 2000. Mid-Proterozoic tectonic evolution along the Orange River on the border between South Africa and Namibia. Communications of the Geological Survey of Namibia 12, 53–62.

Colliston, W.P., Schoch, A.E., Cole, J., 2014. The Grenvillian Namaqua-Natal fold belt adjacent to the Kaapvaal Craton: 1. Distribution of Mesoproterozoic collisional terranes deduced from results of regional surveys and selected profiles in the western and southern parts of the fold belt. Journal of African Earth Sciences 100, 7–19.

Colliston, W.P., Schoch, A.E., Praekelt, H.E., 2008. Comments on the paper by D.H. Cornell and A. Pettersson (SAJG, 110, 575-584 (2007). South African Journal of Geology 111, 465–466. doi:10.2113/gssajg.111.4.465

Cornell, D.H., Pettersson, Å., 2007. Ion probe zircon dating of metasediments from the Areachap and Kakamas Terranes, Namaqua-Natal Province and the stratigraphic integrity of the Areachap Group. South African Journal of Geology 110, 575–584.

Cornell, D.H., Pettersson, Å., Simonsen, S.L., 2012. Zircon U-Pb Emplacement and Nd-Hf crustal residence ages of Straussburg granite and Friersdale charnockite in the Namaqua-Natal Province, South Africa. Geological Society of South Africa 115, 465–484. doi:10.2113/gssajg.115.4.

Cornell, D.H., Pettersson, Å., Whitehouse, M.J., Scherstén, A., 2009. A New Chronostratigraphic Paradigm for the Age and Tectonic History of the Mesoproterozoic Bushmanland Ore District , South Africa. Society of Economic Geologist 104, 385–404.

Cornell, D.H., Thomas, R.J., Moen, H.F.G., Reid, D.L., Moore, J.M., Gibson, R.L., 2006. The Namaqua-Natal Province, in: In: Johnson, M.R, Anhaeusser, C.R and Thomas, R.J. (Eds.), The Geology of South Africa. Geological Society of South Africa. Johannesburg/Council for Geoscience, Pretoria. pp. 325–343.

Coward, M., 1980. Shear zones in the precambrian crust of Southern Africa. Journal of Structural Geology 2, 19–27.

Coward, M.P., Potgieter, R., 1983. Thrust zones and shear zones of the margin of the Namaqua and Kheis mobile belts, southren Africa. Precambrian Research 21, 39–54.

Deer, W.A., Howie, R.A., Zussman, J., 1992. An introduction to the rock forming minerals, second. ed. Pearson Education limited, London.

Eglington, B.M., 2006. Evolution of the Namaqua-Natal Belt, southern Africa - A geochronological and isotope geochemical review. Journal of African Earth Sciences 46, 93–111.

Stellenbosch University https://scholar.sun.ac.za

Eglington, B.M., Armstrong, R.A., 2003. Geochronological and isotopic constraints on the Mesoproterozoic Namaqua-Natal Belt: Evidence from deep borehole intersections in South Africa. Precambrian Research 125, 179–189.

Frei, D., Gerdes, A., 2009. Pricise and accurate in situ U-Pb dating of zircons with high sample throughput by automated LA-SF-ICPMS. Chemical Geology 261, 261–270.

Frimmel, H.E., 2000. Formation of late Mesoproterozoic Supercontinent: The South Africa-East Antarctica connection, in: The precambrian Earth: Tempos and events.

Fusseis, F., Handy, M.R., Schrank, C., 2006. Networking of shear zones at the brittle-to-viscous transition (Cap de Creus, NE Spain). Journal of Structural Geology 28, 1228–1243.

Handy, M.., 1989. Reformation regimes and the rheological evolution of fault zones in the lithosphere : the effects of pressure , temperature , grainsize and time. Tectonophysics 163, 119–152.

Hartnady, C.J.H., Joubert, P., Stowe, C., 1985. Proterozoic crustal evolution in Southwestern Africa. Science 8, 236–244.

Hoffman, P.F., 1991. Did the breakout of Laurentia turn Gondwanaland inside-out? Science 252, 1409–1412.

Humphreys, H.C., Van Bever Donker, J.M., 1987. Aspects of deformation along the namaqua province eastern boundary, kenhardt district, South Africa. Precambrian Research 36, 39–63.

Jacobs, J., Thomas, R., Weber, K., 1993. Accretion and indentation tectonics at the southern margin of the Kaapvall craton during Kibaran (Greenville) orogeny. Geology 21, 203–206.

Jacobs, J., Thomas, R.J., 1994. Oblique collision at about 1.1 Ga along the southern margin of the Kaapvaal continent, south-east Africa. Geologische Rundschau 83, 322–333.

Jefferies, S.P., Holdsworth, R.E., Wibberley, C.A.J., Shimamoto, T., Spiers, C.J., 2006. The nature and importance of phyllonite development in crustal-scale fault cores : an example from the Median Tectonic Line , Japan. Journal of Structural Geology 28, 220–235. doi:10.1016/j.jsg.2005.10.008

Joubert, P., 1986. Namaqualand; a model of Proterozoic accretion? South African Journal of Geology 89, 79 –96.

Lagoeiro, L., Fueten, F., 2008. Fluid-assisted grain boundary sliding in bedding-parallel quartz veins deformed under greenschist metamophic grade. Tectonophysics 446, 42–50. doi:10.1016/j.tecto.2007.10.004

Lambert, C.W., 2013. Granitic melt transport and emplacement along transcurrent shear zones : Case study of the Pofadder Shear Zone in South Africa and Namibia. University of Stellenbosch.

Ludwig, K., 2012. Isoplot/Ex version 3.75: a Geochronological toolkit for Microsoft Excel. Berkeley Geochronology Center, Berkeley.

Macey, P.H., Minnaar, H., Miller, J.A., Lambert, C.W., Groenewald, C., Indongo, J., Angombe, M.T., Hendrik, S., Shifotoka, G., Diener, J., le Roux, P., Frei, D., 2015. The Precambrian Geology of the Region South of Warmbad from Haib to Velloorsdrif, Southern Namibia, An Explanation to 1:50 000 Geological Map Sheets 2818AC, 2818AD, 2818CA, 2818CB,2818CC,2818CD,2818DA,

Stellenbosch University https://scholar.sun.ac.za

2819CA,2819CB, 2819CC, 2819CD and 2819DA.

Maclaren, A.., 1984. The geology of the area east of Pofadder with emphasis on shearing associated with the Pofadder lineament, Northwest Cape. Bulletin, Precambrian research, University of Cape Town 35, 1–123.

Marsh, J.H., Stockli, D.F., 2015. Lithos Zircon U – Pb and trace element zoning characteristics in an anatectic granulite domain : Insights from LASS-ICP-MS depth profiling. Lithos 239, 170–185. doi:10.1016/j.lithos.2015.10.017

Mclaren, A.H., 1988. The geology of the area east of the pofadder with emphasis on the shearing associated with the Poffader Lineament. Bulletin, Precambrian research, University of Cape Town 35, 1–123.

Means, W.D., 1995. Shear zones and rock history. Tectonophysics 247, 157–160.

Meinhold, G., Kostopoulos, D., Frei, D., Himmerkus, F., Reischmann, T., 2010. U-Pb LA-SF-ICP-MS zircon geochronology of the Serbo-Macedonian Massif, Greece: palaeotectonic constrains for Gondwana-derived terranes in the Eastern Mediterranean. international Journal of Earth Sciences 99, 813–832.

Melosh, B.L., Rowe, C.D., Smit, L., Groenewald, C., Lambert, C.W., Macey, P., 2014. Snap, crackle, Pop: Dilational fault breccias record seismic slip below the brittle-plastic transition. Earth and Planetary Science Letters 403, 432–445.

Miller, R.M., 2012. 'Review of Mesoproterozoic magmatism, sedimentation and terrane amalgamation in southwestern Africa.' South African Journal of Geology 115, 417–448.

Miller, R.M., 2008. The geology of Namibia. Hand book, Geological Survey of Namibia,3 volumes.

Minnaar, H., 2012. Composition and Evolution of the Proterozoic Vioolsdrif Batholith (including the Orange river group), Northern cape province, South Africa. University of the Free State.

Moen, H.F.G., Toogood, D.J., 2007. Geology of the Onseepkans Area. Pretoria, South Africa: Council for Geoscience.

Moore, A.C., 1981. The Tantalite Valley shear zone, a major locus for igneous activity in Southern Namibia/South West Africa. Journal of Volcanology and Geothermal Research 10, 383–393.

Nordin, F., 2009. U-Pb dating, Lu-Hf isotopic analysis and geothermobarometry of rocks in the Grunau terrane and Richetersveld sub-province, Namaqua sector, southern Africa. University of Gotenburg, Sweden.

Passchier, C., Trouw, R., 2005. Micro-tectonics, Second. ed. Springer, Berlin.

Passchier, C.W., 1984. The generation of ductile and brittle shear bands in a low-angle mylonite zone. Journal of Structural Geology 6, 273–1984.

Passchier, C.W., Hoek, J.D., Bekendam, R.F., De Boorder, H., Boorder, H.D.E., 1990. Ductile reactivation of Proterozoic brittle fault rocks; an example from the Vestfold Hills, East Antarctica. Precambrian Research 47, 3–16. doi:10.1016/0301-9268(90)90026-M

Pettersson, Å., 2008. Mesoproterozoic crustal evolution in Southern Africa. University of Gothenburg.

Stellenbosch University https://scholar.sun.ac.za

Platt, J.P., Behr, M.W., 2011. Lithospheric shear zones as constant stress experiments. Geology 39, 127–130. doi:10.1130/G31561.1

Ponce, C., Druguet, E., Carreras, J., 2013. Development of shear zone-related lozenges in foliated rocks. Journal of Structural Geology 50, 176–186. doi:10.1016/j.jsg.2012.04.001

Ramsay, J.G., 1980. Shear zone geometry: A review. Journal of Structural Geology 2, 83–99.

Reid, D.L., 1997. Sm-Nd age and REE geochemistry of Proterozoic arc-related igneous rocks in the richtersveld Subprovince, Namaqua Mobile Belt, Southern Africa. Journal of African Earth Sciences 24, 621–633.

Reid, D.L., Barton, E.S., 1983. Geochemical characterization of granitoid in the Namaqualand geotransverse. Spec. publ. geol. Soc. S. Afr 10, 67–82.

Reid, D.L., Welke, H.J., Erlank, A.J., Moyes, A., 1987. The Orange River Group: a major Proterozoic calcalkaline volcanic belt in the western Namaqua Province, southern Africa, in: Pharaoh, T.C. & Rickard, D.(eds) Geochemistry and Mineralization of Proterozoic Volcanic Suites, Geological Society, London, Special Publication No.33. pp. 327–346. doi:10.1144/GSL.SP.1987.033.01.22

Rennie, S.F., Fagereng, Å., Diener, J.F.A., 2013. Strain distribution within a km-scale , mid-crustal shear zone : The Kuckaus Mylonite Zone , Namibia. Journal of Structural Geology 56, 57–69. doi:10.1016/j.jsg.2013.09.001

Samskog, P., 2009. U-Pb , Lu-Hf zircon dating and source magma determination of magmatic rocks in the Richtersveld and Kakamas terrane , Namaqua Province , southern Africa. University of Gothenburg, Sweden.

Simpson, C., 1985. Deformation of granitic rocks across the brittle--ductile transition. Journal of Structural Geology 7, 503–511.

Simpson, C., De Paor, D.G., 1993. Strain and kinematic analysis in general shear zones. Journal of Structural Geology 15, 1–20.

Sláma, J., Košler, J., Condon, D.., Crowley, J.., Gerdes, A., Hanchar, J.., Horstwood, M.S.., Morris, G.., Nasdala, L., Norberg, N., Schaltegger, U., Shoene, B., Tubrett, M.., Whitehouse, M.., 2008. Plešovice zircon-a new natural reference material for U-Pb and Hf isotopic microanalysis. Chemical Geology 249, 1–35.

Stewart, M., Holdsworth, R.E., Strachan, R.A., 2000. Deformation processes and weakening mechanisms within the frictional- viscous transition zone of major crustal-scale faults : insights from the Great Glen Fault Zone , Scotland. Journal of Structural Geology 22, 543–560.

Stipp, M., Kunze, K., 2008. Dynamic recrystallization near the brittle-plastic transition in naturally and experimentally deformed quartz aggregates. Tectonophysics 448, 77–97. doi:10.1016/j.tecto.2007.11.041

Stipp, M., Stünitz, H., Heilbronner, R., Schmid, S.M., 2002. The eastern Tonale fault zone: A 'natural laboratory' for crystal plastic deformation of quartz over a temperature range from 250 to 700 °C. Journal of Structural Geology 24, 1861–1884. doi:10.1016/S0191-8141(02)00035-4

Stellenbosch University https://scholar.sun.ac.za

Thomas, R.J., Agenbacht, A.L.D., Cornell, D.H., Moore, J.M., 1994. The Kibaran of southern Africa: Tectonic evolution and metallogeny. Ore Geology Reviews 9, 131–160.

Toogood, D.J., 1976. Structural and Metamorphic Evolution of a Gneiss Terrain in the Namaqua Belt Near Onseepkans, South West Africa. Bulletin of the Precambrian Research unit, 19, 1–189.

Whitehouse, M.J., Bridgwater, D., 2001. Geochronological constraints on Paleoproterozoic crustal evolution and regional correlations of the northern Outer Hebridean Lewisian complex , Scotland. Precambrian Research 105, 227–245.

Wightman, R.H., Prior, D.J., Little, T.A., 2006. Quartz veins deformed by diffusion creep-accommodated grain boundary sliding during a transient , high strain-rate event in the Southern Alps , New Zealand. Journal of Structural Geology 28, 902–918. doi:10.1016/j.jsg.2006.02.008

Winter, J.D., 2001. An introduction to igneous and metamorphic petrology. Printice Hall, Upper Saddle River, New Jersey.

Stellenbosch University https://scholar.sun.ac.za

APPENDICES

APPENDIX A

List of samples for petrographic, geochronology and structural analysis

Waypoint number	Latitude	Longitude	Sample id number	Sample lithology and description
Petrographic section				
MA14003	-28.60136	18.455357	MA14001	Metagabbro
MA14004	-28.59250	18.457512	MA14002	Cataclasite/mylonite metagabbro
MA14006	-28.58426	18.454949	MA14003	Metagabbro
MA14010	-28.57840	18.464699	MA14004	Amphibolites
MA14022	-28.55221	18.444884	MA14005	Migmatitic banded gneiss
MA14024b	-28.55615	18.448550	MA14008	Amphibolites
MA14026	-28.55177	18.450615	MA14009	Garnet-andalusite quartz-biotite schist
MA14026	-28.55177	18.450615	MA14009	Metapelite (garnet-andalusite quartz-biotite schist)
MA14029	-28.55632	18.460306	MA14010A	Migmatitic banded gneiss
MA14029	-28.55632	18.460306	MA14010C	Migmatitic banded gneiss
MA14037	-28.54343	18.452090	MA14011	Migmatitic banded gneiss
MA14039	-28.53776	18.443596	MA14012	Migmatitic banded gneiss
MA14040	-28.53435	18.440362	MA14014	Phyllonites
MA14061	-28.56167	18.390457	MA14018A	Mesocratic porphyritic granite (Quartz-biotie-feldspar augen gneiss)
MA14061	-28.56167	18.390457	MA14018A	Mesocratic porphyritic granite (Quartz-biotie-feldspar augen gneiss)
MA14061	-28.56167	18.390457	MA14018B	Mesocratic porphyritic granite (Quartz-biotie-feldspar augen gneiss)
MA14061	-28.56167	18.390457	MA14018B	Mesocratic porphyritic granite (Quartz-biotie-feldspar augen gneiss)
MA14102	-28.54396	18.766094	MA14023	Restitic pods within sheared Eureka grey gneiss
MA14102	-28.54396	18.766094	MA14024	Restitic pods within sheared Eureka grey gneiss
MA14102	-28.54396	18.766094	MA14025	Eureka grey gneiss (quartz-bitite schist)
MA14103	-28.54235	18.770566	MA14026	Eureka grey gneiss (quartz-bitite schist)
MA14121	-28.55085	18.482332	MA14028	Leucocratic equigranular granite
MA14127	-28.56288	18.481388	MA14030	Amphibolites
MA14212	-28.48158	18.400953	MA14050	Calc-silicate (Garnet bearing)
MA14219	-28.47877	18.423730	MA14051	Pegmatitic granite
MA14230	-28.47659	18.427116	MA14052	Mylonite-cataclasites (pegmatite)
MA14231	-28.47372	18.430166	MA14053	Metagabbro
MA14255	-28.51104	18.425103	MA14054	Metapelite (restitic grt-quartz-biotite granulite)
MA14525	-28.56929	18.471689	MA14057	Leucocratic equigranular granite
MA14526	-28.56799	18.472276	MA14058	Garnet-bearing migmatitic qtz-bit-augen gneiss
MA14529	-28.57118	18.479502	MA14059	Metapelite cordierite-qtz-bit-grt granulite (100m thick lense)
MA14531	-28.56632	18.482494	MA14060	Leucocratic equigranular granite
MA14533	-28.56519	18.486686	MA14062	Metapelite cordierite-sillimanite pelitic granulite
MA14560	-28.57270	18.407550	MA14063	Leucocratic equigranular granite
MA14582	-28.49885	18.452510	MA14066	Eureka grey gneiss (garnet-quartz-biotite phyllonite)

Stellenbosch University https://scholar.sun.ac.za

MA14584	-28.50234	18.442830	MA14067	Eureka grey gneiss (garrnet-quartz-biotite phyllonite)
MA14686	-28.68426	18.457517	MA14078	Metagabbro
MA15543	-28.38423	18.458004	MA15070	Mesocratic porphyritic granite
MA15542b	-28.38823	18.459600	MA15071	Mesocratic porphyritic granite
MA15562	-28.49172	18.445983	MA15073	Mafic granulites
MA15564	-28.50971	18.429639	MA15074	Mylonite-cataclasite (quartzo-feldspathic gneiss)

Geochronology				
MA15587	-28.51773	18.449392	MA14069	Quartzo-feldspathic gneiss
MA14109	-28.53244	18.482322	MA14027	Leucocratic porphyritic granite
MA15543b	-28.38966	18.456866	MA15042	Metapelite (restitic cordierite-sillimanite-garnet-quartz-feldspar granulite)
MA15580	-28.54447	18.765800	MA15077	Eureka grey gneiss (grarnet-quartz-biotite)
Oriented thin section				
MA14004	-28.59250	18.457512	MA14002	Mylonite-cataclasite (quartz-biotie-feldspar gneiss)
MA14004	-28.59250	18.457512	MA14002	Mylonite-cataclasite (quartz-biotie-feldspar gneiss)
MA14126	-28.56248	18.481517	MA14029	Migmatitic banded gneiss (phyllonites-cataclasites)
MA14146	-28.48601	18.395191	MA14033	Mylonite-cataclasites (quartzo-feldspathic gneiss)
MA14146	-28.48601	18.395191	MA14034	Mylonite-cataclasites (quartzo-feldspathic gneiss)
MA14146	-28.48601	18.395191	MA14035	Amphibolite
MA14146	-28.48601	18.395191	MA14036	Eureka grey gneiss (quartz-biotite phyllonite)
MA14495	-28.56102	18.467150	MA14056	Mylonite-cataclasite (quartz-biotie-feldspar gneiss)
MA14495	-28.56102	18.467150	MA14056	Mylonite-cataclasite (quartz-biotie-feldspar gneiss)
MA14526	-28.56799	18.472276	MA14058	Garnet-bearing migmatitic qtz-bit-augen gneiss
MA14532	-28.56525	18.484612	MA14061	Mylonite-cataclasite (quartz-feldspar-biotite gneiss)
MA14561	-28.56350	18.407143	MA14064	Mylonite-cataclasite (quartz-biotie-feldspar gneiss)
MA14561	-28.56350	18.407143	MA14064	Mylonite-cataclasite (quartz-biotie-feldspar gneiss)
MA14575	-28.51937	18.460554	MA14065	Amphibolite (bECciated)
MA14587	-28.51290	18.443783	MA14068	Mylonite-cataclasites (quartzo-feldspathic gneiss)
MA14646	-28.54185	18.415322	MA14076	Mylonite-cataclasite (quartz-biotie-feldspar gneiss)
MA14646	-28.54185	18.415322	MA14076	Mylonite-cataclasite (quartz-biotie-feldspar gneiss)
MA14652	-28.53188	18.424200	MA14077	Migmatitic banded gneiss (phyllonites-cataclasites)

Stellenbosch University https://scholar.sun.ac.za

APPENDIX B

Geological map attached at the back

Stellenbosch University https://scholar.sun.ac.za

APPENDIX C

List of geochronology analysis (U-Pb, ICP-MS) result tables

Sample MA15077																	
				RATIOS							AGES [Ma]						[]*
Analysis	U [ppm][a]	Pb [ppm][a]	Th/U[a]	$^{207}Pb/^{235}U$[b]	2 s[d]	$^{206}Pb/^{238}U$[b]	2 s[d]	rho[c]	$^{207}Pb/^{206}Pb$[e]	2 s[d]	$^{207}Pb/^{235}U$	2 s	$^{206}Pb/^{238}U$	2 s	$^{207}Pb/^{206}Pb$	2 s	%
77-1	236	51	0.30	2.450	0.077	0.2164	0.0043	0.64	0.0821	0.0020	1257	40	1263	25	1248	48	101
77-2	163	60	0.35	6.303	0.195	0.3657	0.0073	0.65	0.1250	0.0029	2019	62	2009	40	2029	42	99
77-3	973	157	0.90	1.853	0.057	0.1618	0.0032	0.65	0.0831	0.0019	1065	33	967	19	1270	46	76
77-4	278	60	0.49	2.468	0.081	0.2163	0.0044	0.62	0.0827	0.0021	1263	41	1262	26	1263	50	100
77-5	294	65	0.09	2.582	0.088	0.2227	0.0045	0.60	0.0841	0.0023	1296	44	1296	26	1295	53	100
77-6	724	119	0.78	1.957	0.060	0.1643	0.0033	0.65	0.0864	0.0020	1101	34	981	20	1346	45	73
77-7	343	97	0.24	4.469	0.150	0.2819	0.0058	0.61	0.1150	0.0030	1725	58	1601	33	1879	48	85
77-8	667	167	0.55	3.600	0.117	0.2507	0.0051	0.62	0.1042	0.0026	1550	50	1442	29	1700	47	85
77-9	325	95	0.25	4.527	0.143	0.2931	0.0059	0.64	0.1120	0.0027	1736	55	1657	33	1832	44	90
77-10	529	118	0.15	2.588	0.081	0.2224	0.0044	0.64	0.0844	0.0020	1297	40	1294	26	1302	46	99
77-11	456	103	0.73	2.641	0.088	0.2263	0.0046	0.61	0.0847	0.0022	1312	44	1315	27	1308	51	101
77-12	259	57	0.39	2.568	0.083	0.2216	0.0045	0.62	0.0840	0.0021	1291	42	1290	26	1293	49	100
77-13	268	60	0.39	2.586	0.093	0.2228	0.0046	0.57	0.0842	0.0025	1297	47	1297	27	1296	57	100
77-14	270	60	0.38	2.594	0.084	0.2228	0.0045	0.62	0.0845	0.0021	1299	42	1297	26	1303	49	99
77-15	349	78	0.87	2.622	0.085	0.2239	0.0045	0.62	0.0850	0.0021	1307	42	1302	26	1315	49	99
77-17	324	70	0.39	2.465	0.080	0.2170	0.0044	0.62	0.0824	0.0021	1262	41	1266	25	1255	49	101
77-18	430	93	0.47	2.454	0.084	0.2151	0.0044	0.60	0.0828	0.0023	1259	43	1256	26	1264	53	99
77-19	307	28	0.39	0.733	0.027	0.0903	0.0018	0.55	0.0588	0.0018	558	21	557	11	561	67	99
77-20	332	72	0.63	2.485	0.082	0.2169	0.0044	0.61	0.0831	0.0022	1268	42	1265	25	1272	51	99
77-21	503	133	0.52	4.493	0.143	0.2645	0.0053	0.63	0.1232	0.0031	1730	55	1513	30	2003	44	76
77-22	196	66	0.53	5.238	0.171	0.3345	0.0067	0.62	0.1136	0.0029	1859	61	1860	37	1857	46	100
77-23	195	44	0.56	2.669	0.090	0.2257	0.0046	0.60	0.0857	0.0023	1320	45	1312	27	1332	52	98
77-24	255	67	0.48	3.423	0.114	0.2634	0.0053	0.61	0.0943	0.0025	1510	50	1507	30	1514	50	100
77-25	546	105	0.31	2.235	0.073	0.1933	0.0039	0.61	0.0839	0.0022	1192	39	1139	23	1290	51	88
77-26	865	291	0.09	5.297	0.162	0.3370	0.0067	0.65	0.1140	0.0027	1868	57	1872	37	1864	42	100
77-28	252	78	0.66	4.702	0.161	0.3113	0.0064	0.60	0.1096	0.0030	1768	61	1747	36	1792	50	97

Stellenbosch University https://scholar.sun.ac.za

77-29	1262	198	0.10	2.178	0.088	0.1572	0.0034	0.53	0.1005	0.0034	1174	47	941	20	1633	63	58
77-30	376	85	0.34	2.612	0.085	0.2246	0.0045	0.62	0.0844	0.0022	1304	42	1306	26	1301	50	100
77-31	319	119	0.42	6.448	0.202	0.3719	0.0074	0.64	0.1258	0.0030	2039	64	2038	41	2039	43	100
77-32	219	65	0.29	4.446	0.168	0.2956	0.0063	0.56	0.1091	0.0034	1721	65	1669	35	1784	57	94
77-33	267	80	0.86	4.246	0.136	0.2983	0.0060	0.63	0.1032	0.0026	1683	54	1683	34	1683	46	100
77-34	1485	127	0.31	0.814	0.035	0.0858	0.0018	0.50	0.0688	0.0026	605	26	531	11	893	77	59
77-35	473	155	0.48	5.100	0.159	0.3281	0.0065	0.64	0.1127	0.0027	1836	57	1829	36	1844	43	99
77-36	167	28	0.04	1.942	0.144	0.1703	0.0047	0.37	0.0827	0.0057	1096	81	1014	28	1262	135	80
77-37	825	125	0.38	1.769	0.070	0.1518	0.0032	0.53	0.0845	0.0028	1034	41	911	19	1305	65	70
77-38	246	46	0.27	2.169	0.095	0.1855	0.0040	0.49	0.0848	0.0032	1171	51	1097	24	1311	74	84
77-39	1210	190	0.65	1.736	0.058	0.1571	0.0031	0.60	0.0802	0.0022	1022	34	941	19	1201	53	78
77-42	836	204	0.69	3.540	0.119	0.2435	0.0049	0.60	0.1055	0.0028	1536	52	1405	28	1723	49	82
77-44	988	179	1.25	2.727	0.087	0.1810	0.0036	0.62	0.1093	0.0028	1336	43	1072	21	1787	46	60
77-45	588	187	0.85	5.413	0.179	0.3184	0.0064	0.61	0.1233	0.0032	1887	62	1782	36	2004	47	89
77-46	106	24	0.24	2.656	0.106	0.2266	0.0048	0.53	0.0850	0.0029	1316	52	1317	28	1316	66	100
77-47	458	85	0.15	2.187	0.103	0.1866	0.0041	0.47	0.0850	0.0035	1177	56	1103	24	1316	81	84
77-48	574	172	0.19	5.080	0.165	0.2992	0.0059	0.61	0.1231	0.0032	1833	59	1687	33	2002	46	84
77-49	632	175	0.10	4.486	0.151	0.2768	0.0056	0.60	0.1176	0.0032	1728	58	1575	32	1919	49	82
77-50	394	132	0.59	5.270	0.174	0.3352	0.0067	0.60	0.1140	0.0030	1864	62	1864	37	1865	47	100
77-51	908	241	0.27	3.997	0.141	0.2657	0.0054	0.58	0.1091	0.0031	1633	57	1519	31	1784	52	85
77-52	487	80	0.86	1.887	0.072	0.1654	0.0034	0.54	0.0828	0.0027	1076	41	986	20	1263	63	78
77-53	518	173	0.17	5.246	0.176	0.3346	0.0067	0.59	0.1137	0.0031	1860	62	1861	37	1860	49	100
77-54	345	70	0.51	2.644	0.117	0.2033	0.0044	0.49	0.0943	0.0036	1313	58	1193	26	1515	73	79
77-55	157	31	0.77	2.302	0.088	0.1975	0.0041	0.54	0.0845	0.0027	1213	46	1162	24	1305	62	89
77-56	497	106	0.47	2.414	0.083	0.2141	0.0043	0.58	0.0818	0.0023	1247	43	1251	25	1240	55	101
77-57	1522	195	0.35	1.462	0.051	0.1284	0.0026	0.57	0.0826	0.0024	915	32	779	16	1260	56	62
77-58	890	264	0.10	4.755	0.164	0.2963	0.0059	0.58	0.1164	0.0033	1777	61	1673	33	1902	51	88
77-59	1690	344	0.02	2.797	0.096	0.2037	0.0041	0.58	0.0996	0.0028	1355	46	1195	24	1616	52	74
77-60	473	100	0.53	2.429	0.115	0.2125	0.0047	0.47	0.0829	0.0035	1251	59	1242	27	1267	82	98
77-61	548	123	0.30	2.606	0.092	0.2238	0.0045	0.57	0.0845	0.0025	1302	46	1302	26	1303	57	100
77-62	755	147	0.22	2.260	0.079	0.1945	0.0039	0.57	0.0843	0.0024	1200	42	1146	23	1299	56	88
77-63	762	132	0.16	2.013	0.072	0.1734	0.0035	0.56	0.0842	0.0025	1120	40	1031	21	1297	57	79

[a]U and Pb concentrations and Th/U ratios are calculated relative to GJ-1 reference zircon

[b]Corrected for background and within-run U-Pb fractionation and normalised to reference zircon GJ-1 (ID-TIMS values/measured value);

$^{207}Pb/^{235}U$ calculated using $(^{207}Pb/^{206}Pb)/(^{238}U/^{206}Pb * 1/137.88)$

Stellenbosch University https://scholar.sun.ac.za

[c]Rho is the error correlation defined as the quotient of the propagated errors of the $^{206}Pb/^{238}U$ and the $^{207}/^{235}U$ ratio
[d]Quadratic addition of within-run errors (2 SD) and daily reproducibility of GJ-1 (2 SD)
[e]Corrected for mass-bias by normalising to GJ-1 reference zircon (~0.6 per atomic mass unit) and common Pb using the model Pb composition of Stacey & Kramers (1975)
*Concentration

Stellenbosch University https://scholar.sun.ac.za

Sample MA15042

				RATIOS							AGES [Ma]						[]*
Analysis	U [ppm][a]	Pb [ppm][a]	Th/U[a]	$^{207}Pb/^{235}U$[b]	2 s[d]	$^{206}Pb/^{238}U$[b]	2 s[d]	rho[c]	$^{207}Pb/^{206}Pb$[e]	2 s[d]	$^{207}Pb/^{235}U$	2 s	$^{206}Pb/^{238}U$	2 s	$^{207}Pb/^{206}Pb$	2 s	%
42-1	115	26	0.24	2.657	0.091	0.2234	0.0045	0.60	0.0862	0.0024	1316	45	1300	26	1344	53	97
42-2	671	244	0.32	6.152	0.184	0.3630	0.0072	0.66	0.1229	0.0028	1998	60	1997	39	1999	40	100
42-3	280	73	0.51	3.641	0.112	0.2605	0.0052	0.65	0.1014	0.0024	1558	48	1492	30	1649	44	90
42-4	1056	156	0.05	1.599	0.048	0.1474	0.0029	0.65	0.0787	0.0018	970	29	886	18	1165	45	76
42-5	582	121	0.06	2.318	0.071	0.2076	0.0041	0.65	0.0810	0.0019	1218	37	1216	24	1221	46	100
42-6	412	85	0.14	2.291	0.076	0.2055	0.0042	0.61	0.0809	0.0021	1209	40	1205	24	1218	52	99
42-7	645	102	0.17	1.755	0.054	0.1586	0.0032	0.65	0.0802	0.0019	1029	32	949	19	1203	46	79
42-8	506	105	0.06	2.336	0.072	0.2085	0.0041	0.65	0.0813	0.0019	1223	38	1221	24	1228	46	99
42-9	596	124	0.06	2.299	0.072	0.2075	0.0041	0.64	0.0804	0.0019	1212	38	1215	24	1206	47	101
42-10	277	63	0.12	2.667	0.086	0.2283	0.0046	0.63	0.0847	0.0021	1319	42	1326	27	1309	49	101
42-11	216	45	0.18	2.302	0.076	0.2074	0.0042	0.61	0.0805	0.0021	1213	40	1215	24	1209	51	100
42-12	462	96	0.21	2.314	0.073	0.2075	0.0041	0.63	0.0809	0.0020	1217	38	1215	24	1219	48	100
42-13	148	32	0.21	2.454	0.082	0.2147	0.0044	0.60	0.0829	0.0022	1259	42	1254	25	1267	52	99
42-14	365	82	0.03	2.627	0.084	0.2247	0.0045	0.63	0.0848	0.0021	1308	42	1307	26	1311	48	100
42-15	704	145	0.03	2.278	0.072	0.2058	0.0041	0.63	0.0803	0.0020	1205	38	1206	24	1204	48	100
42-16	182	61	0.43	5.150	0.169	0.3316	0.0067	0.62	0.1126	0.0029	1844	60	1846	37	1842	47	100
42-17	665	138	0.04	2.306	0.074	0.2070	0.0042	0.62	0.0808	0.0020	1214	39	1213	24	1216	50	100
42-18	270	56	0.07	2.331	0.076	0.2089	0.0042	0.62	0.0809	0.0021	1222	40	1223	25	1220	51	100
42-19	450	93	0.08	2.310	0.075	0.2078	0.0042	0.62	0.0807	0.0020	1215	39	1217	24	1213	50	100
42-20	156	47	0.45	4.245	0.141	0.2985	0.0061	0.61	0.1032	0.0027	1683	56	1684	34	1682	48	100
42-21	448	134	0.80	4.283	0.142	0.2982	0.0060	0.61	0.1042	0.0027	1690	56	1682	34	1700	48	99
42-22	249	52	0.26	2.293	0.078	0.2066	0.0042	0.60	0.0805	0.0022	1210	41	1211	25	1210	54	100
42-23	294	61	0.08	2.328	0.084	0.2078	0.0043	0.57	0.0813	0.0024	1221	44	1217	25	1228	58	99
42-24	263	57	0.32	2.482	0.084	0.2165	0.0044	0.60	0.0831	0.0023	1267	43	1264	26	1272	53	99
42-25	390	81	0.22	2.307	0.079	0.2067	0.0042	0.60	0.0809	0.0022	1214	41	1211	25	1220	54	99
42-26	544	107	0.19	2.260	0.070	0.1974	0.0039	0.64	0.0830	0.0020	1200	37	1161	23	1270	46	91
42-27	591	131	0.26	2.569	0.078	0.2220	0.0044	0.65	0.0839	0.0019	1292	39	1293	25	1291	45	100
42-28	1068	195	0.51	2.121	0.064	0.1824	0.0036	0.65	0.0843	0.0019	1156	35	1080	21	1299	44	83
42-29	883	180	0.04	2.261	0.068	0.2044	0.0040	0.66	0.0802	0.0018	1200	36	1199	24	1203	45	100
42-30	559	122	0.46	2.483	0.076	0.2175	0.0043	0.64	0.0828	0.0019	1267	39	1269	25	1265	46	100

Stellenbosch University https://scholar.sun.ac.za

42-31	341	72	0.23	2.396	0.076	0.2123	0.0042	0.63	0.0819	0.0020	1241	39	1241	25	1243	48	100
42-32	188	41	0.21	2.511	0.084	0.2190	0.0044	0.60	0.0832	0.0022	1275	43	1277	26	1273	53	100
42-33	323	65	0.13	2.194	0.072	0.2013	0.0040	0.60	0.0791	0.0021	1179	39	1182	24	1173	52	101
42-34	496	134	0.36	3.631	0.113	0.2694	0.0053	0.63	0.0978	0.0024	1556	49	1538	30	1582	45	97
42-35	2717	195	0.00	0.722	0.022	0.0717	0.0014	0.65	0.0730	0.0017	552	17	446	9	1013	47	44
42-36	558	115	0.07	2.293	0.071	0.2068	0.0041	0.64	0.0804	0.0019	1210	37	1212	24	1208	47	100
42-37	909	186	0.02	2.269	0.069	0.2051	0.0040	0.64	0.0803	0.0019	1203	37	1203	24	1203	46	100
42-38	276	59	0.23	2.446	0.079	0.2145	0.0043	0.61	0.0827	0.0021	1256	41	1253	25	1262	50	99
42-39	975	199	0.03	2.254	0.074	0.2044	0.0041	0.61	0.0800	0.0021	1198	39	1199	24	1197	51	100
42-40	742	153	0.07	2.280	0.070	0.2059	0.0041	0.64	0.0803	0.0019	1206	37	1207	24	1205	47	100
42-41	288	90	0.66	4.750	0.155	0.3127	0.0063	0.62	0.1102	0.0028	1776	58	1754	35	1802	47	97
42-42	534	111	0.11	2.328	0.072	0.2086	0.0041	0.64	0.0810	0.0019	1221	38	1221	24	1220	47	100
42-43	432	79	0.03	2.017	0.064	0.1819	0.0036	0.62	0.0804	0.0020	1121	36	1077	21	1207	49	89
42-44	353	82	0.35	2.761	0.091	0.2324	0.0046	0.61	0.0862	0.0022	1345	44	1347	27	1342	50	100
42-45	1031	214	0.02	2.300	0.070	0.2076	0.0041	0.65	0.0804	0.0019	1212	37	1216	24	1206	46	101
42-46	220	68	0.54	4.510	0.143	0.3087	0.0062	0.63	0.1060	0.0026	1733	55	1734	35	1731	45	100
42-47	807	120	0.30	1.684	0.052	0.1489	0.0029	0.64	0.0820	0.0020	1003	31	895	18	1246	47	72
42-48	2262	412	0.16	1.948	0.058	0.1821	0.0036	0.65	0.0776	0.0018	1098	33	1079	21	1136	45	95
42-49	797	178	0.19	2.582	0.080	0.2234	0.0044	0.63	0.0839	0.0020	1296	40	1300	26	1289	47	101
42-50	807	166	0.03	2.283	0.072	0.2056	0.0041	0.63	0.0805	0.0020	1207	38	1205	24	1210	48	100
42-51	337	66	0.12	2.236	0.073	0.1958	0.0039	0.61	0.0828	0.0021	1193	39	1153	23	1265	50	91
42-52	419	79	0.15	2.151	0.070	0.1896	0.0038	0.61	0.0823	0.0021	1165	38	1119	22	1252	50	89
42-53	111	25	0.27	2.655	0.099	0.2263	0.0047	0.55	0.0851	0.0026	1316	49	1315	27	1318	60	100
42-54	866	179	0.03	2.315	0.072	0.2068	0.0041	0.63	0.0812	0.0019	1217	38	1212	24	1226	47	99
42-55	332	96	0.83	4.055	0.129	0.2902	0.0058	0.62	0.1014	0.0025	1645	52	1642	33	1649	46	100
42-56	431	91	0.16	2.368	0.076	0.2109	0.0042	0.62	0.0814	0.0021	1233	40	1234	24	1231	50	100
42-57	839	149	0.03	2.016	0.063	0.1775	0.0035	0.63	0.0824	0.0020	1121	35	1053	21	1255	47	84
42-58	579	121	0.23	2.397	0.076	0.2098	0.0041	0.63	0.0829	0.0020	1242	39	1228	24	1266	48	97
42-59	766	159	0.26	2.341	0.073	0.2080	0.0041	0.63	0.0816	0.0020	1225	38	1218	24	1236	48	99
42-60	163	36	0.37	2.583	0.093	0.2227	0.0045	0.57	0.0841	0.0025	1296	46	1296	26	1296	57	100
42-61	527	108	0.05	2.280	0.073	0.2052	0.0041	0.62	0.0806	0.0020	1206	39	1203	24	1211	49	99
42-62	506	109	0.20	2.453	0.078	0.2153	0.0043	0.62	0.0826	0.0021	1258	40	1257	25	1260	49	100
42-63	1166	198	0.03	1.869	0.058	0.1699	0.0033	0.63	0.0798	0.0019	1070	33	1012	20	1192	48	85
42-64	208	62	0.19	4.233	0.139	0.2975	0.0059	0.61	0.1032	0.0027	1680	55	1679	34	1682	48	100

Stellenbosch University https://scholar.sun.ac.za

42-65	138	34	0.41	3.424	0.152	0.2439	0.0054	0.50	0.1018	0.0039	1510	67	1407	31	1657	71	85
42-66	1088	223	0.02	2.401	0.077	0.2046	0.0040	0.62	0.0851	0.0021	1243	40	1200	24	1319	49	91
42-67	165	52	0.45	4.654	0.154	0.3144	0.0063	0.60	0.1074	0.0028	1759	58	1762	35	1755	48	100
42-68	440	94	0.05	2.408	0.078	0.2133	0.0042	0.61	0.0819	0.0021	1245	40	1247	25	1242	50	100
42-69	945	213	0.30	2.651	0.083	0.2254	0.0044	0.63	0.0853	0.0021	1315	41	1310	26	1323	47	99
42-70	1038	148	0.03	1.555	0.049	0.1430	0.0028	0.62	0.0789	0.0020	952	30	862	17	1168	49	74
42-71	274	87	0.84	4.783	0.155	0.3178	0.0063	0.62	0.1091	0.0028	1782	58	1779	35	1785	46	100
42-72	352	80	0.18	2.660	0.087	0.2274	0.0045	0.60	0.0848	0.0022	1317	43	1321	26	1312	51	101
42-73	206	35	0.32	2.037	0.072	0.1722	0.0035	0.57	0.0858	0.0025	1128	40	1024	21	1334	56	77
42-74	586	122	0.05	2.348	0.077	0.2089	0.0041	0.61	0.0815	0.0021	1227	40	1223	24	1234	51	99
42-75	456	89	0.25	2.229	0.074	0.1952	0.0039	0.60	0.0828	0.0022	1190	39	1149	23	1265	52	91
42-76	847	174	0.10	2.299	0.074	0.2055	0.0041	0.61	0.0811	0.0021	1212	39	1205	24	1225	50	98
42-77	295	61	0.08	2.302	0.079	0.2058	0.0041	0.58	0.0811	0.0023	1213	42	1207	24	1225	55	99
42-78	303	102	0.23	5.346	0.177	0.3376	0.0067	0.60	0.1149	0.0030	1876	62	1875	37	1878	48	100
42-79	155	48	0.44	4.538	0.178	0.3100	0.0066	0.54	0.1062	0.0035	1738	68	1741	37	1735	61	100
42-80	528	112	0.51	2.424	0.085	0.2123	0.0043	0.57	0.0828	0.0024	1250	44	1241	25	1265	56	98
42-81	285	64	0.12	2.634	0.090	0.2253	0.0045	0.58	0.0848	0.0024	1310	45	1310	26	1311	54	100
42-82	905	208	0.25	2.727	0.088	0.2298	0.0045	0.61	0.0861	0.0022	1336	43	1333	26	1340	49	100
42-83	338	76	0.09	2.587	0.089	0.2231	0.0045	0.58	0.0841	0.0024	1297	45	1298	26	1295	55	100
42-84	411	84	0.10	2.299	0.078	0.2045	0.0041	0.59	0.0815	0.0022	1212	41	1199	24	1234	54	97
42-85	612	128	0.10	2.406	0.079	0.2091	0.0041	0.60	0.0834	0.0022	1244	41	1224	24	1280	51	96
42-86	200	45	0.39	2.586	0.092	0.2229	0.0045	0.57	0.0842	0.0025	1297	46	1297	26	1296	57	100
42-87	88	20	0.33	2.703	0.130	0.2284	0.0051	0.47	0.0858	0.0037	1329	64	1326	30	1335	82	99
42-88	1059	218	0.01	2.309	0.076	0.2060	0.0041	0.60	0.0813	0.0021	1215	40	1208	24	1228	51	98
42-89	144	32	0.39	2.544	0.095	0.2201	0.0045	0.55	0.0838	0.0026	1285	48	1283	26	1289	61	100
42-90	476	103	0.24	2.491	0.085	0.2160	0.0043	0.58	0.0837	0.0023	1269	43	1261	25	1284	54	98
42-91	286	60	0.16	2.338	0.082	0.2086	0.0042	0.57	0.0813	0.0023	1224	43	1221	24	1228	57	99
42-92	254	80	0.51	4.752	0.163	0.3164	0.0064	0.58	0.1089	0.0030	1777	61	1772	36	1781	51	99
42-93	348	71	0.10	2.283	0.083	0.2036	0.0041	0.56	0.0813	0.0024	1207	44	1195	24	1229	59	97
42-94	829	157	0.03	2.133	0.074	0.1898	0.0038	0.58	0.0815	0.0023	1160	40	1121	22	1234	55	91
42-95	710	137	0.15	2.248	0.076	0.1927	0.0038	0.59	0.0846	0.0023	1196	40	1136	23	1307	53	87
42-96	797	171	0.20	2.796	0.093	0.2141	0.0042	0.59	0.0947	0.0025	1354	45	1251	25	1522	51	82
42-97	315	65	0.10	2.307	0.081	0.2071	0.0042	0.57	0.0808	0.0023	1214	43	1213	24	1216	57	100
42-98	941	190	0.05	2.233	0.075	0.2014	0.0040	0.59	0.0804	0.0022	1191	40	1183	23	1207	53	98

Stellenbosch University https://scholar.sun.ac.za

42-99	344	74	0.12	2.469	0.088	0.2160	0.0043	0.56	0.0829	0.0024	1263	45	1261	25	1267	57	99
42-100	748	162	0.11	2.473	0.084	0.2167	0.0043	0.58	0.0828	0.0023	1264	43	1264	25	1264	54	100
42-101	193	42	0.29	2.473	0.092	0.2163	0.0044	0.54	0.0829	0.0026	1264	47	1262	26	1267	61	100
42-102	2103	234	0.01	1.178	0.040	0.1112	0.0022	0.59	0.0768	0.0021	790	27	680	13	1117	55	61

[a]U and Pb concentrations and Th/U ratios are calculated relative to GJ-1 reference zircon

[b]Corrected for background and within-run U-Pb fractionation and normalised to reference zircon GJ-1 (ID-TIMS values/measured value);

$^{207}Pb/^{235}U$ calculated using $(^{207}Pb/^{206}Pb)/(^{238}U/^{206}Pb * 1/137.88)$

[c]Rho is the error correlation defined as the quotient of the propagated errors of the $^{206}Pb/^{238}U$ and the $^{207}/^{235}U$ ratio

[d]Quadratic addition of within-run errors (2 SD) and daily reproducibility of GJ-1 (2 SD)

[e]Corrected for mass-bias by normalising to GJ-1 reference zircon (~0.6 per atomic mass unit) and common Pb using the model Pb composition of Stacey & Kramers (1975)

*Concentration

Stellenbosch University https://scholar.sun.ac.za

Sample MA14069

				RATIOS							AGES [Ma]						[]*
Analysis	U [ppm][a]	Pb [ppm][a]	Th/U[a]	$^{207}Pb/^{235}U$[b]	2 □[d]	$^{206}Pb/^{238}U$[b]	2 □[d]	rho[c]	$^{207}Pb/^{206}Pb$[e]	2 □[d]	$^{207}Pb/^{235}U$	2 □	$^{206}Pb/^{238}U$	2 □	$^{207}Pb/^{206}Pb$	2 □	%
69-1	218	45	0.23	2.277	0.072	0.2057	0.0047	0.72	0.0803	0.0018	1205	38	1206	25	1205	43	100
69-2	170	35	0.33	2.273	0.073	0.2049	0.0047	0.71	0.0805	0.0018	1204	39	1202	25	1208	45	99
69-3	191	39	0.65	2.275	0.072	0.2050	0.0047	0.72	0.0805	0.0018	1205	38	1202	25	1209	43	99
69-4	139	29	0.33	2.284	0.074	0.2069	0.0047	0.71	0.0801	0.0018	1207	39	1212	25	1198	45	101
69-5	352	67	0.23	2.132	0.069	0.1914	0.0044	0.71	0.0808	0.0019	1159	38	1129	24	1216	45	93
69-6	148	29	0.33	2.187	0.071	0.1963	0.0045	0.71	0.0808	0.0018	1177	38	1156	24	1216	44	95
69-7	57	12	0.53	2.298	0.080	0.2064	0.0048	0.67	0.0808	0.0021	1212	42	1210	26	1216	51	100
69-8	296	62	0.05	2.323	0.075	0.2081	0.0047	0.70	0.0810	0.0019	1219	39	1219	25	1221	45	100
69-9	87	17	1.03	2.162	0.084	0.1953	0.0045	0.59	0.0803	0.0025	1169	45	1150	24	1204	61	96
69-10	214	42	0.64	2.170	0.069	0.1946	0.0044	0.72	0.0809	0.0018	1171	37	1146	24	1219	43	94
69-11	322	66	0.24	2.281	0.074	0.2053	0.0047	0.71	0.0806	0.0018	1206	39	1204	25	1212	45	99
69-12	141	29	0.26	2.256	0.073	0.2054	0.0047	0.70	0.0797	0.0018	1199	39	1204	25	1189	46	101
69-13	228	45	0.58	2.172	0.071	0.1958	0.0045	0.70	0.0805	0.0019	1172	38	1153	24	1208	46	95
69-14	192	40	0.21	2.284	0.076	0.2064	0.0047	0.69	0.0802	0.0019	1207	40	1210	25	1203	47	101
69-15	171	34	0.30	2.188	0.070	0.1976	0.0045	0.71	0.0803	0.0018	1177	38	1162	24	1205	44	96
69-16	121	25	0.43	2.270	0.075	0.2054	0.0047	0.70	0.0802	0.0019	1203	40	1204	25	1201	46	100
69-17	112	23	0.51	2.273	0.078	0.2053	0.0047	0.67	0.0803	0.0020	1204	41	1204	25	1204	50	100
69-18	199	38	0.14	2.116	0.088	0.1923	0.0044	0.55	0.0798	0.0028	1154	48	1134	24	1192	68	95
69-19	123	24	0.54	2.138	0.077	0.1933	0.0045	0.64	0.0802	0.0022	1161	42	1139	24	1202	54	95
69-20	76	15	0.53	2.139	0.076	0.1922	0.0044	0.65	0.0807	0.0022	1162	41	1133	24	1215	53	93
69-21	56	14	0.53	3.420	0.118	0.2563	0.0059	0.67	0.0968	0.0025	1509	52	1471	31	1564	47	94
69-22	184	38	0.58	2.271	0.074	0.2054	0.0047	0.71	0.0802	0.0018	1203	39	1204	25	1202	45	100
69-23	159	33	0.37	2.281	0.082	0.2058	0.0047	0.64	0.0804	0.0022	1206	44	1206	25	1207	54	100
69-24	528	103	0.32	2.162	0.070	0.1940	0.0044	0.70	0.0808	0.0019	1169	38	1143	24	1217	45	94
69-25	92	19	0.87	2.293	0.077	0.2063	0.0047	0.68	0.0806	0.0020	1210	41	1209	25	1213	48	100

[a]U and Pb concentrations and Th/U ratios are calculated relative to GJ-1 reference zircon

$^{207}Pb/^{235}U$ calculated using ($^{207}Pb/^{206}Pb$)/($^{238}U/^{206}Pb$ * 1/137.88)

[b]Corrected for background and within-run U-Pb fractionation and normalised to reference zircon GJ-1 (ID-TIMS values/measured value);

[c]Rho is the error correlation defined as the quotient of the propagated errors of the $^{206}Pb/^{238}U$ and the $^{207}/^{235}U$ ratio

[d]Quadratic addition of within-run errors (2 SD) and daily reproducibility of GJ-1 (2 SD)

[e]Corrected for mass-bias by normalising to GJ-1 reference zircon (~0.6 per atomic mass unit) and common Pb using the model Pb composition of Stacey & Kramers (1975)

*Concentration

Stellenbosch University https://scholar.sun.ac.za

Sample MA14027

				RATIOS							AGES [Ma]						[]*
Analysis	U [ppm][a]	Pb [ppm][a]	Th/U[a]	$^{207}Pb/^{235}U$[b]	2 s[d]	$^{206}Pb/^{238}U$[b]	2 s[d]	rho[c]	$^{207}Pb/^{206}Pb$[e]	2 s[d]	$^{207}Pb/^{235}U$	2 s	$^{206}Pb/^{238}U$	2 s	$^{207}Pb/^{206}Pb$	2 s	%
27-01	25	9	0.24	5.77	0.50	0.3530	0.0091	0.30	0.1185	0.0098	1941	168	1949	44	1933	144	101
27-02	233	82	0.16	5.81	0.23	0.3527	0.0095	0.67	0.1195	0.0035	1948	78	1947	45	1948	52	100
27-03	312	116	1.15	6.42	0.22	0.3707	0.0096	0.77	0.1256	0.0027	2035	69	2033	45	2038	38	100
27-04	394	130	0.62	5.68	0.20	0.3296	0.0085	0.75	0.1250	0.0028	1928	66	1837	41	2029	40	91
27-05	257	51	0.39	2.28	0.09	0.1964	0.0051	0.63	0.0841	0.0027	1205	50	1156	28	1294	61	89
27-07	387	164	0.12	8.41	0.28	0.4238	0.0110	0.77	0.1440	0.0031	2276	77	2278	50	2275	37	100
27-09	86	19	0.88	2.61	0.18	0.2219	0.0059	0.38	0.0852	0.0056	1303	92	1292	31	1320	124	98
27-10	99	22	0.95	2.63	0.10	0.2255	0.0059	0.72	0.0847	0.0021	1310	47	1311	31	1308	48	100
27-11	350	116	0.36	5.18	0.18	0.3323	0.0086	0.76	0.1130	0.0025	1849	63	1849	42	1848	39	100
27-12	121	27	0.59	2.58	0.10	0.2224	0.0058	0.71	0.0841	0.0022	1295	48	1294	31	1295	50	100
27-13	1392	92	0.23	0.77	0.03	0.0657	0.0017	0.71	0.0844	0.0022	577	21	410	10	1303	50	32
27-14	191	46	1.22	3.96	0.14	0.2410	0.0064	0.72	0.1193	0.0030	1626	59	1392	33	1945	45	72
27-15	181	17	0.21	1.08	0.06	0.0932	0.0024	0.49	0.0842	0.0039	745	40	574	14	1298	89	44
27-16	77	26	0.97	5.29	0.19	0.3354	0.0088	0.73	0.1144	0.0028	1867	67	1865	43	1870	43	100
27-17	440	53	0.55	1.75	0.06	0.1216	0.0032	0.75	0.1046	0.0024	1028	36	740	18	1708	42	43
27-18	185	62	0.84	5.30	0.20	0.3359	0.0088	0.69	0.1145	0.0032	1869	71	1867	42	1872	50	100
27-19	601	179	0.27	4.62	0.17	0.2985	0.0078	0.72	0.1123	0.0028	1753	64	1684	39	1837	45	92
27-20	160	35	0.23	2.81	0.14	0.2188	0.0058	0.54	0.0932	0.0038	1358	66	1276	30	1491	77	86
27-21	161	30	0.30	1.97	0.07	0.1876	0.0049	0.72	0.0764	0.0019	1107	40	1108	27	1104	50	100
27-25	63	13	0.46	2.35	0.09	0.2097	0.0056	0.68	0.0812	0.0023	1226	48	1227	30	1225	55	100
27-26	135	28	0.35	2.35	0.09	0.2098	0.0055	0.71	0.0812	0.0021	1227	45	1228	29	1226	50	100
27-27	120	40	0.77	5.28	0.19	0.3354	0.0088	0.73	0.1142	0.0028	1866	67	1865	43	1868	44	100
27-29	111	19	0.90	1.68	0.06	0.1682	0.0044	0.69	0.0726	0.0020	1002	38	1002	25	1003	56	100

[a]U and Pb concentrations and Th/U ratios are calculated relative to GJ-1 reference zircon

[b]Corrected for background and within-run U-Pb fractionation and normalised to reference zircon GJ-1 (ID-TIMS values/measured value);

$^{207}Pb/^{235}U$ calculated using $(^{207}Pb/^{206}Pb)/(^{238}U/^{206}Pb * 1/137.88)$

[c]Rho is the error correlation defined as the quotient of the propagated errors of the $^{206}Pb/^{238}U$ and the $^{207}/^{235}U$ ratio

[d]Quadratic addition of within-run errors (2 SD) and daily reproducibility of GJ-1 (2 SD)

[e]Corrected for mass-bias by normalising to GJ-1 reference zircon (~0.6 per atomic mass unit) and common Pb using the model Pb composition of Stacey & Kramers (1975)

*Concentration

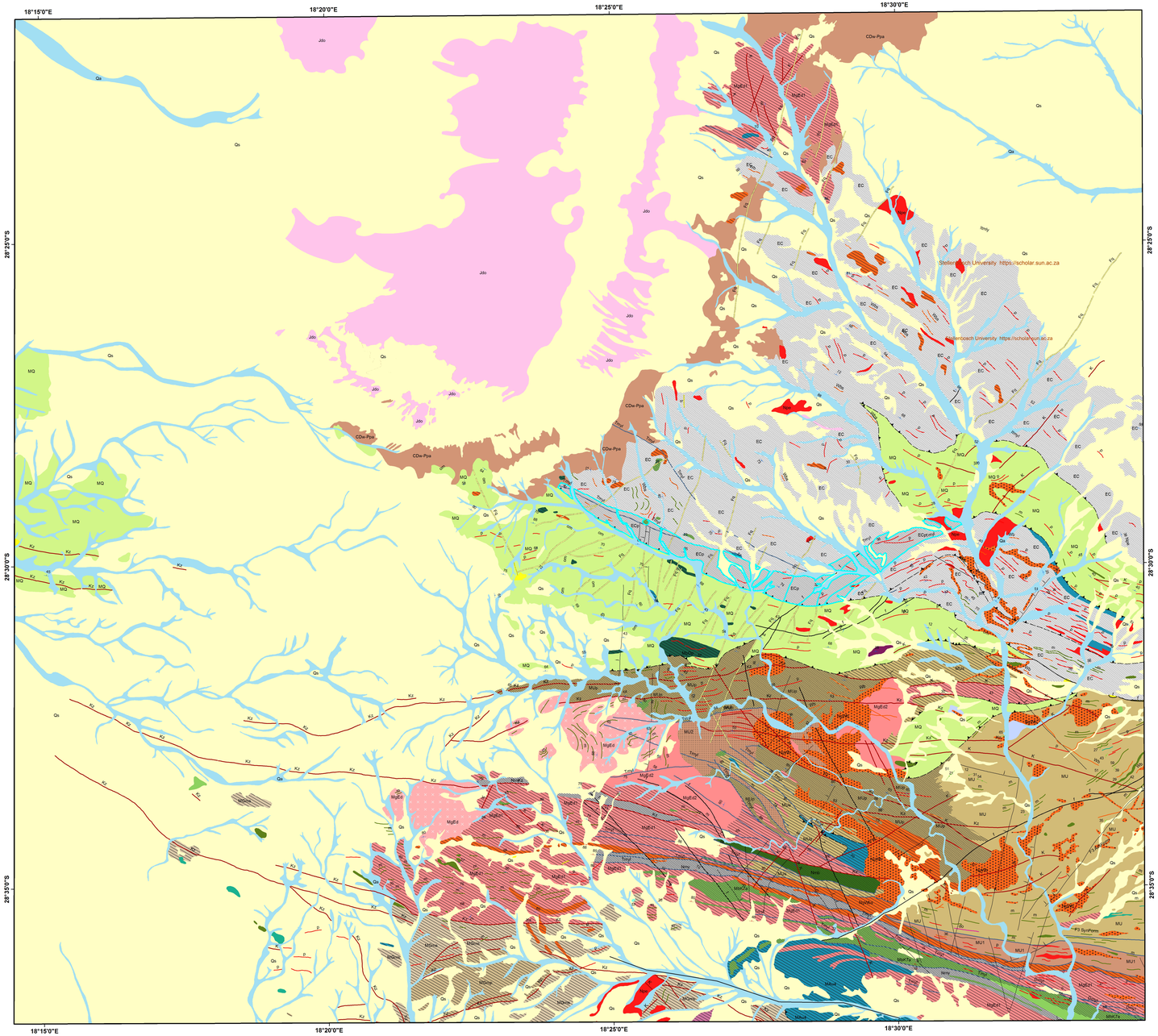

GEOLOGICAL LEGEND

PHANEROZOIC
- CENOZOIC
- PALEOZOIC
  - JURASSIC
  - TRIASSIC
  - PREMIAN
  - CARBONIFEROUS

Qa — Alluvium; residual soil, sand, gravel, scree

Qs — Surficial Cenozoic deposit (undifferentiated mobile sand and weathered regolith)

Jdo — Dolerite sills (Jdo) and picrobasalt dyke (do) } KAROO DOLERITE SUITE } KAROO SUPERGROUP

CDw-Ppa — Basal glacial diamictite (Dwyka Group) overlain by interbedded shale and siltstone (Prince Albert Formation)

PROTEROZOIC
- EDIACARAN
- NEOPROTEROZOIC
- TONIAN

j — Master joints

f, fq — Fault (f) and fault hosting quartz vein (fq)

k, kz — Fractures, faults and discrete shear zones(kz), associated with low grade country rock fluid alteration (mainly K-metasomatism and saussertisation)

q_v — Quartz veins and plugs (q)

q

NgWb — NgWbs — Wb — Wbs — Fine- to medium-grained leucocratic equigranula granite, plutons (NgWb), dykes (Wb). Sheared = NgWbs, Wbs } WARMBAD SUITE *1003 Ma*

Npe — Pegmatite (sheared and unsheared, dyke; p) *1005-958 Ma*

p

Discrete & truncating mylonite shear zones with or without quartz vein and/or pegmatite fill

Mphy — Polylithic shear zone including sheared rocks from both Pella and Gordonia domains hosting the cryptic Lower Fish River-Onseepkans thrust

Nmb — Mafic mylonite and cataclasite

Nmg — Felsic/granitic mylonite and cataclasite

Nmy — Undifferentiated mylonite and cataclasite } Marshall Rocks-Pofadder Shear Zone

ECp — Undifferentiated phyllonite of the reworked eureka complex and interlayered amphibolite and quartzo-feldspathic gneiss

EC — Lithotectonic pakage hosting sheared rocks of the reworked eureka complex (eureka grey gneiss, phyllonites and resistitic zsillimanite garnet-quartz-biotite granulitic pelites) } Polylithic shear zone hosting sheared rocks from both Pella and Gordonia domains hosting the cryptic Lower Fish River-Onseepkans Thrust } sheared Z2 thrust

PROTEROZOIC
- MESOPROTERZOIC
- PALEOPROTEROZOIC

MgEd1 — Variably sheared mesoporphyritic granite

MgEd2 — Unsheared/weakly mesoporphyritic granite

MgEd — Subcropping mesoporphyritic granite } EENDORN SUITE

MQ — om — Lithotectonic pakage hosting sheared rocks of the interlayered amphibolite and quartzo-feldspathic gneiss (MQ), dykes of amphibolite (om) associated with MQ. Mafic granulite (MbGp) } LORFIT ZONE

RICHTERSVELD SUBPROVINCE

Pella Domain

m — MbG — Amphibolite gneiss and rare mafic schist Amphibolite meta-dykes (m). } GIRTIS SUITE

c — MGc — Diopside-plagioclase-quartzstremolite-zsphene smicroclinesepidote calc-silicate granofels

mc — MbGc — Mixed amphibolite and calc-silicate granofels } METASOMATIC ROCKS

MGms — MPg — MU — MU2 — Heterogenous package dominated by migmatitic hornblende-biotite-quartz-feldspar gneiss and phyllonite, interlayered with quartz-feldspar gneiss, amphibolite (MbG), calc-silicate (MGc) and occasional layers of antophyllite-bearing gneiss and garnet-biotite-quartz-feldspar schist.Sheared in the MRPSZ= MGms, sheared in the Eureka Shear Zone

Biotitegarnet schist (MU2) and phyllonite (MUp) } ORANGE RIVER GROUP Umtis Gneiss

1979±5 Ma

MGmm — MGmp — Heterogenous interlayered package of gneisses dominated by biotite-hornblende porphyroblastic gneiss together with layers of biotite gneiss and phyllonite, quartz-feldspar gneiss, sporadic layers of antophyllite bearing gneiss,meta-agglomerate, amphibolite (MbG) and calc-silicate(MGc) and various foliation parallel sheets of Vioolsdrif intrusive rocks. Sheared = MGms; Phyllonite and cataclasite=MGmp } Gladkopm Gneiss

2052±14 Ma & 1975±6 Ma

GORDONIA SUBPROVINCE

Kakamas Domain

a — ak — Fine- to medium-grained alkali granite } SAMBOK SUITE

MbK7a — MbK7 — Metagabbro and metagabbronorite (MbK7); sheared metagabbroic rocks (MbK7a)

MAu2 — Restitic sillimanite-K-spar-cordieritesgarnet pelite granulite

MAu4 — Sheared biotite-muscovitesgarnet schist/ phyllite/phyllonite with unsheared outcrop-scale inclusions of peitic granulite } Aruga Gneiss

STRUCTURAL LEGEND

Tectonic lines
- f: Faults
- J: Joints and fractures
- Kz & K: Faults, fractures & discrete shear zones
- Fq: Faults hosting quartz vein
- Qv: Quartz vein
- Tmyl: Descrete &truncating mylonites
- Cryptic Thrust

Structural points

Foliation
- S4b
- S4
- S2/S4

Stretching lineation
- L4b
- L4
- L2/L4

MAP AREA

Authors:
This study
Mapped by Macey et al.,2015

Namibia

Map Projection: UTM (Zone 33S), Transverse Mercator

Datum: WGS 1984

1:50 000

0 1.25 2.5 5 Kilometers

Map Legend and layers, modified after Macey et al., 2015